

### **Distribution Agreement**

In presenting this dissertation as a partial fulfillment of the requirements for an advanced degree from Emory University, I hereby grant to Emory University and its agents the non-exclusive license to archive, make accessible, and display my thesis or dissertation in whole or in part in all forms of media, now and hereafter known, including display on the world wide web. I understand that I may select some access restrictions as part of the online submission of this thesis or dissertation. I retain all ownership rights to the copyright of the thesis or dissertation. I also retain the right to use in future works (such as articles or books) all or part of this thesis or dissertation.

Signature:

---

Alessandra M. Richardson

---

Date

More than a biomarker: vimentin function in lung cancer invasion and metastasis

By

Alessandra M. Richardson  
Doctor of Philosophy

Graduate Division of Biological and Biomedical Science  
Cancer Biology

---

Adam Marcus, Ph.D.  
Advisor

---

Paula Vertino, Ph.D.  
Committee Member

---

Hans Grossniklaus, M.D. M.B.A.  
Committee Member

---

George Beck Jr., Ph.D.  
Committee Member

---

Sumin Kang, Ph.D.  
Committee Member

---

Melissa Gilbert-Ross, Ph.D.  
Committee Member

Accepted:

---

Lisa A. Tedesco, Ph.D.  
Dean of the James T. Laney School of Graduate Studies

---

Date

More than a biomarker: vimentin function in lung cancer invasion and metastasis

By

Alessandra M. Richardson  
B.S., University of North Carolina at Chapel Hill, 2012

Advisor: Adam Marcus, Ph.D.

An abstract of  
A dissertation submitted to the Faculty of the  
James T. Laney School of Graduate Studies of Emory University  
in partial fulfillment of the requirements for the degree of Doctor of Philosophy  
in  
Graduate Division of Biological and Biomedical Sciences  
Cancer Biology  
2017

## Abstract

More than a biomarker: vimentin function in lung cancer invasion and metastasis

By Alessandra M. Richardson

Vimentin expression has been shown for decades to correlate with increased metastatic potential across solid tumor types including lung, breast and prostate cancers. However, it has never been demonstrated whether vimentin is a necessary contributor to the metastatic cascade. The work in this dissertation demonstrates with *in vitro* models, *in vivo* models, and clinical samples that vimentin is more than a biomarker and contributes to the metastatic cascade through a role in the tumor microenvironment.

We identified a role for vimentin in cell motility using lung cancer cell line models. Here we demonstrate that vimentin enters focal adhesion sites where it acts as a scaffold to promote EGF mediated phosphorylation of VAV2, the guanine exchange factor for the rho GTPase Rac1. Phosphorylation of VAV2 activates Rac1 to its GTP bound form where it promotes FAK activation at focal adhesion sites.

To further elucidate the role of vimentin in lung cancer metastasis, we moved our work into a genetically engineered mouse model (GEMM). For this study we developed a novel GEMM by crossing the Cre-dependent lung cancer metastasis model *LSL-Kras<sup>G12D</sup>/LKBI<sup>fl/fl</sup>* (*KLV<sup>+/+</sup>*) to a whole body vimentin knockout mouse to generate the *LSL-Kras<sup>G12D</sup>/LKBI<sup>fl/fl</sup>/Vim<sup>-/-</sup>* mouse (*KLV<sup>-/-</sup>*). Comparison of the *KLV* models show that vimentin loss does not impact tumor formation or burden. However, loss of vimentin does significantly reduce the rate of metastasis to the mediastinal lymph node. Immunohistochemical analysis of the primary lung tumors demonstrates that vimentin expression is reserved to the tumor microenvironment. This expression pattern was consistent with lung adenocarcinoma patient tissue samples irrespective of genotype. Further analysis shows vimentin to be predominantly expression in cancer-associated fibroblasts (CAFs). These CAFs support collective invasion and metastasis via heterotypic CAF-cancer cell interactions.

Overall this dissertation highlights the importance of vimentin as a functional player in cell motility and demonstrates a novel role in lung adenocarcinoma metastasis. Follow-up studies on the impact of vimentin on the tumor microenvironment will provide further insight on the role of vimentin on tumor progression.

More than a biomarker: vimentin function in lung cancer invasion and metastasis

By

Alessandra M. Richardson  
B.S., University of North Carolina at Chapel Hill, 2012

Advisor: Adam Marcus, Ph.D.

A dissertation submitted to the Faculty of the  
James T. Laney School of Graduate Studies of Emory University  
in partial fulfillment of the requirements for the degree of Doctor of Philosophy  
in  
Graduate Division of Biological and Biomedical Sciences  
Cancer Biology  
2017

## Acknowledgements

I have been very fortunate to have a great deal of support and encouragement on and off campus throughout the course of my dissertation work. First, I would like to thank those who guided me scientifically. My advisor, Adam Marcus, has instilled in me the importance of thinking critically while never losing sight of the big picture: why we are here and who benefits from our research. Thank you for taking a chance on me all those years ago. I know you will continue to inspire generations of young scientists with your mission and drive.

I would also like to thank my thesis committee for engaging with me in this project. I have really enjoyed our meetings as they have provided invaluable insight into my project and cancer biology as a whole.

Thank you to all those who worked on the manuscripts described in this dissertation. I appreciate all of your hard work and hope you all continue to be successful.

To my Atlanta support system (GDBBS Class of 2012, CC Crew, my labmates, JustFaith Family, and all my Kweens), thank you for sharing with me in the joys and struggles of graduate school. You all have helped make Atlanta my home. I am eternally grateful for all of your friendships.

For me, inspiration to pursue this degree came from both scientific and patient perspectives within my own family. Andy and Michelle, thank you for leading the way. I never would have found this path if it wasn't for all your guidance. Thank you for your support at every step from setting up my first research experience to helping me study for my qualifying exams. Abuelo, Ka, Ito; I would like to dedicate this dissertation to you in honor of your battles against cancer.

I would also like to thank God and my family for their love and support since day one. Thank you Mom and Dad for instilling in the three of us the importance of education. Mom, you have always been my role model. Thank you for actually taking the time to understand my project and for showing me what girls can do. Dad, thank you for keeping me grounded and reminding me 'it's not having what you want, it's wanting what you've got.' To my brothers, Cristian and Daniel, thanks for putting up with me. Your presence in Atlanta has provided so much comfort and joy throughout the years.

Thank you also to the rest of our ever-growing family: Ito, Ita, Abuela, Ana, El Pueblo, El Pueblito, The Other Salgueiros, and The Richardsons.

Finally, I would like to thank my husband Christopher. Thank you for supporting me through the distance, the weekends in lab, the presentation practices, and the late nights writing. We made it! Thank you.

## More than a biomarker: vimentin function in lung cancer invasion and metastasis

1. Introduction .....	5
1.1. Lung cancer .....	6
1.1.1. Histology .....	6
1.1.2. Genetic drivers .....	8
1.1.3. Current treatments .....	9
1.2. Metastasis .....	11
1.2.1. Migration strategies .....	12
1.2.1.1. Focal adhesion signaling .....	15
1.2.2. Intravasation, circulation, extravasation .....	15
1.3. Tumor microenvironment .....	17
1.3.1. Microenvironmental factors .....	18
1.3.1.1. Fibroblasts.....	18
1.3.1.2. Immune cells.....	19
1.3.1.3. Vasculature.....	19
1.3.1.4. The role of the microenvironment in metastasis.....	20
1.4. Metastatic biomarkers.....	20
1.4.1. History and applications .....	20
1.5. Vimentin structure and function .....	21
1.5.1. Intermediate filament structure .....	21
1.5.2. Vimentin in signal transduction .....	22
1.6. Current research models .....	22

1.6.1. Transplantation models .....	24
1.6.2. Genetically engineered mouse models (GEMMs) .....	26
1.7. Scope of Dissertation .....	27
2. Vimentin regulates lung cancer cell adhesion through a VAV2-Rac1 pathway to control focal adhesion kinase activity.....	29
2.1. Introduction.....	30
2.2. Experimental Procedures.....	31
2.3. Results.....	39
2.4. Discussion.....	62
3. Vimentin is required for lung adenocarcinoma metastasis via heterotypic tumor cell-cancer-associated fibroblast interactions during collective invasion.....	65
3.1. Introduction.....	66
3.2. Experimental Procedures.....	67
3.3. Results.....	74
3.4. Discussion.....	103
4. Discussion of Dissertation.....	105
4.1. Vimentin is identified as a key player in lung cancer invasion and metastasis	106
4.2. A novel mechanism of vimentin-mediated cell adhesion <i>in vitro</i> .....	107
4.3. Vimentin is necessary for lung cancer metastasis <i>in vivo</i> .....	108
4.4. Lung adenocarcinoma metastasis occurs via vimentin-mediated collective invasion.....	109
4.5. Context-dependent roles for vimentin.....	112
4.6. Postulated mechanisms of vimentin-mediated stroma-cancer cell crosstalk..	113



4.7. Future directions and translational implications.....	114
5. References.....	116

## **List of Figures**

**Figure 1-1: Metastasis and migration strategies**

**Figure 1-2: Summary of commonly used mouse models**

**Figure 2-1: Phospho-proteomic screen for cell motility proteins with an altered phosphorylation status upon vimentin depletion**

**Figure 2-2: pY142-VAV2 localizes to focal adhesions in vimentin positive cells**

**Figure 2-3: Vimentin depletion reduces the number and intensity of activated FAK positive focal adhesion sites**

**Figure 2-4: Vimentin regulates FAK activation and expression**

**Figure 2-5: Vimentin regulates FAK-mediated cell adhesion**

**Figure 2-6: VAV2 regulates vimentin dependent FAK activation and cell adhesion**

**Figure 2-7: Vimentin regulates VAV2-mediated Rac1 activation**

**Figure 2-8: Vimentin regulates FAK activity through a VAV2-Rac1 dependent pathway**

**Supplemental Figure 2-1: Vimentin loss reduces cell motility and invasion**

**Supplemental Figure 2-2: Vimentin loss reduces invasion and metastasis**

**Supplemental Figure 2-3: Phosphoproteomic screen for altered phosphorylation status upon vimentin depletion**

**Supplemental Figure 2-4: Vimentin is important for focal adhesion formation**

**Figure 3-1: KLV<sup>+/+</sup> and KLV<sup>-/-</sup> mice have a similar primary tumor burden**

**Figure 3-2: Vimentin depletion inhibits invasion and metastasis**

**Figure 3-3: Vimentin is required for collective invasion pack (CIP) formation**

**Figure 3-4: Vimentin+ cancer-associated fibroblasts surround CIPs**

**Figure 3-5: Vimentin regulates CAF invasion and stroma-cancer cell crosstalk**

**Figure 3-6: Vimentin is expressed in cancer-associated fibroblasts of lung cancer patient CIPs, which lack EMT in tumor cells**

**Supplemental Table 3-1: Infection rate and histology of lentiviral-Cre treated mice of both *KLV*<sup>+/+</sup> and *KLV*<sup>-/-</sup> mice**

**Supplemental Figure 3-1: Generation of an *LSL-Kras*<sup>G12D</sup>/*LKB1*<sup>fl/fl</sup>/*Vim*<sup>-/-</sup> GEMM (*KLV*<sup>-/-</sup>)**

**Supplemental Figure 3-2: *KLV* model survival analysis**

**Supplemental Figure 3-3: Vimentin antibody validation**

**Supplemental Figure 3-4: CIP biology is similar in both *KLV*<sup>+/+</sup> and *KLV*<sup>-/-</sup> tumors**

**Supplemental Figure 3-5: CAFs are present at the invasive front**

**Supplemental Figure 3-6: Macrophage recruitment is similar in both *KLV* models**

**Supplemental Figure 3-7: Probing Members of the tumor microenvironment**

**Supplemental Figure 3-8: Circularity of invasive areas in 3D spheroid assay**

**Supplemental Figure 3-9: Vimentin pathology Q score**

**Figure 4-1: Proposed model of vimentin-dependent CAF/CIP interactions.**

## List of Key Abbreviations

ANOVA	Analysis of variance
CA	Constitutively active
CAFs	Cancer-associated fibroblasts
CIP	Collective invasion pack
CTC	Circulating tumor cell
DIC	Differential interference contrast
DN	Dominant negative
ECM	Extracellular matrix
EGF	Epidermal Growth Factor
EGFR	Epidermal Growth Factor Receptor
ELISA	Enzyme Linked Immunosorbent Assay
EMT	Epithelial-mesenchymal transition
FA	Focal adhesion
FAK	Focal Adhesion Kinase
FBS	Fetal Bovine Serum
FFPE	Formalin-fixed paraffin embedded
FGF	Fibroblast Growth Factor
FSP1	Fibroblast-specific protein 1
GAPDH	Glyceraldehyde 3-phosphate dehydrogenase
GEF	Guanine exchange factor
GEMM	Genetically engineered mouse model
GFP	Green Fluorescent Protein
H&E	Hemotoxylin & Eosin
HBEC	Human bronchial epithelial cells
IF	Immunofluorescence
IHC	Immunohistochemistry
KLV	Kras/LKB1/Vimentin
KO	Knockout
Kras	Kirsten rat sarcoma
LKB1	Liver kinase B 1
LV-Cre	Lentiviral Cre
MMP	Matrix metalloprotease
NA	Numerical aperture
NSCLC	Non-small cell lung cancer
OCT	Optimal cutting temperature
PBS	Phosphate Buffer Saline
PCR	Polymerase Chain Reaction
PFS	Progression Free Survival
Pro-SPC	Pro-Surfactant Protein C
ROI	Region of interest
SCC	Squamous Cell Carcinoma

SDS	Sodiumdodecylsulphate
SHG	Second harmonic generation
shRNA	Short hairpin ribonucleic acid
siRNA	Small interference ribonucleic acid
$\alpha$ -SMA	Alpha Smooth Muscle Actin
TAM	Tumor Associated Macrophage
TBST	Tris Buffer Saline with Tween
TGF $\beta$ 1	Transforming Growth Factor Beta 1
TNF1 $\alpha$	Tumor Necrosis Factor 1 Alpha
TNM	Tumor Node Metastasis
TP53	Tumor Protein 53
VEGF	Vascular Endothelial Growth Factor
vim	Vimentin
WT	Wild-Type

## 1. Introduction

## **1.1 Lung Cancer**

Lung cancer is the second most common cancer diagnosis among both men and women and is the leading cause of cancer-related deaths worldwide (1). In 2017 alone there are predicted to be 222,500 newly diagnosed cases and 115,870 estimated deaths in the United States (1). This high incidence of death is largely due to the high prevalence of metastatic disease upon diagnosis, with lung cancer patients most frequently diagnosed at metastatic stage IV (2). Globally, lung cancer patients with aggressive metastatic disease have a 5-year survival rate of 18% (1). Metastasis is an important prognostic factor not just for lung cancer patients, but also across solid tumor types since 90% of cancer-related deaths are due to metastatic disease (3). Therefore, elucidating mechanisms of metastasis is a vital area of research not only in the context of lung cancer, but all cancers.

The most common cause of lung cancer is tobacco use, exposure to which accounts for 80% of lung cancer cases in the United States (American Cancer Society). However, epidemiologic studies show that there is a link between lung cancer susceptibility and family history (4). Specifically, SNP variations have been identified within two genes encoding subunits of nicotinic acetylcholine receptor alpha, which is regulated by nicotine exposure (4).

Lung cancer risk is also impacted by DNA repair capacity. Individuals with impaired DNA repair pathways are more susceptible to develop lung cancer, especially when accompanied with exposure to tobacco smoke or other carcinogens (4).

### **1.1.1 Histology**

Lung cancer is a broad term that describes a heterogeneous class of diseases. Broadly, lung cancer is divided into two main histological groups: small cell lung cancer

and non-small cell lung cancer (NSCLC). Non-small cell lung cancer accounts for 85% of lung cancer cases (5). Non-small cell lung cancer can be further divided into three histological subtypes: squamous cell lung cancer, adenocarcinoma, and large cell lung cancer.

Squamous cell lung cancer makes up 20-30% of NSCLC cases (6) and has the strongest historical association with cigarette smoking (4). Squamous cell carcinoma (SCC) is typically found in the proximal bronchi and is characterized by extensive areas of keratinization associated with an inflammatory component; however, less differentiated cases lose keratinization (7). The immunoprofile of SCC tends to be TTF-1 negative, but positive for CK 5/6, CK7 and P63 (6). As smoking has decreased and cigarettes have been modified, incidence of SCC has decreased in recent years (8).

The majority of NSCLC cases (50-70%) (6) are lung adenocarcinoma. Adenocarcinoma is a heterogeneous subtype consisting of bronchioloalveolar carcinoma, acinar, papillary, solid type, and mixed subtypes (9). They are marked immunohistochemically by positive markers Pro-SPC (10) and TTF-1 (11). While adenocarcinoma, like squamous cell carcinoma, is associated with cigarette smoking, the majority of never smokers (especially young women) who are diagnosed with lung cancer present with lung adenocarcinoma (7). Most adenocarcinomas are peripheral, presenting at surface alveolar epithelium or bronchial mucosal glands (7). Adenocarcinoma can be especially difficult to diagnose in early stages since most patients present as asymptomatic with metastatic disease (7) making overall prognoses worse.



Large cell lung cancer is typically defined as any NSCLC lacking the histological features found in squamous cell carcinoma or adenocarcinoma. It is the least common of the three main subtypes and as such does not have a defined treatment regimen (7).

Each histology has its own characteristic prognosis and metastatic phenotype. For example, small cell lung cancer and adenocarcinomas both preferentially metastasize to the brain whereas squamous cell carcinoma typically invades through the thoracic wall (2).

### **1.1.2 Genetic drivers**

Histological characterization has been instrumental in cancer diagnosis and treatment for decades. However, in recent years oncogenic mutations that drive lung cancer progression, specifically adenocarcinoma, have been uncovered. These ‘driver’ mutations are defined as those oncogenic mutations that initiate and maintain tumorigenesis (12). The most prevalent oncogenic drivers of lung adenocarcinoma include *EGFR*, *HER2*, *KRAS*, *ALK*, *BRAF*, *PIK3CA*, *AKT1*, *ROS1*, *NRAS* and *MAP2K1* (5). The majority of these driver mutations are mutually exclusive of each other with the exception of *PIK3CA*, which may co-occur with *EGFR* mutations (12).

Despite this oncogenic exclusivity, lung adenocarcinomas are not confined to single mutations. Many oncogenes are often co-mutated with tumor suppressors that exhibit loss of heterozygosity. These co-mutations add another level of complexity to lung cancer biology and treatment options. The most common tumor suppressors lost in adenocarcinomas include *TP53*, *LKB1* (*STK11*), *CDKN2A8*, *KEAP1*, and *SMARCA4* (13).

*KRAS* is the most common oncogenic mutation in NSCLC lung cancer (13). A member of the Ras family of proteins, *KRAS* is most often mutated at G12 in lung adenocarcinoma cases with 40% mutated as G12C and 22% as G12V (14, 15). Constitutive activation of *KRAS* results in sustained proliferative growth signaling, a hallmark of cancer (16).

While *KRAS* activation is sufficient to drive tumor growth (17), it is frequently co-mutated with key tumor suppressors. Common concomitant mutations include loss of heterozygosity in *LKB1* (18) and *TP53* (19). Mutation of *LKB1* occurs in approximately one-third of *KRAS* mutated patients and generates particularly aggressive and metastatic tumors that have been under extensive study in recent years (20-24).

Increased understanding of the genetic landscape of lung adenocarcinoma has been instrumental in developing and informing treatment options for patients. However, the vast majority of NSCLC patient tumors do not contain mutations in known drivers, making lung cancer an especially challenging diagnosis.

### **1.1.3 Current treatments**

While NSCLC is a heterogeneous class of diseases, the different subtypes often cluster into similar protocols for diagnosis, staging, and treatment. Over the last several decades, the prognosis of advanced NSCLC cases has improved by the development of tolerable platinum doublet based chemotherapies (25). However, patient survival in these advanced cases has not drastically increased beyond the 12-month mark (25).

Staging is the main determinant for prognosis and treatment regimens. A number of factors are incorporated into tumor staging and treatment, including tumor size and location, histologic type, tumor grade, surgical margins, lymph node involvement, and

distant metastasis (8). These factors are combined to group tumors into three main staging groups: surgically resectable disease, locally or regionally advanced disease, and distant metastatic disease. Staging groups are further subdivided using TNM staging, which takes into account tumor size (T0-T4), lymph node involvement (N0-N3), and distant metastasis (M0-M1) (26).

NSCLC patients have relatively few treatment options. The majority of these patients undergo surgical resection to remove the primary lung tumors as well as any other accessible metastases. Depending on extent of disease, neoadjuvant or adjuvant chemotherapy and/or radiation therapy may be recommended. Neoadjuvant chemotherapy in combination with radiation therapy is typically used to shrink tumors prior to surgery. Adjuvant chemotherapy (sometimes with radiation) is prescribed to reduce recurrence and treat metastatic disease after surgical resection (8). Platinum-based chemotherapies such as cisplatin are typically used in combination with other chemotherapies such as gemcitabine or pemetrexed since these therapies have been shown to improve overall survival (25, 27).

While treatment regimens are typically determined by tumor stage and histology, the genetic background of a tumor can determine whether a patient will respond to therapeutics. For example, *KRAS/LKBI* and *KRAS/TP53* co-mutations significantly reduce sensitivity to docetaxal as compared to “*KRAS* only” mutated tumors (28).

This information sheds light on the need for precision therapeutics that target the specific mutations of each tumor. Currently, targeted immunotherapy approaches are only standard of care for *recurrent* NSCLC cases (8). These immunotherapies include Nivolumab, Pembrolizumab, Erlotinib, Gefitinib, and Crizotinib (8). Nivolumab and

Pembrolizumab target the programmed death-1 (PD-1) co-inhibitory immune checkpoint. Nivolumab has improved overall survival in patients with metastatic disease as compared to previously standard docetaxel treatment (29, 30) while Pembrolizumab significantly improves progression free survival (PFS) in patients expressing PDL-1 (PD-1 ligand) in over 50% of their cells (31).

While many patients benefit from targeted immunotherapies, over time tumors often develop resistance mechanisms and the response to therapy diminishes. Further, there has yet to be any success in developing therapeutics beneficial to patients outside of those exhibiting *EGFR* or *ALK* mutations. The majority of NSCLC cases are either *KRAS* mutated or have unknown molecular drivers and do not have many treatment options beyond standard of care (5).

Overall, lung cancer patients have limited treatment options regardless of whether targeted therapies are available to them. Therefore, in order to better treat all lung cancer patients, research needs to focus on what is common to all cases. High incidence of metastatic disease is the leading cause of cancer-related deaths across cancer types (3) and is highly prevalent at lung cancer diagnosis (2). If metastasis could be targeted, prevented, and reduced, then patient outcomes would improve across the board. To target metastatic disease, its central players and mechanisms need to be better elucidated.

## **1.2 Metastasis**

The vast majority of cancer-related deaths (90%) are due to metastatic spread to vital organs such as the brain, liver, and kidney (3). The key steps to metastasis that allow cancer cells to migrate to a secondary site are invasion, intravasation, circulation, extravasation, and metastatic colonization and growth. Each of these steps is energy

intensive (32), resulting in cancers evolving different mechanisms by which they achieve the ultimate goal of metastatic spread.

### **1.2.1 Migration Strategies**

Cancer cells may escape the primary tumor through either individual or collective migration strategies. During individual cell invasion, single cancer cells may utilize an amoeboid or mesenchymal migration pattern (33). Amoeboid migrating cells squeeze through extracellular matrix (ECM) fibers by rapidly cycling through morphological expansion and contraction. This mode of migration utilizes a ‘gliding’ motion in which the cells have light transient interactions with the surrounding ECM (33).

Mesenchymal cancer cells have undergone an epithelial-to-mesenchymal transition (EMT) in which they undergo genetic (34) and epigenetic (35) alterations resulting in the loss of epithelial markers and morphology and the gain of mesenchymal morphology and markers (36). EMT is a transient and reversible program (37-39) that is regulated by transcription factors Snail and Twist (40). The migration pattern of mesenchymal cells is highly dependent on focal adhesion signaling (41) and strong interactions with the ECM (42). As mesenchymal cells migrate, they secrete matrix metalloproteases (MMPs), which degrade the ECM and facilitate migration (43).

Through collective migration, cancer cells maintain cell-cell contacts through adhesion molecules and other communication junctions (44) and typically retain their epithelial morphology (45). Collectively invading cells may form a chain or pack of cells as they work as a cohesive unit to invade out from the primary tumor (33). Chains of streaming cancer cells maintain contact with the primary tumor as they reach out toward the blood vessels, whereas packs of cells bud off and migrate on their own, finding the

path of least resistance (33). Whether in streams or packs a collectively invading group has a “leading edge” that uses integrins and proteases to move through the extracellular matrix of the tumor microenvironment (46). Studies in breast and lung cancer models demonstrate that cells leading collective invasion are genetically and morphologically distinct from “followers” (46, 47).

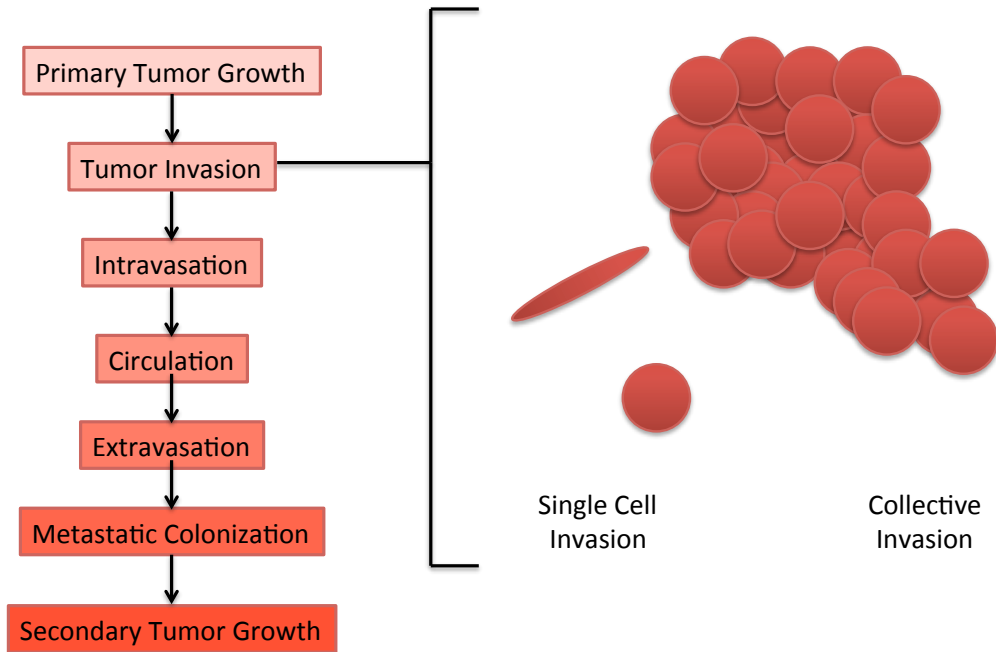


**Figure 1-1. Metastasis and Migration Strategies.**

One of the first steps of metastasis is tumor invasion. Cancer cells employ different invasion strategies based upon intrinsic mutations and the tumor microenvironment

### **1.2.1.1 Focal Adhesion Signaling**

As previously mentioned, focal adhesion signaling is integral to cell migration, particularly in the case of mesenchymal cells (41). Focal adhesions (FAs) are signaling complexes found at the cell-matrix interface of motile cells (48). The key players at these hubs include focal adhesion kinase (FAK), Src, integrins, Rho GTPases, and the cytoskeleton (48).

At sites of focal contact with the ECM transmembrane integrin heterodimers bind to ECM fibers such as fibronectin to activate an intracellular signaling cascade (49). This outside-in signaling induces autophosphorylation of the non-receptor tyrosine kinase, FAK, and its downstream effectors (50). Autophosphorylation of FAK in turn promotes inside-out signaling as it further activates integrins and strengthens adhesion to the ECM (51).

Cytoskeletal proteins such as actin and vimentin directly enter focal adhesion sites where they promote FA maturation and stability (52, 53). As a result, FA signaling has been extensively studied in the context of cancer cell motility, and FAK expression and activity have been shown to correlate with poor patient prognosis and malignant, metastatic disease (54, 55).

### **1.2.2 Intravasation, circulation, and extravasation**

Cancer cells invade through the tumor microenvironment to reach blood vessels where they undergo intravasation to enter the bloodstream. Secreted factors such as epidermal growth factor (EGF) and tumor necrosis factor 1 $\alpha$  (TNF1 $\alpha$ ) help recruit invading cancer cells to blood vessels. Upon arrival at the blood vessels, cancer cells



undergo transendothelial migration via paracellular and transcellular mechanisms (56). Transforming growth factor  $\beta$  (TGF $\beta$ ) and vascular endothelial growth factor (VEGF) weaken the endothelial barrier and allow more cancer cells to intravasate into the bloodstream (57).

Upon entering the bloodstream, cancer cells are under extreme stress, as they must combat anoikis, shear stress, and immunological assaults prior to reaching their secondary site (56, 58). In order to survive, circulating tumor cells (CTCs) may cluster together (59). It has been well documented that CTCs traveling in homotypic clusters have an over 50 times greater chance of survival than individual CTCs (60-62).

Heterotypic clusters have also been shown to form between CTCs and different stromal partners including platelets (63) and fibroblasts (64). CTCs may adhere to activated platelets via integrins, using them as a shield as they flow through the bloodstream as well as using them to facilitate extravasation via cell arrest and adhesion to the endothelium (63). In a similar way, fibroblasts carried over from the primary site improve the efficiency of metastatic colonization by providing a “native soil” for the metastatic seeds to grow (64).

As mentioned previously, a cancer preferentially metastasizes to certain organs based on its organ of origin and histological subtype. CTCs of over 23 different cancers are “homed” to preferential sites of metastasis via CXCR4/CXCL12 signaling (65). CXCL12 binds to the CXCR4 receptor to activate many cell responses that contribute to metastatic spread, including proliferation, chemotaxis, and survival (66).

As CTCs approach the site of homing, they are often mechanically trapped in the microcapillaries to prevent further circulation (67). Once lodged in place, CTCs may

extravasate by breaching vascular walls (68). Depending on the organ site of metastasis, CTCs may activate expression of certain genes to facilitate extravasation into a particular site (69). These intrinsic genetic programs, in addition to extrinsic stromal factors (70, 71), facilitate successful extravasation and metastatic colonization (67, 70).

The final steps of metastasis are colonization and expansion. Colonization is a huge hurdle as the CTCs, which developed at the primary tumor in co-evolution with tumor-associated stroma, now must adapt and survive in a new environment. These final steps are predominantly dependent on pro-tumorigenic signaling within the metastatic organ microenvironment (72). Since stromal components are more favorable for colonization in certain organs and CTCs preferentially settle in these same organs, the “seed and soil” hypothesis was formed and validated over decades of research (73). The “seed and soil” hypothesis, established by Stephen Paget in 1889, proposed that metastatic colonization depends on crosstalk between selected cancer cells (the 'seeds') and specific organ microenvironments (the 'soil') (73). Therefore, without strong ‘seeds’ and good ‘soil’ metastatic spread is impossible.

Despite these advances in understanding, cancer metastasis remains a complex multi-step process that is difficult to predict in patients and impossible to investigate *in vitro*. As a result, many animal models have been developed to determine key factors that contribute to metastasis and ultimately identify actionable therapeutic targets.

### **1.3 Tumor Microenvironment**

As noted in the review of current research models, a key factor in determining the translational efficacy of a tumor mouse model is the presence of an active and communicative tumor microenvironment. As Hanahan and Weinberg postulated in their

seminal review, cancer research has moved away from a reductionist view to a perspective that includes heterotypic cell biology by integrating microenvironmental factors into research models (74). Understanding the role of the microenvironment within tumor progression is an area of active research (75) as the membership and complexity of the tumor microenvironment have been shown to impact patient prognosis and therapeutic response (76, 77).

### **1.3.1 Microenvironmental Factors**

The tumor microenvironment co-evolves with the cancer and includes various stromal cells that, depending on the context, may facilitate or inhibit tumor growth and progression (78, 79). The central players of the tumor microenvironment across solid tumor types, including lung cancer, are fibroblasts, immune cells, and vasculature (80).

#### **1.3.1.1 Fibroblasts**

Cancer-associated fibroblasts (CAFs) are among the most prevalent stromal cells within the tumor microenvironment of most solid tumors. CAFs may be derived from local fibroblasts or converted from other cell types including endothelial cells and adipose tissue, forming a heterogeneous population (79, 81). Activated CAFs typically express markers such as fibroblast-specific protein 1 (FSP1, also known as S100A4), fibroblast-activating protein (FAP), and alpha-smooth muscle actin ( $\alpha$ -SMA) (79).

CAFs are best defined by whether they promote or inhibit tumor growth and progression (79). CAFs have been shown to augment carcinogenesis by promoting cancer cell proliferation (82, 83), stemness (84) and migration (85) via paracrine signaling (86). Many of these tumor-promoting pathways are stimulated by a wound-healing response activated in tumor adjacent CAFs (87). Another key function of CAFs is their ability to

modulate tumor architecture and rigidity via secretion of extracellular matrix (ECM) proteins (including fibronectin and type I collagen) and matrix metalloproteases (MMPs) (79). Specifically within lung cancer CAFs have been shown to regulate lung cancer stem cell plasticity via paracrine signaling through the IGFII/IGF1R pathway (88).

The tumor inhibitory effects of CAFs have not been as extensively investigated. However, some studies demonstrate CAFs inhibiting cancer cell proliferation and early tumor progression (89, 90).

Aside from direct interactions with cancer cells, CAFs can further impact the tumor microenvironment via secretion of pro-inflammatory factors that recruit either tumor-promoting or –inhibiting immune responses (91, 92).

#### **1.3.1.2 Immune Cells**

Tumor-promoting inflammation is an enabling characteristic of cancer (16). Across solid tumors, immune cell infiltration is prevalent with tumor-associated macrophages (TAMs), cytotoxic T cells, myeloid derived stem cells (MDSCs), and neutrophils all present and active within the tumor microenvironment (93, 94). These infiltrating immune cells not only modulate inflammation and immune system response to the tumor's presence but also secrete growth factors that stimulate cancer cell proliferation and stromal recruitment, including epidermal growth factor (EGF), transforming growth factor  $\beta$  (TGF-  $\beta$ ), fibroblast growth factors (FGFs) and interleukins (ILs) (95).

#### **1.3.1.3 Vasculature**

As tumors grow, resources become depleted; therefore, cancer cells rely on complex vascular networks to maintain access to oxygen and other nutrients. These

networks include existing neighboring vessels, angiogenic or vasculogenic vessels, and vasculogenic networks formed by the cancer cells (96-98). To recruit, form, and maintain tumor vasculature, cancer cells and other stromal cells secrete growth factors such as vascular endothelial growth factors (VEGFs), transforming growth factor betas (TGF- $\beta$ s), fibroblast growth factors (FGFs), and epidermal growth factor (EGF) (96).

Once tumors activate the “angiogenic switch” and recruit their own vasculature, they gain access not only to oxygen and nutrients for further proliferation but also a route for tumor cell dissemination and metastasis via the blood stream (99, 100).

#### **1.3.1.4 The role of the microenvironment in metastasis**

All three of the main components of the tumor microenvironment contribute to the metastatic cascade through different pathways. Infiltrating immune cells and CAFs secrete not only growth factors, but also matrix metalloproteases, which facilitate cancer cell escape and invasion by breaking down the tumor ECM and promoting cell motility (93, 101, 102). Tumor vasculature is typically quite leaky as it loosely associates with pericytes (103). This results in increased cell traffic in and out of the blood vessels. Through these weak structures, immune cells can further infiltrate the tumor microenvironment and cancer cells can escape into the circulatory system (93).

### **1.4 Metastatic Biomarkers**

#### **1.4.1 History and Prognostic Applications**

One canonical mechanism of cancer cell metastasis is the epithelial-to-mesenchymal transition (EMT) (104). EMT is a developmental program involving changes in genetic and epigenetic expression to convert immotile, polarized, epithelial cells to motile, invasive, mesenchymal cells (104). EMT in cancer invasion and

metastasis has been extensively studied (105, 106). As a result, the majority of metastatic biomarkers for solid tumors, including lung cancer, are mesenchymal cell markers including fibronectin, N-cadherin, and vimentin (107-109). These mesenchymal markers have been shown to correlate with increased invasiveness and metastatic potential in clinical samples (110-112) and, as such, are used as prognostic markers to help determine the likelihood of cancer progression and metastasis in patients.

Vimentin expression specifically has been shown to correlate with high nuclear grade (113), increased metastatic potential (114, 115), and poor overall survival (116, 117) across solid tumor types.

### **1.5 Vimentin structure and function**

Vimentin is a type III intermediate filament that is highly dynamic as it interconverts between three assembly states: particles, “squiggles”, and elongated filaments (118-120). Historically, intermediate filaments have been viewed purely as structural components of the cytoskeleton whose only function is to maintain cell integrity. However, recent studies have shown that intermediate filaments are integral cellular components, the disruption of which, can lead to many different diseases (121).

#### **1.5.1 Intermediate filament structure**

All intermediate filament monomers, including vimentin, have a tripartite structure with a highly conserved alpha-helical central “rod” capped by variable “head” and “tail” domains (122). The smallest functional unit of vimentin within cells is the tetramer. Vimentin tetramers further assemble into protofilaments, which require the head domains for successful assembly (123). Vimentin assembly is regulated by phosphorylation of serine sites by a few key kinases, namely PKA, PAK1, and PKC (124,

125). Phosphorylation sites have been identified at both ends of the vimentin monomer, with the majority located in the critical head domain (124).

### **1.5.2 Vimentin in signal transduction**


In mesenchymal cells, vimentin filaments extend throughout the cell to control cell morphology (126), lamellipodia formation (127), cell integrity under stress (128), and signaling (129, 130).

As mentioned previously, vimentin dynamics are regulated by phosphorylation at serine sites. Phosphorylation at certain sites not only regulates vimentin assembly but also influences binding partners and downstream signaling. For example, it has been shown that phosphorylated vimentin regulates cell cycle pathways via 14-3-3 (131) and can inhibit caspase-induced proteolysis, increasing cell survival and motility (132). As these studies demonstrate, vimentin has emerged as an important component of cell signaling and motility in recent years.

### **1.6 Current research models**

*In vivo* models are integral tools for investigating not only carcinogenesis and drug treatments but also modeling the metastatic cascade. Cancer metastasis models, specifically, have been developed in many different animal models including drosophila, mice, zebrafish, and rats (133-135). The most versatile and informative models of metastasis are murine models, which provide opportunities to ask different experimental questions via transplantation models and genetically engineered mouse models (GEMMs).

Figure 2. Mouse Models



Features	Xenograft Transplant		Syngeneic Transplant		GEMM
	Subcutaneous/ Tail Vein	Orthotopic Injection	Subcutaneous/ Tail Vein	Orthotopic Injection	
Active Immune System	✗	✗	✓	✓	✓
Tumor Host Organ	✗	✓	✗	✓	✓
Primary Tumor Formation	✗	✓	✗	✓	✓
Secondary Tumor Formation	✓	✓	✓	✓	✓
Spontaneous Metastasis	✗	✓	✗	✓	✓
Mimics Early Tumor Initiation	✗	✗	✗	✗	✓

**Figure 1-2. Summary of commonly used mouse models.**



### **1.6.1 Transplantation models**

Transplantation models involve the injection of human or murine cell lines or tumor fragments into one of three main locations: the tail vein, under the skin (subcutaneous), or at the orthotopic site of the tumor's origin (i.e. breast cancer injected into a mammary fat pad). Each of these transplantation models has different advantages and disadvantages and probes distinct experimental questions.

Tail vein injection is the most commonly used experimental metastasis model (135). In this model, as with all experimental metastasis models, cancer cells are injected directly into circulation without the formation of a primary tumor. These experimental models skip the early steps of metastasis and instead probe a cell line's capacity for surviving circulation, extravasating, and seeding the metastatic site (136, 137).

Spontaneous metastasis transplantation models were developed to better mimic the full cascade of metastasis. These models may involve ectopic or orthotopic injection of tumors into mice, resulting in drastically different phenotypes.

The most popular ectopic injection site is under the skin. Subcutaneous injection of cancer cell lines or tumor fragments, while sometimes useful, have generally proved to be an inadequate model for assessing tumor progression and metastasis. Because of the ectopic location of subcutaneous injections, the tumor microenvironment is often not suitable for the cancer cells, altering the doubling time and tumor progression (138). As a result, distant metastases do not often form, and testing therapeutics in these models may not accurately translate to the endogenous human setting (138, 139).

Orthotopic transplantation models most closely mimic human disease as evidenced by assessment of tumor histology, vascularity, tumor-stroma interactions, gene expression profiles, metastasis, and therapeutic response (140, 141). Direct transplantation into the orthotopic site may come from direct injection of cancer cells or surgical implantation of intact fragments of tumor (135). Surgical implantation has been shown to improve the reproducibility and metastatic outcomes within many orthotopic models (142).

As mentioned previously, transplantation models may inject either human (xenograft) or murine (syngeneic) samples into the mouse. Use of either a xenograft or of syngeneic transplantation has its advantages and disadvantages. Xenograft models, while more similar to human disease, require the use of immunodeficient mice so that the tumor grafts will survive and progress (135, 143). While immunodeficiency facilitates tumor seeding and metastasis, without a functioning immune system, the functional contribution of the immune system to tumor progression and metastasis cannot be assessed in this model (144). Xenografts may be further impaired by inhibited growth factor signaling between the tumor microenvironment and the cancer cells. Species specificity of cytokine/cytokine receptor systems can limit the effectiveness of murine stromal components on human cancers (144, 145).

Syngeneic transplantation models overcome the microenvironment issues presented in xenograft models. However, because murine cells injected into the tumor site are derived from inbred mouse strains, genetic heterogeneity is drastically reduced as compared to human patient samples (135, 143).

### 1.6.2 Genetically engineered mouse models (GEMMs)

Genetically engineered mouse models or GEMMs provide further insight into cancer progression, as they allow for the study of early neoplasms in addition to metastatic disease. GEMMs have major advantages over transplantation models (146) including an intact tumor microenvironment (147) and the ability to manipulate gene expression in time and space using viral systems (148, 149). This tight regulation of gene expression is especially useful in cases where systemic expression or disruption of a gene has debilitating impacts such as embryonic lethality and sterility (137).

Another key advantage of GEMMs over transplantation models is their translation to the clinic. Preclinical therapeutic investigations in GEMMs provide better insight into therapeutic success due to their more realistic timeline and orthotopic microenvironment (150). Because GEMMs display the full spectrum of tumor progression from tumor initiation to metastasis, they are ideal models for testing anti-metastatic therapies (137, 151).

GEMMs are particularly useful in lung cancer where orthotopic transplantation into the lungs, though possible (152), is technically difficult. The most frequently used lung cancer model is the Cre-inducible *LSL-Kras<sup>G12D</sup>* model (137). In this model a LoxP-Stop-LoxP transcriptional stop cassette is located upstream of the oncogenic *Kras<sup>G12D</sup>* mutation and is removed in a Cre-dependent manner (153). Cre administration via viral inhalation in the *LSL-Kras<sup>G12D</sup>* model produces lung adenocarcinomas (153, 154). Concomitant mutations of *Kras<sup>G12D</sup>* with loss of tumor suppressors *Trp53<sup>fl/fl</sup>*, *LKB1<sup>fl/fl</sup>*, or *INK4a<sup>fl/fl</sup>* via gene flanking LoxP sites result in aggressive metastatic lung adenocarcinoma (154).

Of the *Kras*<sup>G12D</sup> models, the *Kras*<sup>G12D</sup>, *LKB1*<sup>fl/fl</sup> model has been most extensively studied (20, 23, 24) as it combines two of the most common mutations found in lung adenocarcinoma patients (155, 156) and is a robust model of tumor initiation, growth, invasion and metastasis within a host murine microenvironment (21).

### **1.7 Scope of Dissertation**

Despite advances in vimentin cell biology research, little is known about the functional role of vimentin within the context of lung cancer. This dissertation seeks to bridge the gap between cell biology and clinical data by exploring the role of vimentin within lung cancer cell invasion and metastasis. First we identify a role for vimentin within focal adhesion signaling using *in vitro* lung cancer cell line models and xenograft studies. This work was published in *Oncogene* in 2014 and details a model in which vimentin is directly inserted in focal adhesion sites to promote EGFR-mediated phosphorylation of VAV2, which activates Rac1 to induce FAK activation.

This initial study inspired the main focus of my dissertation, which was characterization of lung cancer metastasis in a vimentin null mouse. For this study we developed a novel genetically engineered mouse model (GEMM) by crossing the Cre-dependent lung cancer metastasis model *LSL-Kras*<sup>G12D</sup>/*LKB1*<sup>fl/fl</sup> (*KLV*<sup>+/+</sup>) to a whole body vimentin knockout mouse to generate the *LSL-Kras*<sup>G12D</sup>/*LKB1*<sup>fl/fl</sup>/*Vim*<sup>-/-</sup> mouse (*KLV*<sup>-/-</sup>). Comparisons of these models show that loss of vimentin does result in a significant reduction in metastasis to the mediastinal lymph node. Further study identified that vimentin expression in cancer-associated fibroblasts (CAFs) supports collective invasion and metastasis via heterotypic CAF-cancer cell interactions in which CAFs physically

lead collective chains of cancer cells into the extracellular matrix (ECM) via cell-cell interactions.

Both studies further our understanding of vimentin within the context of lung cancer and provide a springboard for future studies on the role of vimentin within the tumor microenvironment.

**Chapter 2: Vimentin regulates lung cancer cell adhesion through a VAV2-**

**Rac1 pathway to control focal adhesion kinase activity**

Lauren S. Havel, Erik R. Kline, Alessandra M. Salgueiro, and Adam I. Marcus

This chapter is adapted from a manuscript published by L Havel, E Kline, A Salgueiro, and A Marcus. *Vimentin regulates lung cancer cell adhesion through a VAV2-Rac1 pathway to control focal adhesion kinase activity*. *Oncogene* 2014. doi:

0.1038/onc.2014.123

AMS contribution: manuscript review and experimental design and execution of HBEC experiments

## 2.1 Introduction

Lung cancer is the leading cause of cancer-related deaths in the United States (157). Non-small cell lung cancer (NSCLC), specifically, constitutes 80% of lung cancer deaths (158). The poor survival results from the aggressive nature of lung cancer. Most often, patients are diagnosed with advanced stage disease where metastasis of the primary tumor has already occurred (158).

Metastasis is a hallmark of cancer (74) that is initiated by genetic and epigenetic alterations that transform stationary epithelial cells into motile mesenchymal cells (159). This transition is referred to as the epithelial to mesenchymal transition or EMT (160). EMT is characterized by alterations in cell morphology, cell-matrix interactions, cytoskeletal rearrangements, and protein expressions (38). One canonical biomarker of EMT is the intermediate filament protein, vimentin. Vimentin has been shown to correlate with increased metastatic potential and poor patient prognosis in NSCLC patients (161). While the role of vimentin as a biomarker has been well characterized, the functional role of vimentin in cancer metastasis is undefined.

Increasing evidence indicates vimentin as a regulator of focal adhesions and cell motility. Vimentin has been shown to directly enter and strengthen focal adhesion sites (125) and vimentin expression increases focal adhesion (FA) turnover (130). However, the exact molecular mechanism connecting vimentin to focal adhesion signaling, specifically focal adhesion kinase (FAK) is yet to be elucidated.

In this manuscript we identify a novel vimentin-dependent mechanism for cell adhesion and motility. We identified that phosphorylation at Y142 on VAV2, a guanine nucleotide exchange factor (GEF) for Rac1, is dependent on vimentin expression. Having

identified this dependence, we tested a vimentin-based model of lung cancer cell motility and invasion. In this model we found that vimentin promotes phosphorylation of VAV2, which, in turn, activates Rac1 at focal adhesions, leading to stabilization of FAK. These data provide a novel mechanism for vimentin-mediated cell motility within a lung cancer model. Since alterations in motility are among the first steps of metastasis, this work may provide mechanistic insight into those factors driving lung cancer metastasis.

## **2.2 Experimental Procedures**

### **Cell Culture**

H1299, H460 and H1792 cell lines were grown in RPMI 1640 media supplemented with 10% FBS and 1% penicillin/streptomycin and maintained in a humidified chamber at 37 °C with 5% CO<sub>2</sub>. HEK 293 cells were grown in DMEM media supplemented with 10% FBS and 1% penicillin/streptomycin. All tissue culture plates and coverslips used for experiments were covered with 5 µg/cm<sup>2</sup> human plasma fibronectin (Millipore) diluted in PBS and incubated for 30 min at 37 °C prior to cell seeding.

### **Antibodies**

Antibodies against pY397-FAK (Invitrogen), FAK (BD Biosciences), GAPDH (Cell Signalling), vimentin (Sigma), pY142-VAV2 (Full Moon Biosystems), pY172-VAV2 (Abcam), VAV2 (Full Moon Biosystems), GFP (Covance, Princeton, NJ), pY418-Src (Invitrogen) and FLAG (Sigma) were used for Western blotting, immunofluorescence and immunoprecipitation. HRP-conjugated secondary antibodies (Jackson ImmunoResearch) were used for Western blotting.



## Transfections and Drug Treatments

Lipofectamine 2000 and Plus reagents (Invitrogen) were used to transfect the FLAG, WT FAK-FLAG, Y397E FAK-FLAG, Y397F FAK-FLAG, GFP, WT FAK-GFP, Y397E FAK-GFP, WT VAV2-GFP, CA VAV2-GFP, inactive VAV2-GFP, WT Rac1-GFP, Q61L Rac1-GFP, T17N Rac1-GFP, WT cdc42-GFP, Q61L cdc42-GFP and T17N cdc42-GFP constructs according to the Invitrogen supplied protocol. The RevTet-On system (Clontech), which includes pRevTRE carrying the human vimentin gene and pRevTet-On, was used. Oligofectamine (Invitrogen) was used to transiently transfect cells with VAV2 small interfering RNA (siRNA) (Qiagen FlexiTube VAV2 6. Cat. No. SI02662947), vimentin siRNA (Qiagen FlexiTube Hs\_VIM\_13. Cat. No. SI04201890) or FAK siRNA (ThermoScientific ON-TARGET plus PTK2 Cat. No. L-003164-00-0005) according to the manufacturer's protocol. Two successive 24-hour transfections were performed before cell harvesting. For the production of stable vimentin knock-down H1299, H460 and H1792 lung cancer cells, vimentin shRNA (ThermoScientific, Catalog No. RHS3979-201759429, clone ID TRCN0000029122) and shVIM clone 2 were (ThermoScientific, Catalog No. RHS3979-201759427, clone ID TRCN0000029119) delivered in pLKO.1 lentiviral vectors (ThermoScientific). The shVIM sequence is 5' - TTGAACTCGGTGTTGATGGCG-3' and the shVIM clone 2 sequence is 5' - AATAGTGTCTTGGTAGTTAGC-3' . To produce the virus, HEK 293T cells were transfected with the shRNA and helper plasmids (pHRCMV8.2 $\Delta$ R and CMV-VSVG) using LT1 transfection reagent (Myrius). To harvest the lentiviral stock, the media was centrifuged at 250g for 5 min then filtered through a syringe. Cells were infected with a 1:4 dilution of lentivirus in complete media containing 8  $\mu$ g/mL polybrene. The next day,

the media was changed to complete media containing 2  $\mu\text{g}/\text{mL}$  puromycin. For the cyclohexamide (CHX) experiment, H1299 cells were treated with 20  $\mu\text{g}/\text{mL}$  cyclohexamide (Sigma) in complete RPMI media.

### Adhesion Assays

For the detachment assays, cells were plated at  $1 \times 10^5$  or  $1.5 \times 10^5$  cells/well of a 12-well plate, respectively. After 24 hours, each well was trypsinized for lengths of time ranging from 0 to 5 min. At each time point, 2 times the trypsin volume of complete RPMI media was added to the well. The non-adherent cell containing media was aspirated off and each well was washed with 1X PBS. The remaining adherent cells were trypsinized and counted. The number of adherent cells in each well was normalized to the total number of cells (0 time point). For the attachment assays, the concentration of each cell line after collection by trypsinization was equalized to  $5 \times 10^5$  cells/mL. 1 mL of cells was added to each well of a 12-well plate and incubated for varying lengths of time ranging from 10 to 90 min. At each time point, the non-adherent cells were aspirated off. The adherent cells were washed gently with PBS, trypsinized then counted.

### Western Blotting

Cells were harvested and lysed in cold TNES buffer (50 mM Tris pH 7.5, 100 mM NaCl, 2 mM EDTA, 1% Nonidet P-40, 1X Roche Complete Protease Inhibitors, 10 mM NaF, 1 mM  $\text{NaVO}_4$ , 2 mM sodium pyrophosphate, and 2 mM  $\beta$ -glycerophosphate). Protein concentrations were determined using a protein assay kit (Pierce). Equal protein concentrations of whole cell lysate were solubilized in SDS sample buffer, separated on a 10% SDS-polyacrylamide gel, and transferred to a methanol soaked polyvinylalide

difluoride (PVDF) membrane, which was then blocked with 10% milk in 1X TBST. Primary antibody, diluted in 5% milk in TBST, was added to the membrane while rocking overnight at 4°C. After 3 TBST washes, the appropriate HRP conjugated secondary antibody diluted in 5% milk in TBST was added to the blot for 1 h at room temperature. After 3 more TBST washes, proteins were visualized using a chemiluminescent substrate (Denville).

#### Wound-healing assay

Cells were cultured to 100% confluence on glass coverslips. An X shaped wound was made using a small pipette tip followed by a brief 1X PBS wash. Cells were incubated for 16-24 hours at 37 °C then fixed and mounted onto slides. Coverslips were imaged using a 10X objective on a Zeiss Axioplan 2 microscope with a Zeiss Axiocam II camera. Identical imaging parameters were used for all images.

#### Matrigel Invasion assay

5 x 10<sup>4</sup> cells in serum free media were plated in BD Biocoat Matrigel invasion chambers (BD Biosystems). The well containing the insert was partially filled with complete RPMI media also containing fibronectin at 5 µg/cm<sup>2</sup>. The cells were incubated at 37 °C for 18-24 h. The membrane from the insert was removed, fixed and stained according to the manufacturer's protocol then mounted on slides for imaging with a Zeiss Axioplan upright microscope using the 10X objective.

## Xenotransplantation and tumor analysis

All animal experiments were performed within institutional guidelines. Female HSD Balb/c Jhan Hsd-Prkdc SCID mice (7-8 weeks old) were subcutaneously injected with  $1.5 \times 10^6$  cells/mL (in 200  $\mu$ L PBS) of the H460 human large-cell lung cancer cell line into the left abdominal wall. For each cell line, 6 mice were injected. Primary tumors at the injection site were measured using digital calipers. Tumor volumes (in mm<sup>3</sup>) were calculated as follows:  $\text{volume} = (\text{length} \times \text{width}^2)/2$ . Mice were sacrificed after 4-6 weeks. Using a dissecting microscope, the number of metastatic lung nodules was counted prior to fixation of the lung with 10% buffered formalin overnight at room temperature. The tissues were then processed by the Pathology Core at Emory University for hematoxylin and eosin (H&E) staining. The number of micrometastases on the stained slides was counted. Images of the lungs were taken with a Sony camera using an automatic exposure time.

## Drug Treatments

Epidermal Growth Factor (EGF) was used at a concentration of 100 ng/mL in ddH<sub>2</sub>O. The calpain inhibitors, calpeptin (Calbiochem) and PD150606 (Calbiochem), were both used at a concentration of 200  $\mu$ M in DMSO.

## Cdc42 activation assays

The G-LISA cdc42 colorimetric activation assay kit (Cytoskeleton, Denver, CO) was used to measure cdc42 activity in H1299 shVIM and pLKO.1 cells transfected with GFP, CA VAV2-GFP, WT VAV2-GFP or inactive VAV2-GFP. Cells were lysed in the

supplied lysis buffer. Lysates were diluted to 0.3 ug/uL then processed according to the supplied protocol. Readings were obtained using a BioTek spectrophotometer.

### Quantitative Real-Time PCR

Total RNA was isolated using an RNeasy Mini Kit (Qiagen) then reverse transcribed with M-MLV Reverse Transcriptase (Invitrogen). The cDNA product was amplified using sequence specific primers to FAK (forward- TGGTGAAAGCTGTCATCGAG, reverse- TCATCCACAGTGGCCAATAA) and analyzed by real-time PCR using SYBR green detection. 25µL reactions contained 1 µL DNA, 0.2 µM of each primer, and 12.5 µL IQ SYBR Green Supermix (Bio-Rad). The following PCR protocol was used: 3 min hot start at 95 °C followed by cycles of 95 °C, 10 s; 55 °C 60 s. Melt curve analysis verified a single product. Relative RNA quantities were calculated then standardized to levels of 18S rRNA.

### Immunofluorescence

Cells were fixed on 1.5mm glass coverslips with PHEMO buffer (68 mM, PIPES, 25 mM HEPES, 15 mM EGTA, 3 mM MgCl<sub>2</sub>, 10% DMSO) plus 3.7% formaldehyde, 0.05% glutaraldehyde and 0.5% Triton X-100 for 10 min at room temperature. After three 5 min washes with PBS, the coverslips were blocked with 10% normal goat serum for 1 h at room temperature. Primary antibodies were diluted in 5% normal goat serum and added to the coverslips overnight at 4 °C. After 3 PBS washes, the coverslips were incubated for 1 h at room temperature with a fluorophore conjugated secondary antibody diluted in 5% normal goat serum. After 3 PBS washes, the coverslips were incubated

with 350 nM DAPI stain diluted in 1X PBS for 10 min at room temperature. The coverslips were mounted on glass slides using Prolong gold mounting medium (Invitrogen). The slides were imaged using Zeiss LSM 510 META confocal microscope using a 100X oil Plan-Apo objective (NA = 1.46). The images were processed using ZEN 2009 software. A Nikon N-SIM microscope housed within the Emory Integrated Cellular Imaging Core was utilized to acquire super-resolution images of vimentin directly entering FAs. Images were acquired using a 100× 1.49 NA oil objective. All images within an experiment were taken under identical settings. Intensity levels were adjusted equally on all samples within an experiment.

#### Immunofluorescence Image Quantification

To assess focal adhesion site size and intensity, images were analyzed in ImageJ/Fiji. A 100  $\mu\text{m}^2$  rectangle was used as a region of interest (ROI) at the leading edge of cells. Pixels within this ROI were then thresholded to remove background and the same threshold was used for all samples stained with the same antibody. The “Analyze Particle” function was then implemented to detect objects. All objects less than 0.5micrometers were then removed using a size filter. The intensities and size of the remaining objects were then quantified and imported into Excel.

#### Co-Immunoprecipitation

Cells were harvested and lysed in NP-40 lysis buffer (50 mM Tris pH 7.4, 50 mM NaCl, 0.1% Triton X-100, 1% NP-40) plus 1X Roche Complete Protease Inhibitors, 10 mM NaF, 1 mM NaVO<sub>4</sub>, 2 mM sodium pyrophosphate and 2 mM  $\beta$ -glycerophosphate.

For co-immunoprecipitations involving vimentin, total lysate was used. For all other co-immunoprecipitations, lysate was centrifuged at  $14,000 \times g$  at  $4^{\circ}C$  for 10 min. 10  $\mu g$  of primary antibody was incubated with 500  $\mu g$  of protein at  $4^{\circ}C$  overnight while rotating. Each sample was incubated with 50  $\mu L$  of Dynabeads (Invitrogen) for 1 hour at  $4^{\circ}C$  while rotating. After three 20 min washes with NP-40 lysis buffer, the protein-antibody complex was eluted from the beads in 2X Laemmli buffer at  $100^{\circ}C$  for 10 min.

### Phosphorylation Screen

H460 pLKO.1 and shVIM cell lysates were analyzed using the Phospho Explorer Antibody Array (Full Moon Biosystems), which is a microarray containing 1,318 phospho-specific antibodies spotted on a coated glass slide in duplicate. Cell lysates were given to Full Moon Biosystems for processing and analysis. Lysates were labeled with biotin then bound to the array's antibodies. The phosphorylated protein in each sample was detected using Cy3-streptavidin. The array was scanned with an Axon GenePix scanner to measure phosphorylation levels of individual proteins in each sample. The ratio of phosphorylated to total protein was calculated for both pLKO.1 and shVIM cells and reported as a fold change upon vimentin loss. The percent change in phosphorylation upon vimentin depletion was calculated as a ratio of phosphorylated:total protein in shVIM cells to phosphorylated:total protein in pLKO.1 cells.

### Rac1 Activation Assays

The G-LISA rac1 luminescence-based activation assay kit (Cytoskeleton, Denver, CO) was used to measure rac1 activity in stably adherent cells. The cells were lysed in

the supplied lysis buffer. Lysates were diluted to 1 ug/uL then processed according the supplied protocol. Readings were obtained using spectraMax luminometer. For the timecourse experiment on trypsinized cells that were re-plated, we used a Rac1 activation pull-down kit (Cytoskeleton, Denver, CO). Cells were lysed in the supplied lysis buffer then diluted to 1.5  $\mu\text{g}/\mu\text{L}$  and processed according to the supplied protocol. The pull-down products were analyzed by western blotting using a Rac1 antibody from BD Biosciences.

### Statistical Analysis

P-values of significance were obtained using one- or two-way ANOVA analysis followed by a multiple comparison test. In the case of the xenograft and qRT-PCR studies, a Student's t-test was employed.

## 2.3 Results

### **Vimentin regulates lung cancer cell migration, invasion, and metastasis**

The role of vimentin in cell motility has been extensively studied by other groups (130); however, to verify this correlation in lung cancer cells, we depleted vimentin expression in H1299 lung cancer cells by siRNA (Supplemental Figure 2-1A). Knockdown of vimentin within lung cancer cells decreased their motility and invasive phenotypes as assessed by wound healing and Matrigel Boyden chamber assays (Supplemental Figure 2-1B and 2-1C).

These studies were further validated by an *in vivo* xenograft model with H460 lung cancer cells. H460 cells stably expressing vimentin shRNA (shVIM) or vector



control shRNA (pLKO.1) were generated for these studies (Supplemental Figure 2-2A). H460 shVIM cells were significantly less invasive *in vitro* as compared to pLKO.1 cells (Supplemental Figure 2B). The pLKO.1 and shVIM H460 cells were injected subcutaneously into the flanks of nude mice. Primary tumor volume was not significantly different between the two experimental groups (Supplemental Figure 2-2C); however, there was a significant decrease in the number of metastatic lung nodules in the H460 shVIM cohort compared to control (Supplemental Figure 2-2D and 2-2E). Furthermore, the H460 shVIM cells also generated fewer micrometastases. Together, these data indicate that vimentin contributes to *in vitro* lung cancer cell motility and invasion as well as *in vivo* metastasis.

### **Vimentin regulates VAV2 phosphorylation and localizes VAV2 to FAs**

To determine the role of vimentin within lung cancer cell motility signaling, a phospho-proteomic screen was performed using H460 pLKO.1 and H460 shVIM cells to identify which cell motility proteins had the greatest change in phosphorylation upon vimentin depletion. Lysates from the H460 cell lines were probed with 1,318 phospho-specific antibodies and their corresponding non-phosphorylated antibodies (Supplemental Figure 2-3 and Supplemental Table 1). The ratio of phosphorylated to total protein was calculated for each screened protein. For each protein, the ratio of phosphorylated/total in H460 shVIM was plotted against the H460 pLKO.1 cells (Figure 1A). This analysis revealed the guanine nucleotide exchange factor (GEF) VAV2 as having the greatest decrease in percentage of phosphorylation (at Y142) upon vimentin depletion (Figure 2-1B and 2-1C). VAV2 is the GEF for Rac1 and cdc42 Rho GTPases, and has been shown to contribute to cell motility, spreading, and invasion (162, 163). VAV2 is regulated by

phosphorylation at tyrosines 142, 159, and 172 by EGFR (164). To validate the phospho-proteomic screen, western blotting of H460 and H1299 shVIM and pLKO.1 cell lines was performed. Consistent with the screen, VAV2 phosphorylation at Y142 decreased upon vimentin depletion in both H460 and H1299 cell lines (Figure 2-1D and 2-1E). Conversely, when GFP-tagged vimentin (hVIM-GFP), which was under the control of a doxycycline inducible promoter, was expressed in HEK293 cells, VAV2 phosphorylation increased at Y142 (Figure 2-1F). Based on these data we have identified a novel GEF whose phosphorylation is mediated by vimentin expression.

Immunofluorescence of pY142-VAV2 and vimentin in pLKO.1 and shVIM H460 cells was performed to determine localization of activated VAV2. In pLKO.1 H460s pY142-VAV2 was localized to the edge of the cell membranes in punctate structures resembling focal adhesions. However, cells lacking vimentin demonstrated more of a nuclear localization of pY142-VAV2 (Figure 2-2A and 2B). Analysis of focal adhesion sites revealed that while size and intensity of pY142-VAV2 focal adhesions remained unchanged, the number of pY142-VAV2 positive focal adhesion sites significantly decreased with vimentin loss (Figure 2-2C). Tyrosine 172, another marker of VAV2 activity, was also probed by immunofluorescence. In H1299 cells pY172-VAV2 was also localized to focal adhesions. Because VAV2 phosphorylation is mediated by the EGFR signaling pathway, we sought to determine whether vimentin regulates EGFR-mediated phosphorylation of VAV2. Our results show that vimentin regulates EGFR-mediated phosphorylation of VAV2 at Y142 and Y172 as shVIM cells had reduced levels of pY142- and pY172-VAV2 levels compared to pLKO.1 control cells after the addition of EGF.

To examine the interaction of vimentin and VAV2, we performed a co-immunoprecipitation experiment that showed that pY142-VAV2 formed a complex with vimentin in whole cell lysates (Figure 2-2D). To determine if pY142-VAV2 was, in fact, localized to focal adhesions as predicted by the staining pattern, we performed dual immunofluorescence for pY142-VAV2 and focal adhesion kinase (FAK), which marks focal adhesions. Co-staining revealed that pY142-VAV2 colocalizes with FAK at the cell periphery (Figure 2-2E). These data were further validated by co-IP in which pY142-VAV2 associated with FAK (Figure 2-2F). Together, these data demonstrate that VAV2 is active in the focal adhesion complex and that vimentin is necessary for phosphorylation and localization of VAV2.

#### **Vimentin loss leads to decreased FAK activation at FA sites**

Because vimentin is integral for VAV2 activation and localization to focal adhesion sites, we tested whether vimentin is necessary for proper FAK localization. Immunofluorescence of pY397-FAK was performed in pLKO.1 and shVIM isogenic cell lines (in H1299 and H460 lung cancer cell lines) and focal adhesions at the leading edge of motile cells were imaged by confocal microscopy. Cells lacking vimentin exhibited significantly fewer, smaller, and less intense pY397-FAK sites than isogenic vector control cells (Figures 2-3A-F). Immunofluorescence of total FAK showed a similar staining pattern in which shVIM cell lines exhibited fewer total FAK adhesion sites (Figure 2-3G). In both pLKO.1 cell lines (H460 and H1299), vimentin filaments and squiggles directly entered pY397-FAK sites (Figures 2-3A, 2-3B, and 2-3E), suggesting a potential interaction between the pY397-FAK and vimentin.

To further elucidate the impact of vimentin expression on FAK, we probed three different pairs of isogenic shVIM and pLKO.1 whole cell lysates for pY397-FAK and total FAK by western blot. In all cell line pairs, pY397-FAK and total FAK levels decreased with vimentin loss, confirming that vimentin is required for both FAK expression and activation (Figure 2-4A). An independent shRNA vimentin clone was used to validate these results (Figure 2-4B). Quantitative real-time PCR revealed that FAK mRNA levels did not differ between the isogenic pairs, indicating that vimentin regulation of FAK does not occur at the transcriptional level (Figure 2-4C). Because total FAK levels decreased with vimentin depletion, vimentin regulation on FAK protein stability was investigated by cyclohexamide (CHX) treatment of H1299 pLKO.1 and shVIM isogenic cell lines, which prevented new protein translation. FAK protein was still present in pLKO.1 cells after 12 hours of CHX treatment; however, after only 2 hours of CHX treatment of shVIM cells there was very little total FAK remaining (Figure 2-4D). Since calpains can degrade FAK (165), we investigated whether vimentin regulates calpain-mediated degradation of FAK using two calpain inhibitors. The calpain inhibitors did not significantly increase FAK stability, suggesting that vimentin-mediated FAK degradation goes through a different degradation pathway.

To assess vimentin-mediated promotion of pY397-FAK and total FAK levels, a GFP-tagged vimentin (hVIM-GFP) plasmid under control of a doxycycline-inducible promoter was expressed in HEK-293 cells. Western blot of whole cell lysates show that both pY397-FAK and total FAK expression increase with doxycycline induction of hVIM-GFP expression (Figure 2-4E). These data demonstrate that vimentin overexpression can induce FAK expression and activation. In combination with the

previous data, vimentin overexpression studies support that vimentin loss leads to increased FAK instability.

To follow up on immunofluorescence data showing vimentin entering FAK sites, we tested FAK/vimentin interactions by co-immunoprecipitation. A co-IP was performed for endogenous vimentin and FAK from H1299 cells and the proteins were shown to associate (Figure 2-4F). We hypothesized Y397 would be critical for this interaction. To probe this mechanism, FLAG-tagged phosphomimetic (Y397E) and unphosphorylatable (Y397F) FAK mutant constructs were generated. A co-IP of each of these mutants with vimentin demonstrated a nearly complete loss of vimentin association upon inhibition of phosphorylation in the Y397F FAK mutant, while the phosphomimetic Y397E FAK mutant still associated with vimentin (Figure 2-4G). These results indicate that phosphorylation at Y397 on FAK is critical for vimentin-mediated stabilization of FAK expression and activation.

### **Vimentin-mediated cell adhesion is dependent on FAK activation**

To determine the impact of vimentin-mediated FAK stability on cancer cell adhesion, we performed attachment and detachment assays with pLKO.1 and shVIM isogenic pairs in H460 and H1299 cell lines. Cellular attachment and detachment rates were measured on fibronectin-coated surfaces. Attachment rates were significantly lower in both shVIM cell lines compared to pLKO.1 control lines (Figure 2-5A, B). Detachment rates for the shVIM cell lines were also significantly decreased, indicating an overall decrease in adhesion upon vimentin depletion in shVIM cell lines.

We hypothesized that these adhesion defects were mediated by FAK. To test this hypothesis H1299 shVIM cells were transfected with constitutively active (CA) Y397E

FAK-GFP, wild-type (WT) FAK-GFP, or GFP. Transfected FAK was found to have a slightly higher expression level than endogenous FAK. Adhesion defects in the shVIM cell lines were completely rescued with introduction of WT or Y397E FAK constructs (Figure 2-5E, F). These results show that vimentin-dependent adhesion defects can be restored by WT- or CA-FAK expression.

### **VAV2 regulates vimentin-dependent FAK activation and cell adhesion**

Because vimentin associates with, and regulates both VAV2 and FAK activation and localization to focal adhesion sites, we hypothesized that vimentin regulates FAK via VAV2. Transfection of VAV2 siRNA in H1299 cells resulted in a decrease in FAK phosphorylation at Y397 compared to control siRNA transfected cells (Figure 2-6A). There was, however, no change in total FAK expression, indicating that VAV2 regulates FAK activation. Conversely, FAK siRNA transfection in H1299s revealed no impact on VAV2 activation at Y142 or Y172, indicating that FAK does not regulate VAV2 activation directly (Figure 2-6B).

To determine if VAV2 could rescue FAK activation and stability in shVIM cell lines, a GFP-tagged constitutively active (CA) VAV2 (CA VAV2-GFP) was used in which the first 184 amino acids of VAV2 were deleted (162). A GFP-tagged dominant negative VAV2 mutant was also used as a negative control. Transfection of CA VAV2-GFP in shVIM cell lines, but not WT VAV2-GFP, rescued pY397-FAK levels lost upon vimentin depletion (Figure 2-6C). Expression of CA VAV2-GFP also rescued the adhesion defects previously seen in the shVIM cell lines. These results indicate that an active VAV2 can rescue both FAK activation and cell adhesion defects in vimentin-depleted cells.

### **Vimentin regulates VAV2-mediated Rac1 activation**

As VAV2 is the guanine nucleotide exchange factor (GEF) for Rac1 and cdc42 (162), key Rho GTPases in cell motility, we hypothesized that VAV2 acted through Rac1 and/or cdc42 to regulate FAK. Rac1 activity assays revealed that Rac1 activity was significantly decreased upon vimentin depletion in shVIM cells (Figure 2-7A). This Rac1 defect was rescued by CA VAV2, but not WT VAV2 or the dominant negative mutant, in vimentin-depleted cells (Figure 2-7B). While VAV2 acts as the GEF for cdc42, there were no defects in cdc42 activity in shVIM cells, indicating that vimentin regulates Rac1 but not cdc42 in lung cancer cells.

To test Rac1 regulation of FAK in the lung cancer context, rescue experiments were performed. H1299 shVIM cells were transfected with constitutively active Q61L Rac1, WT Rac1, or dominant negative T17N Rac1 (166) and whole cell lysates were probed for pY397-FAK. CA Q61 Rac1, but not WT or dominant negative constructs, was able to rescue pY397-FAK levels in shVIM cells (Figure 2-7C). A similar experiment was performed with cdc42 constructs but a rescue was not observed (Supplemental Figure 8B). Confocal imaging of CA Q61 Rac1 transfected shVIM cells revealed an increased number of pY397-FAK adhesion sites at the leading edge (Figure 2-7D). Together, these data show that CA Q61 Rac1 can rescue focal adhesion defects in vimentin-depleted lung cancer cells. Finally to test whether Rac1 is active during cell spreading we performed cell spreading assays on pLKO.1 and shVIM H1299 cells. In this experiment serum starved cells were trypsinized and then replated in full serum media. Peak Rac1 activity was observed after 2 hours of cell spreading in pLKO.1 cells; however, activity peak was achieved in shVIM cells (Figure 2-7E). These results suggest

that vimentin-depleted cells exhibit Rac1 activity defects during cell spreading. Together these data support a model in which vimentin mediates VAV2-Rac1 activation to regulate FAK-based cell adhesion.



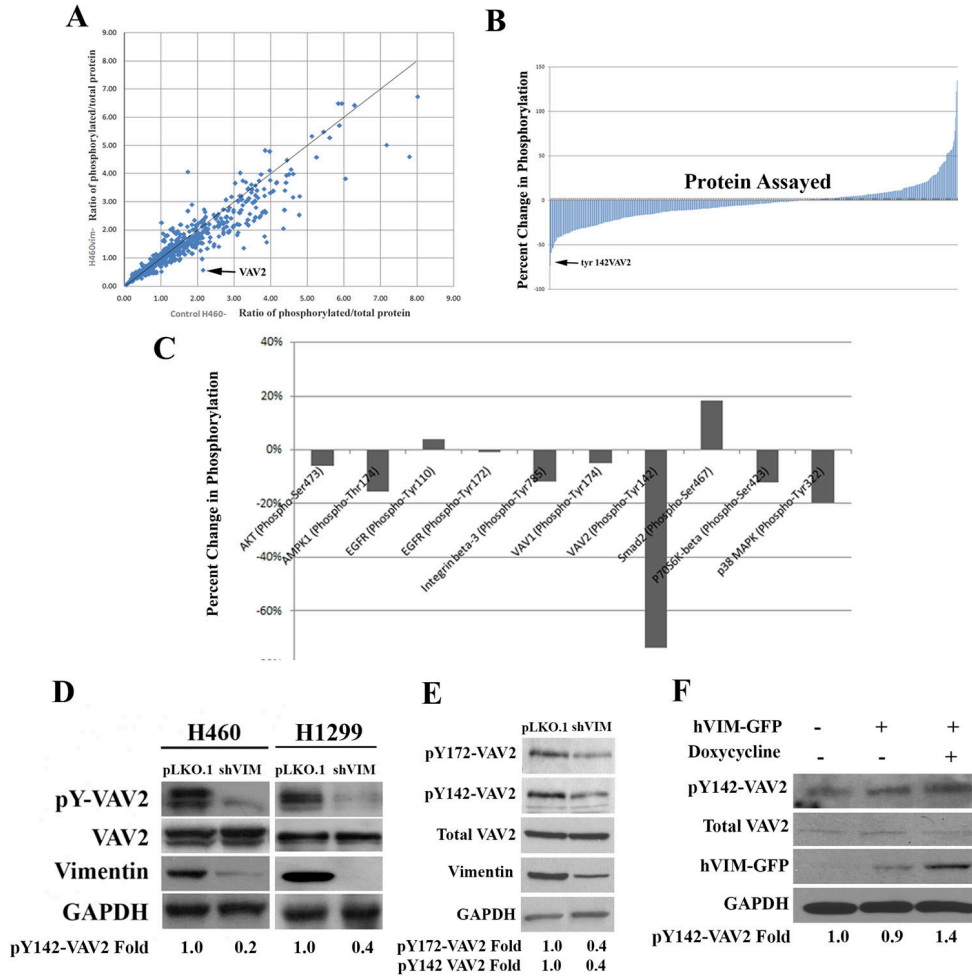


**Figure 2-1. Phospho-proteomic screen for cell motility proteins with an altered phosphorylation status upon vimentin depletion.**

(A) For each protein analyzed, the ratio of phosphorylated/total protein in H460 shVIM cells was plotted against the same ratio in H460 pLKO.1 cells. (B) Bar graphs showing that VAV2 had the greatest decrease in percent phosphorylation of all proteins screened. (C) Bar graph comparing VAV2 to other relevant proteins. (D) The reduction in VAV2 phosphorylation at Y142 was verified by western blot in H460 and H1299 cells. (E) Lysates from H1299 pLKO.1 or shVIM cells were analyzed by western blot for pY172-VAV2 levels. pY172-VAV2 levels are decreased in shVIM cells. (F) Representative western blot of lysate from HEK293 cells transfected with hVIM-GFP shows a 40% increase in pY142-VAV2 upon induction of vimentin expression with doxycycline. Fold changes determined by densitometry

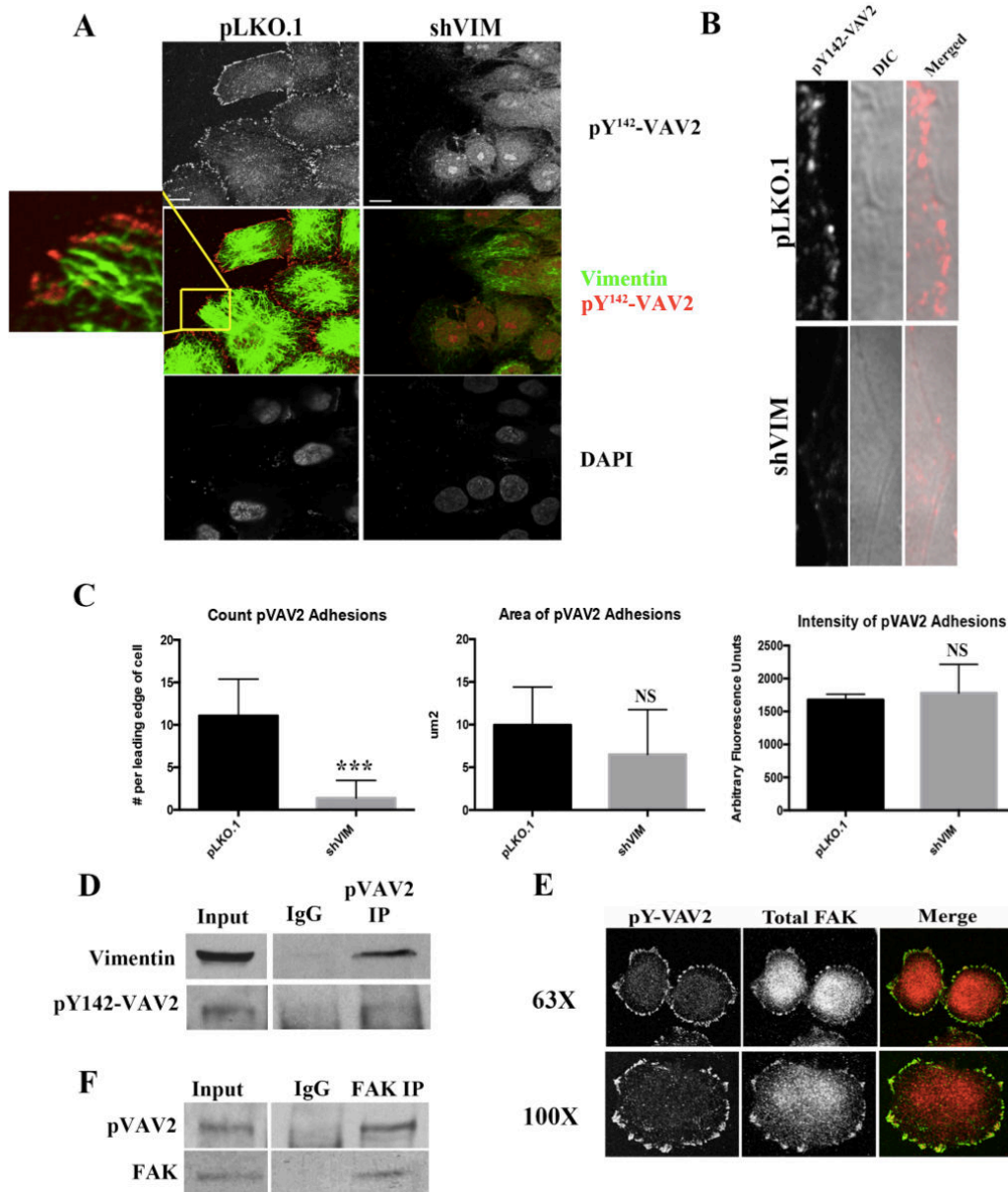


**Figure 2-2. pY142-VAV2 localizes to focal adhesions in vimentin positive cells.**

(A) H460 pLKO.1 and shVIM lung cancer cells co-stained for pY142-VAV2 (red) and vimentin (green). Scale bars = 10 $\mu$ m. (B) H1299 and pLKO.1 and shVIM cells stained for pY142-VAV2. (C) Quantification of the count, area, and intensity of pVAV2 adhesions. (D) Co-immunoprecipitation shows association between endogenous pY142-VAV2 and vimentin in H460 whole cell lysates. (E) Immunofluorescence of pY142-VAV2 (green) and FAK(red) in H460 cells. (F) Co-immunoprecipitation of endogenous pVAV2 and FAK.

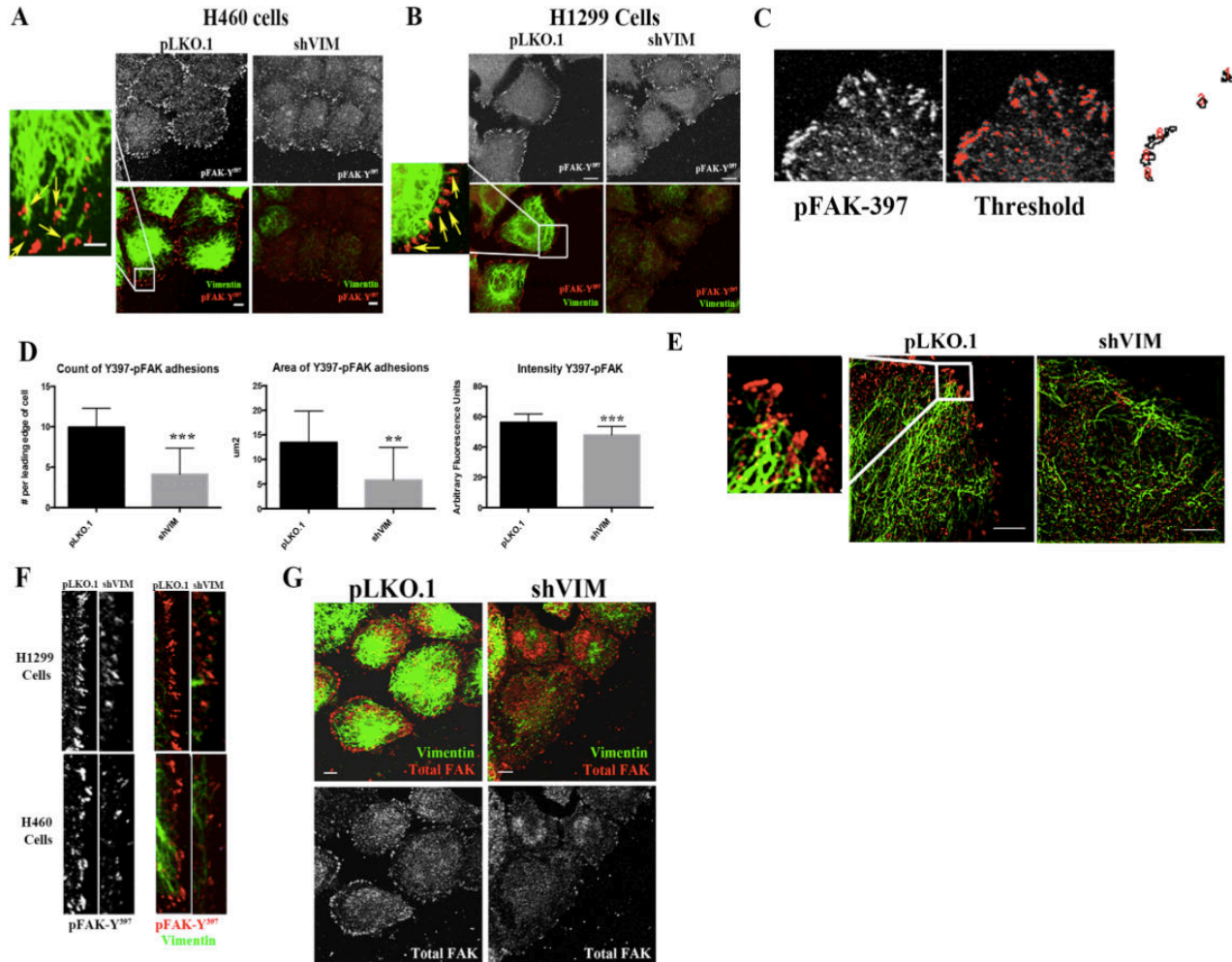


**Figure 2-3. Vimentin depletion reduces the number and intensity of activated FAK positive focal adhesion sites.**

(A and B) Immunofluorescence images of pY396-FAK (red) and vimentin (green) in H460 and H1299 cells from wound healing assay. Yellow arrows indicate where vimentin filaments and squiggles enter the pY397-FAK sites. (scale bar= 10 $\mu\text{m}$ ). (C) The ROI at the leading edge of the cells, whose pixels were thresholded to remove background. (D) Quantification of the number, size, and intensity of focal adhesions in H460 pLKO.1 and shVIM cells. (N-SIM super resolution microscopy shows vimentin filaments (green) directly entering FAK sites (red)). (G) H460 pLKO.1 and shVIM cells co-stained for vimentin (green) and total FAK (red) (scale bar= 10 $\mu\text{m}$ ).

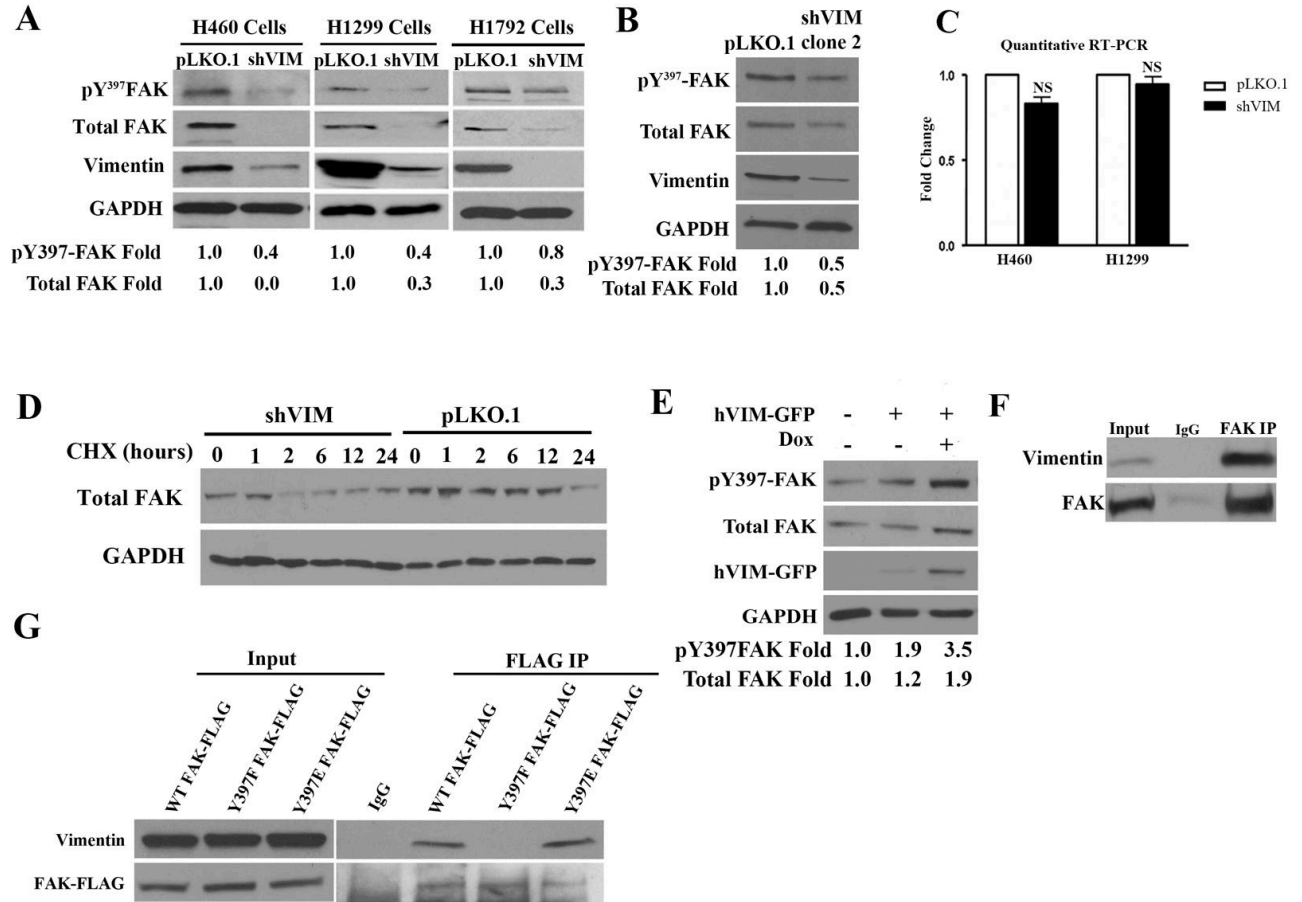


**Figure 2-4. Vimentin regulates FAK activation and expression.**

(A) Representative western blot of H460, H1299 and H1792 pLKO.1 and shVIM lung cancer cell lines show a reduction in FAK Y397 phosphorylation upon vimentin depletion. Fold changes determined by densitometry. (B) Western blot of H1299 pLKO.1 and shVIM clone 2 cells measuring FAK expression and Y397 phosphorylation levels. (C) Quantitative real-time PCR analysis of FAK mRNA levels in H460 and H1299 pLKO.1 and shVIM cells. (D) H1299 shVIM and pLKO.1 cells treated with CHX were analyzed by western blot for total FAK levels. (E) Western blot of FAK expression and Y397 upon doxycycline induction of hVIM-GFP expression in HEK293 cells. (F) Co-immunoprecipitation shows association between endogenous FAK and vimentin in H1299 total cell lysates. (G) Lysates from H1299 cells transfected with WT FAK-FLAG, Y397F FAK-FLAG or Y397E FAK-FLAG were used for immunoprecipitation between transiently expressed FAK and endogenous vimentin.

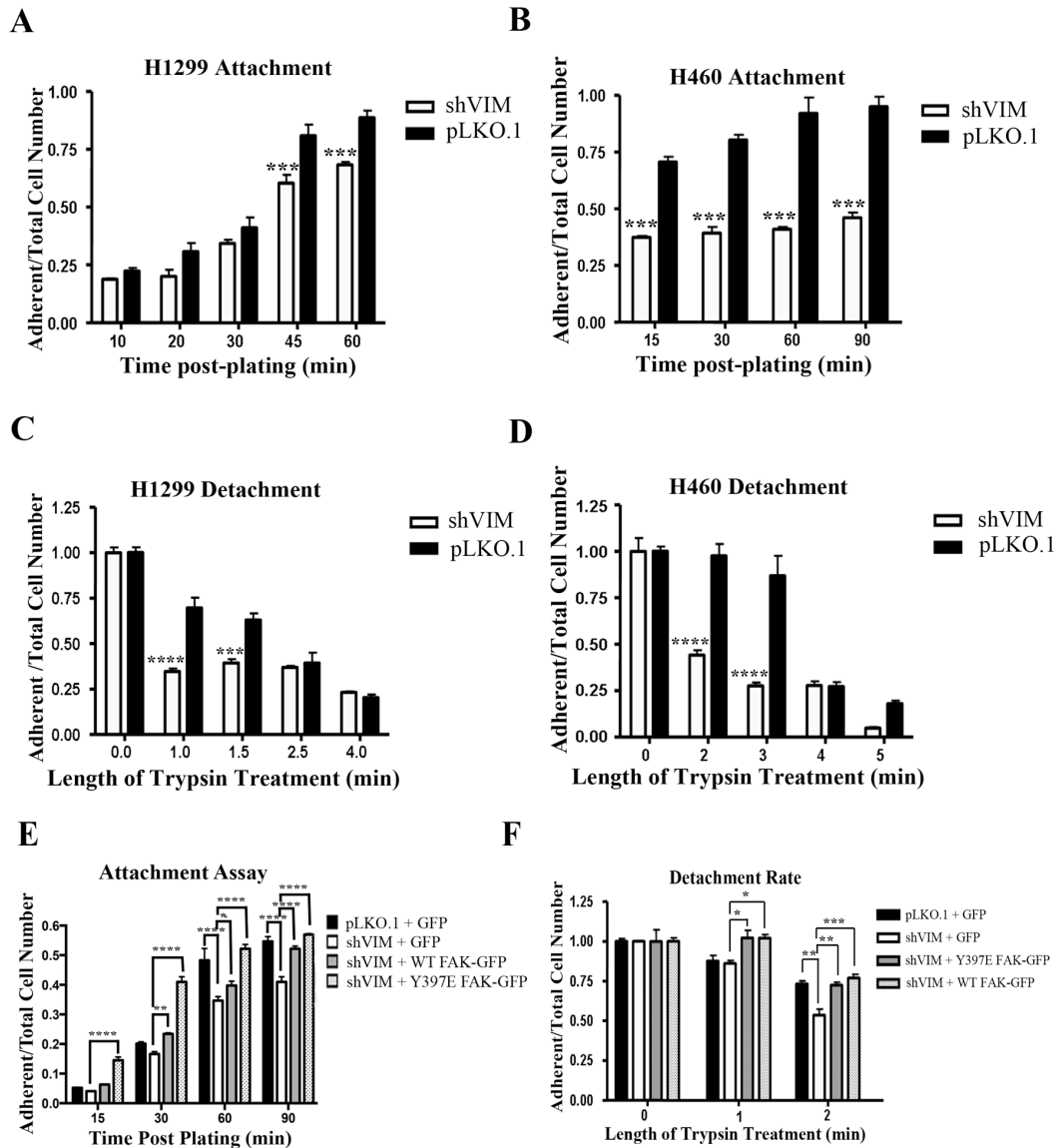


**Figure 2-5. Vimentin regulates FAK-mediated cell adhesion.**

(A-B) Adhesion assays performed with H1299 or H460 cells plated on fibronectin over time. Ratio of adherent to total cells plated was calculated for each cell type at each time point (\*\* $p < 0.001$ ). (C-D) Detachment assays performed with H1299 or H460 pLKO.1 and shVIM cells measured by trypsinizing cells over time. For each time point, the ratio of adherent cells to the total cells was calculated. (\*\* $p < 0.001$ , \*\*\*\* $p < 0.0001$ ). (E) Attachment rate was determined for H1299 pLKO.1 cells transfected with GFP and H1299 shVIM cells transfected with GFP, Y397E FAK-GFP or WT FAK-GFP. (\* $p < 0.05$ , \*\* $p < 0.01$ , \*\*\*\* $p < 0.0001$ ). (F) The detachment rate was determined for H1299 pLKO.1 cells transfected with GFP and H1299 shVIM cells transfected with GFP, Y397E FAK-GFP or WT FAK-GFP (\* $p < 0.05$ , \*\* $p < 0.01$ , \*\*\*\* $p < 0.0001$ ).

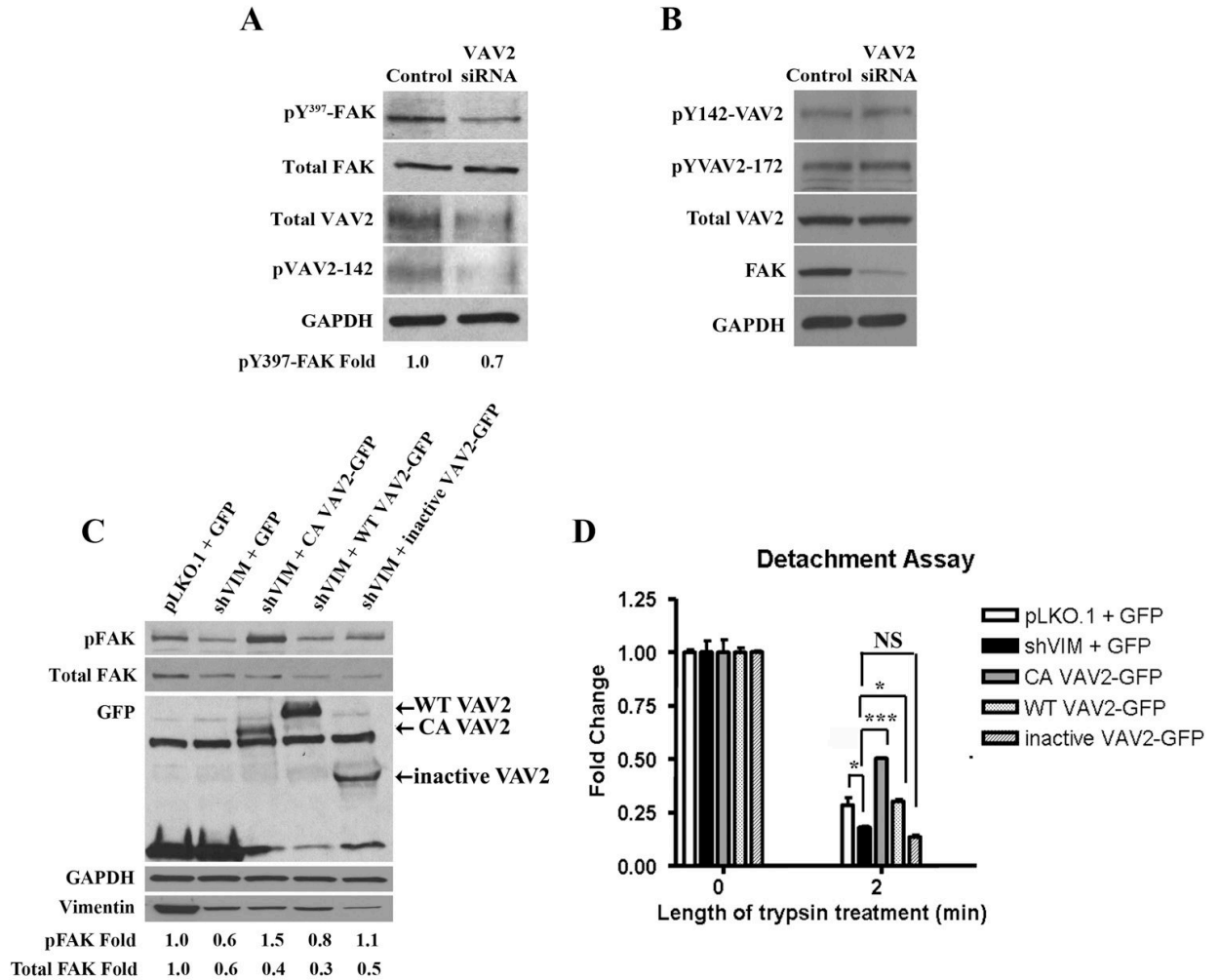


**Figure 2-6. VAV2 regulates vimentin dependent FAK activation and cell adhesion.**

(A) Lysates from H1299 cells transfected with VAV2 or control siRNA analyzed by western blot. Fold changes were determined by densitometry. (B) Lysates from H1299 cells transfected with FAK or control siRNA were analyzed by western blot. (C) Western blot of H1299 pLKO.1 cells transfected with GFP and H1299 shVIM cells transfected with GFP, CA VAV2-GFP, WT VAV2 or inactive VAV2. Fold changes determined by densitometry. (D) A detachment assay with H1299 pLKO.1 cells transfected with GFP and H1299 shVIM cells transfected with GFP, CA VAV2-GFP, WT VAV2 or inactive VAV2 (\* $p < 0.05$ , \*\*\* $p < 0.001$ ).

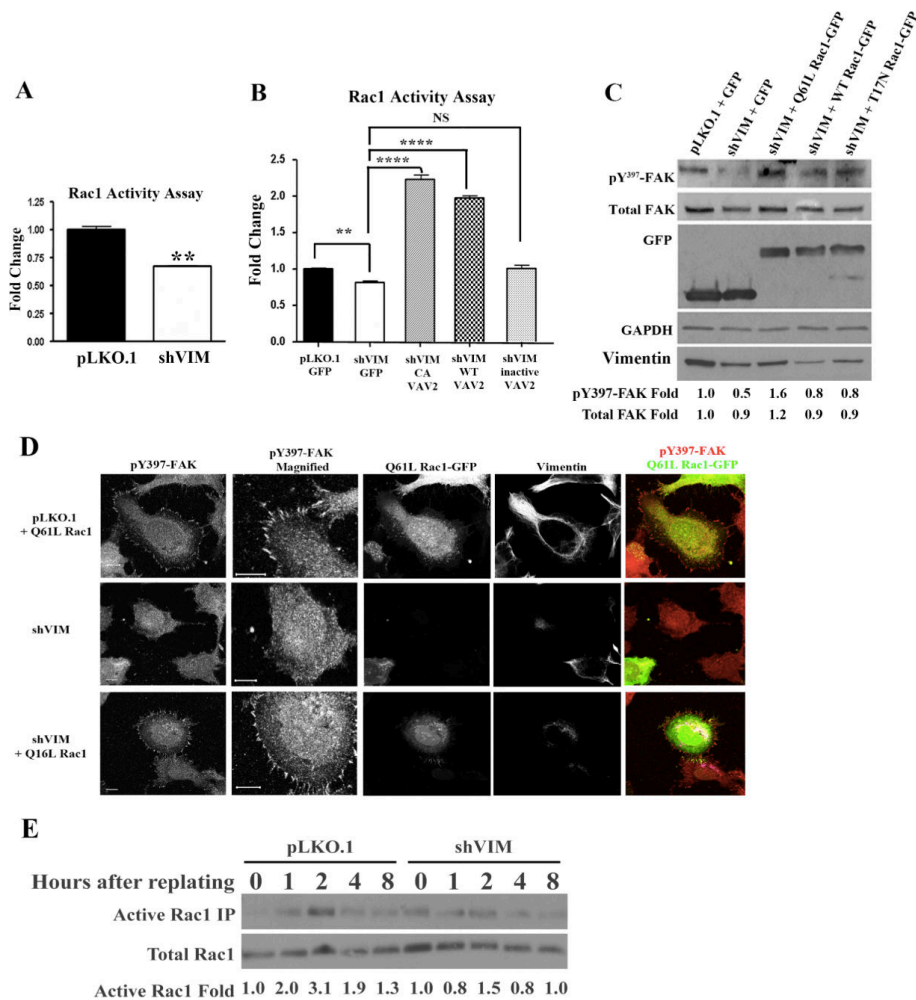


**Figure 2-7. Vimentin regulates VAV2-mediated Rac1 activation**

(A) An ELISA based Rac1 activation assay showed that Rac1 activity was reduced in shVIM cells compared to pLKO.1 cells (\*\* $p < 0.01$ ). (B) H1299 pLKO.1 cells transfected with GFP and shVIM cells were transfected with GFP, CA VAV2-GFP, WT VAV2-GFP or inactive VAV2-GFP (\*\* $p < 0.01$ , \*\*\*\* $p < 0.0001$ ). (C) Western blot of H1299 pLKO.1 cells transfected with GFP and shVIM cells transfected with GFP, Q61L Rac1-GFP, WT Rac1-GFP or T17N Rac1-GFP. Fold changes were determined by densitometry. (D) A rac1 activity pull-down assay on serum starved cells that were trypsonized then replated showed that cells expressing vimentin have a higher level of Rac1 activity during cell spreading than those depleted for vimentin (E) H1299 pLKO.1 shVIM cells were transfected with Q61L Rac1-GFP. Co-staining of Q61L Rac1-GFP (green), pY397-FAK (red) and vimentin (greyscale). Expression of Q61L Rac1 restored FAK-positive focal adhesions in vimentin shRNA cells (scale bars=10 $\mu$ m).

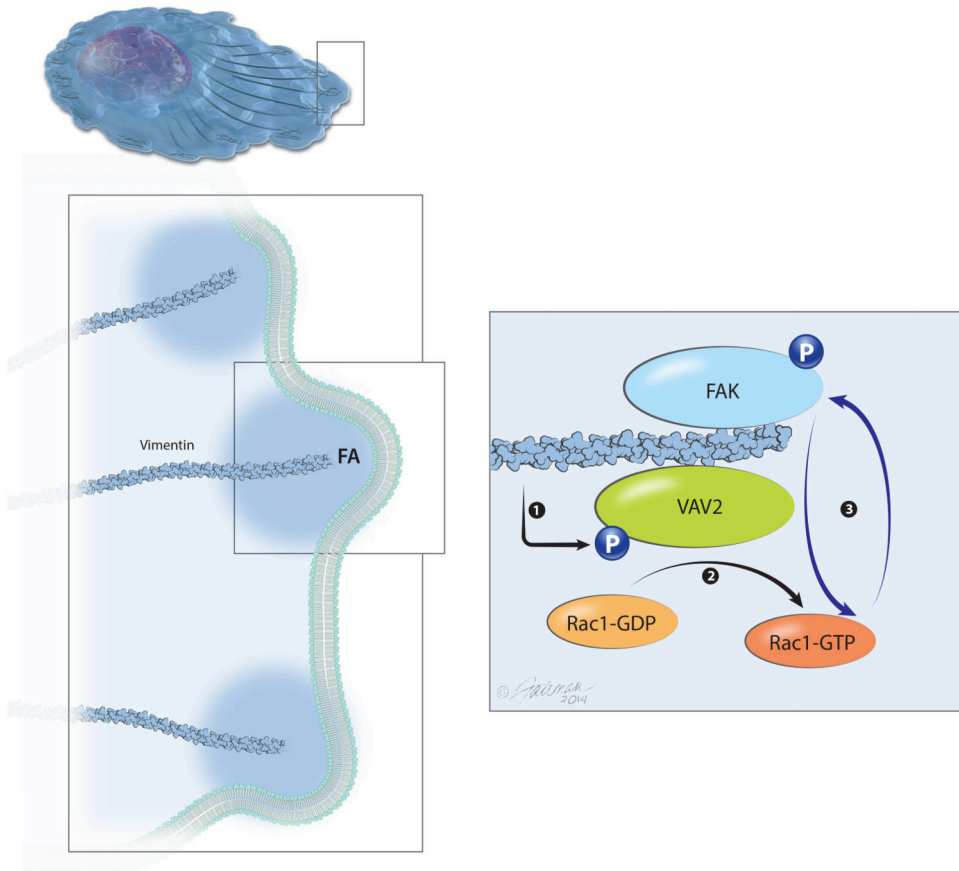
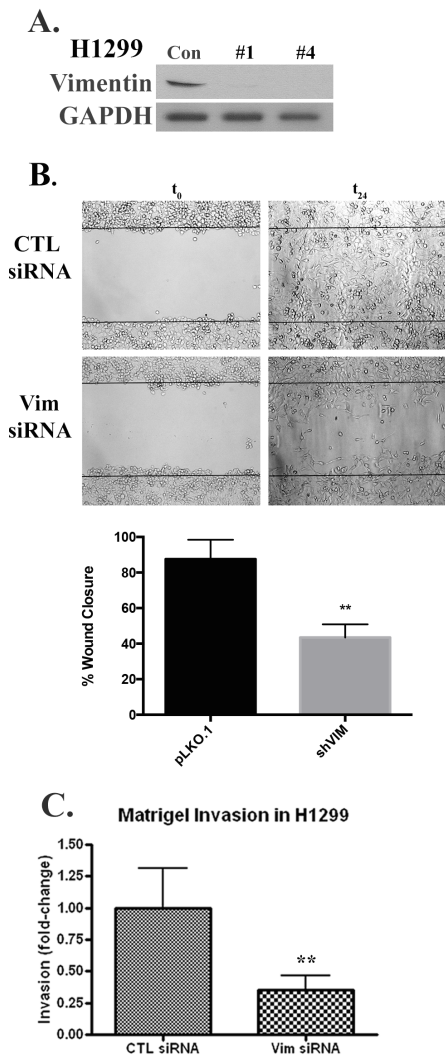


**Figure 2-8. Vimentin regulates FAK activity through a VAV2-Rac1 dependent pathway.**

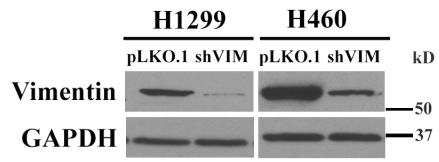
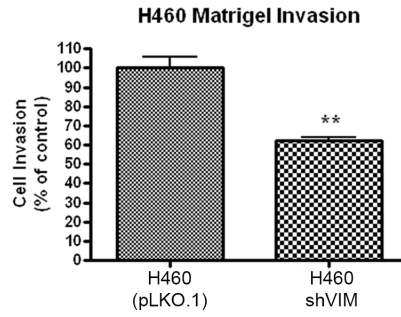
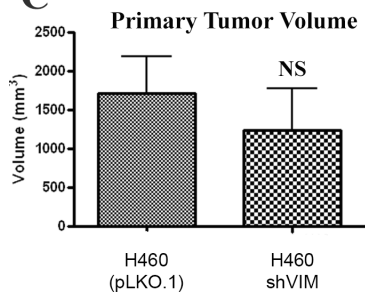
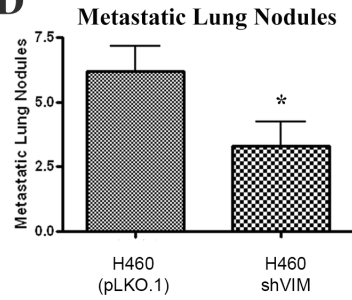
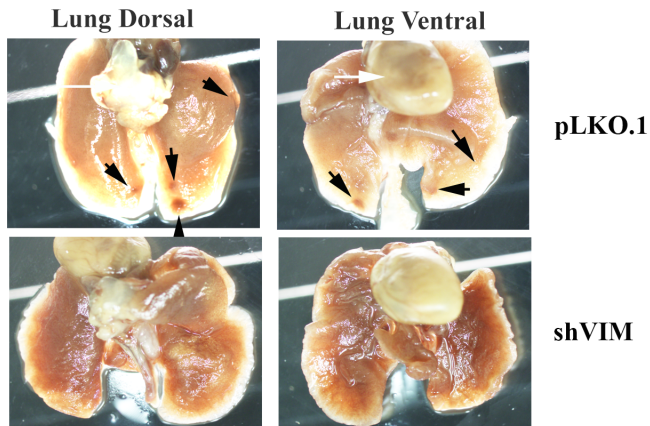
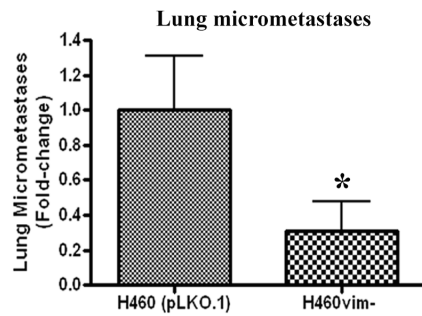
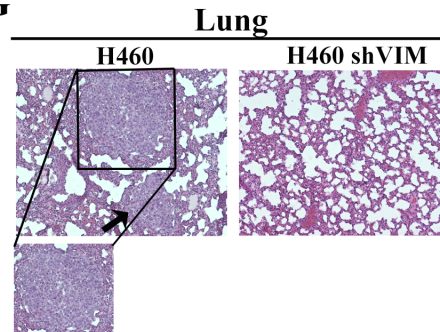
In the presence of vimentin, VAV2 is phosphorylated at Y142 and localizes to the focal adhesions with FAK and vimentin. Phosphorylated VAV2 activates Rac1, which allows FAK activation at the focal adhesions.



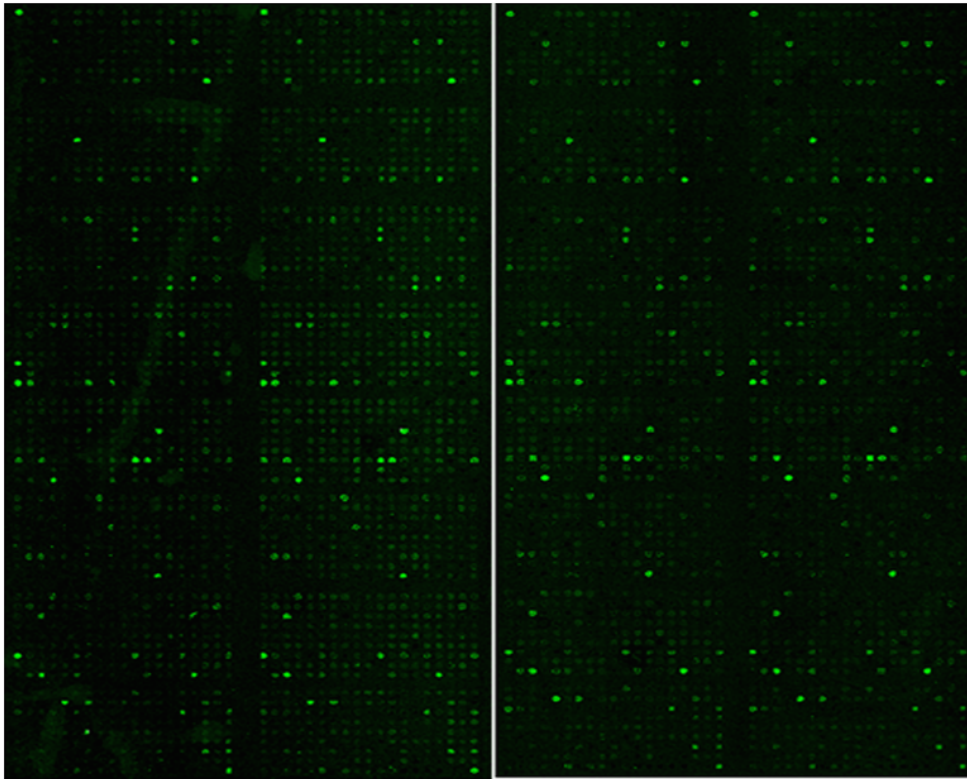
## Chapter 2 Supplemental Figures



**Supplemental Figure 2-1. Vimentin loss reduces cell motility and invasion.** (A) H1299 cells were transfected with two different vimentin siRNAs. Western blot analysis shows significant loss of expression. (B) A scratch wound was induced on a confluent monolayer of H1299 cells. White solid lines represent the initial wound front at time zero. After 24 hours, the cells transfected with control siRNA closed 88% of the wound whereas those transfected with vimentin siRNA only closed 43% of the wound. (C) An invasion assay in control and vimentin siRNA treated H1299 cells showed a significant decrease in invasion upon vimentin depletion. \*\*  $p < 0.01$ .

**A****B****C****D****E****F****G**

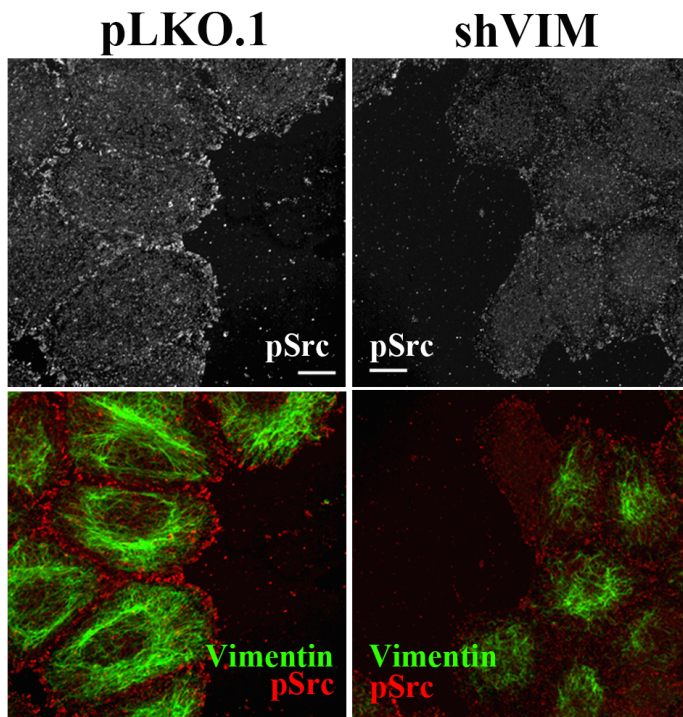
**Supplemental Figure 2-2. Vimentin loss reduces invasion and metastasis.** (A) Isogenic pairs of H1299 and H460 cells stably expressing shVIM or the pLKO.1 vector were produced. Western blotting verified depletion of vimentin protein. (B) An invasion assay showed decreased invasion of shVIM cells compared to pLKO.1 cells. \*\*  $p < 0.01$ . (C-G) H460 shVIM or pLKO.1 cells were injected into 7-8 week nude mice. (C) Bar graph showing that primary tumor volume was not significantly different between shVIM and control pLKO.1 injected mice. (D) Bar graph showing there were fewer metastatic lung nodules in shVIM mice compared to control mice.  $p < 0.05$ . (E) Images showing that control mice developed more metastatic lung nodules (marked by black arrows) than shVIM mice. (F) Bar graph showing that H&E staining of lung sections showed significantly fewer micrometastases in shVIM than control mice. \*  $p < 0.05$ . (G) Images of H&E staining showing micrometastases in the control mice but not in the shVIM mice. There are two micrometastases; the largest one is surrounded by a box and is independently shown below while the smaller one is indicated by an arrow.



**H460 control**

**H460 shVIM**

**Supplemental Figure 2-3. Phospho-proteomic screen for altered phosphorylation status upon vimentin depletion.** A phospho proteomic screen for cell motility proteins whose activity is vimentin dependent. An array with 1,318 different phospho antibodies spotted in a grid was incubated with either biotin labeled H460 shVIM lysate or H460 pLKO.1 lysate then exposed to streptavidin with a fluorescent tag. The intensity of the fluorescence corresponds to the phosphorylation level of a particular protein.



**Supplemental Figure 2-4. Vimentin is important for focal adhesion formation.** H460 pLKO.1 and shVIM cells were grown to confluency. A scratch wound was induced prior to co-staining for vimentin (green) and pY418-Src (red). The shVIM cells showed fewer pY418-Src positive focal adhesion sites than the pLKO.1 cells. Scale bar = 10  $\mu$ m.

## 2.4 Discussion

Vimentin expression has been repeatedly shown to correlate with increased metastatic potential and cell motility (116, 130). However, the exact mechanism by which vimentin regulates cancer cell invasion has been severely understudied. Here we demonstrate a novel role for vimentin as a hub of focal adhesion signaling and regulator of cellular adhesion and motility within lung cancer cells. Our data show that vimentin is required for proper FAK activation and localization at the leading edge of motile lung cancer cells (Figures 2-3 and 2-4). We demonstrate that FAK is regulated by vimentin in a VAV2-Rac1 dependent manner (Figure 2-8). First we showed that vimentin depletion inhibits VAV2 and pY397-FAK expression as well as Rac1 activity. Vimentin-dependent changes in focal adhesion protein expression translate into adhesion defects; all of which are rescued by CA VAV2, indicating that VAV2 acts upstream of both Rac1 and FAK.

Surprisingly, the dominant negative VAV2 mutant demonstrated a partial rescue of pY397-FAK, perhaps due to an incomplete inactivation of VAV2 activity in the mutant. We further demonstrate that vimentin is necessary for proper localization of VAV2 to FAK-positive focal adhesion sites. VAV2 associates with both vimentin and FAK and we believe this occurs at focal adhesion sites as vimentin directly enters VAV2/FAK-positive sites. Interestingly, we found that FAK autophosphorylation at Y397 is necessary for FAK-vimentin association as inhibition of phosphorylation by point mutation prevents association between the two proteins. Finally we show that CA Rac1 can rescue FAK expression and adhesion defects in vimentin-depleted cells by restoring pY397-FAK expression and localization to the leading edge of motile cells.

Based on these findings, we propose a molecular model in which vimentin is required for proper localization and activation of VAV2 at focal adhesions. VAV2 serves as the Rac1 GEF and an active Rac1 is able to promote FAK-positive focal adhesion assembly (Figure 2-8). These data support previous findings that demonstrate Rac1 as a key regulator of focal adhesions (167). Therefore, vimentin promotes focal adhesion formation and stability via VAV2-Rac1 to regulate cell motility in lung cancer cells.

Our proposed model is consistent with findings showing vimentin stabilizes and increases the size of focal adhesions (168). These results indicate that vimentin expression promotes VAV2 activation, which has been shown to regulate cell invasion and spreading (163, 169) as well as be linked to cancer invasion and metastasis (170). Both VAV2 and VAV3 have been shown to promote tumorigenesis and metastasis in breast cancer models that metastasize to the lung (61).

Rac1 activity is only slightly decreased upon vimentin depletion in stably adherent cells, which is indicative of VAV2 being only one of many potential GEFs that can activate Rac1 and compensatory GEFs remaining active in the absence of vimentin. While VAV2 acts as a GEF for both Rac1 and cdc42, which are both key players in cell motility, only Rac1 activity was dependent on vimentin expression. While VAV2 has been well characterized as a GEF of Rac1 (162), its GEF activity on cdc42 remains controversial (171). As mentioned, Rac1 is a critical player in cell motility via regulation of focal adhesion assembly (172). Our data show that CA Rac1 can rescue defects in cell adhesion and FAK signaling caused by vimentin depletion. Therefore, we believe that it is loss of Rac1 activity that reduces FAK autophosphorylation, activation, and localization to focal adhesion sites. Others have shown that pFAK is necessary for Rac1



activation and proper localization to focal adhesions (172); therefore, we propose a feedback loop in which increased FAK activation can in turn activate Rac1. However, this pathway does not likely act through VAV2 as VAV2 activity was unaffected by FAK depletion (Figure 2-6B).

Together our data details the role of vimentin as a regulator of focal adhesion assembly and signaling via VAV2-Rac1 signaling. Because proper focal adhesion assembly is necessary for cell motility and metastasis, our proposed mechanism lays the groundwork for future studies investigating the role of vimentin as not only a metastatic biomarker but an important regulator of the metastatic cascade. We would predict, based on our findings, that *in vivo* vimentin would continue to play an important role in cellular motility within the context of an invasive and metastatic tumor.

**Chapter 3: Vimentin is required for lung adenocarcinoma metastasis via heterotypic tumor cell-cancer-associated fibroblast interactions during collective invasion**

Alessandra M. Richardson, Lauren S. Havel, Allyson E. Koyen, Jessica M. Konen, John Shupe, W. G. Wiles IV, W. David Martin, Hans E. Grossniklaus, Gabriel Sica, Melissa Gilbert-Ross, Adam I. Marcus

This chapter is adapted from a manuscript by A Richardson, L Havel, A Koyen, J Konen, J Shupe, W Wiles, W Martin, H Grossniklaus, G Sica, M Gilbert-Ross, A Marcus.

*Vimentin is required for lung adenocarcinoma metastasis via heterotypic tumor cell-cancer-associated fibroblast interactions during collective invasion.* Clinical Cancer Research 2017. Accepted.

AMR author contribution: wrote and reviewed the manuscript and designed and executed the vast majority of the experiments for this manuscript

### 3.1 Introduction

Epithelial to mesenchymal transition (EMT) has served as a guiding principle underlying the initiation and progression of metastatic disease (173). During EMT, epithelial cells from the primary site undergo genetic (34) and epigenetic (35) alterations that trigger cancer cell invasion. A hallmark of EMT is the loss of epithelial proteins such as E-cadherin (174) and gain of mesenchymal proteins such as vimentin(175). These events can be transient as cells transition through partial and reversible EMT states (37-39, 176). and it has been debated whether these transitions are necessary for metastasis to occur (177, 178).

Lung adenocarcinoma often presents as advanced metastatic disease, which is associated with a 5-year survival rate that can approach 4% (155). As the genomic drivers of lung adenocarcinoma initiation and progression have become well-characterized, co-mutations in *KRAS* and *LKBI* are recognized as major drivers of the disease (28, 156). The *KRAS* and *LKBI* co-mutation has previously been modeled in a Cre-dependent LSL-*Kras*<sup>G12D</sup>, *LKB1*<sup>fl/fl</sup> genetically engineered mouse model (GEMM) (21) to investigate *LKBI* loss in the context of metabolism (23), therapeutic response (20, 24), and microenvironment remodeling (179). In this GEMM, primary lung tumors develop at 8 to 10 weeks with 52% of these mice having metastatic disease to draining lymph nodes (20, 21). When Cre is delivered intranasally via lentiviral infection, 100% of primary tumors are lung adenocarcinomas that reproduce the stages of tumor progression from adenocarcinoma *in situ* to invasive disease (20).

To assess EMT in lung adenocarcinoma, and more specifically the role of the canonical mesenchymal marker vimentin, we generated an *LSL-Kras*<sup>G12D</sup>/*Lkb1*<sup>fl/fl</sup>/*Nim*<sup>-/-</sup>

(*KLV*<sup>-/-</sup>) metastatic lung adenocarcinoma GEMM model, which contains a whole body vimentin knockout (180) in the *Kras/Lkb1* GEMM (176, 181). Vimentin is an intermediate filament protein, which is associated with increased metastatic potential (182), high nuclear grade (113), and poor overall survival (183) across most solid tumor types including lung, prostate, and breast cancers (116, 184, 185). Since vimentin is integral for the structural integrity of the cell (128), lamellipodia formation (127), and adhesion signaling (53, 129), downregulating vimentin expression is sufficient to alter cell morphology *in vitro* (130) as well as inhibit cell motility and invasion (132).

The data from these GEMM, human lung adenocarcinoma, and *in vitro* 3-D models show that vimentin is required for lung adenocarcinoma to metastasize at an early stage by acting in cancer associated fibroblasts (CAFs) that surround epithelial-like collective invasion packs (CIPs). These data support the concept that vimentin is critical for lung adenocarcinoma metastasis and could be a potential target for anti-metastatic therapies.

### 3.2 Experimental Procedures

#### Transgenic Mouse Model

*KLV*<sup>-/-</sup> mouse was generated by crossing the LSL-*Kras*<sup>G12D</sup>/*LKB1*<sup>fl/fl</sup> mouse (21) with the Vimentin<sup>-/-</sup> (180) mouse until a homozygous *KLV*<sup>-/-</sup> mouse was generated. *KLV*<sup>-/-</sup> mouse took approximately four generations over 7 months to create. *KLV*<sup>+/-</sup> mice were generated by crossing *KLV*<sup>+/+</sup> mice with *KLV*<sup>-/-</sup> mice. All mice were housed and treated according to Institutional Animal Care and Use Committee protocol #2003525 by the Emory University Division of Animal Resources. *Kras* and *Lkb1* mutant mice were

purchased from The Jackson Laboratory. Vimentin null mice were obtained from the EMMA repository. Lentiviral Cre ( $1.2 \times 10^7$  i.u.) was administered intranasally to mice 8-12 weeks old that were sedated with Avertin (20mg/mL working dilution). Infected mice were then monitored until tumorigenic symptoms (ie weight loss greater than 10%, respiratory distress, inactivity) presented. All mice infected with lentiviral Cre were monitored to a 25 weeks post infection endpoint and were sacrificed prior if they presented with clinical symptoms including weight loss, respiratory distress, and/or hunching. Upon sacrifice, lungs and mediastinal lymph nodes were harvested in either 10% formalin or flash frozen in OCT pending use.

#### Human Lung Adenocarcinoma Tissue

De-identified human lung adenocarcinoma tissue is a mixed cohort of samples from Emory and Wellstar tumor banks and Emory clinical formalin-fixed paraffin-embedded (FFPE) tumor specimens (IRB00009857). All Emory samples were sequenced using a workflow described (20). Lung adenocarcinoma staging was performed by a board certified thoracic pathologist according to the AJCC Cancer Staging Manual Seventh Edition. Vimentin IHC was scored by a board certified thoracic pathologist with a 40X objective on a scale from 0-3 based on stain intensity and was stratified by stromal or tumor compartment. Q score was determined by the multiplication of stain intensity by percent of cells staining at that intensity for a given cell compartment (i.e. 30% of stromal cells at level 3 stain has Q score of 90).

#### Immunohistochemistry

Formalin-fixed paraffin embedded (FFPE) tissues were hydrated in a series of washes from xylenes to ethanol dilutions to water. Heat-mediated antigen retrieval was conducted with citrate buffer when necessary. Endogenous peroxidase activity was blocked with 3% hydrogen peroxide. Samples were blocked with 2.5% Normal Goat Serum (Vector Labs) and incubated in primary antibody overnight in 1:1 NGS:PBS solution (Vimentin R28 Cell Signaling 1:300, alpha SMA Invitrogen 1:1000, Pro-SPC Santa Cruz FL-197 1:150, CD31 ab28364 1:50 CD3 ab16669 1:100). Samples were incubated in secondary antibody (Rabbit 1:200), biotin, and streptavidin (Vector Labs). Staining was developed using Peroxidase Substrate Kit DAB (Vector Labs). Proliferation was measured by staining for Ki67 (ab16667, 1:200) using IMMpact Kit (Vector Labs).

#### Immunofluorescence

Tissue: Tissue sections frozen in OCT Compound were sliced in 10 $\mu$ m sections and fixed in 100% acetone. Sections were stored at -80°C until used. Sections were blocked for 1 hour in 10% Normal Goat Serum in PBS. Primary antibodies were incubated in PBS overnight overnight for the following antibodies at indicated concentrations: vimentin R28 Cell Signaling 1:50, F4/80 abcam 1:100, FSP1 ab27957 1:200. FFPE tissues were hydrated as described above. Heat-mediated antigen retrieval was also conducted as above. A blocking buffer of 5% BSA in PBS was used. Primary antibodies were incubated at 4°C overnight in 1% BSA in PBS (FSP1 ab27957 1:200; E-cadherin BD Biosciences 610181 1:1000). Secondary antibodies were incubated on tissues for 1 hour (1:1000).

Cells: CAFs were fixed and stained as described (53). Primary antibodies were diluted in 5% normal goat serum (Vimentin R28 Cell Signaling 1:50) and added to the coverslips overnight at 4 °C. The coverslips were mounted on glass slides using Prolong diamond mounting medium (Invitrogen). The slides were imaged using Leica SP8 confocal microscope.

Spheroids: Spheroids embedded in matrigel were fixed with 4% paraformaldehyde for 20 min. Glycine rinse (TBS/glycine 130 mM NaCl, 7 mM Na<sub>2</sub>HPO<sub>4</sub>, 3.5 mM NaH<sub>2</sub>PO<sub>4</sub>, 100 mM glycine) performed three times for 10 min at room temperature. Blocked in immunofluorescence (IF) buffer (130 mM NaCl, 7 mM Na<sub>2</sub>HPO<sub>4</sub>, 3.5 mM NaH<sub>2</sub>PO<sub>4</sub>, 0.2% Triton X-100, 0.05% Tween-20) plus 3% BSA, 5% goat serum and 0.3% Triton X-100 for 2 hours at room temperature. Primary antibodies incubated overnight in blocking buffer (FSP1 1:250) at room temperature. IF buffer used for three 20 min washes. Secondary antibody diluted 1:500 in blocking buffer (Phalloidin 488 1:40 and DAPI added) and incubated at room temperature overnight. Fluorescence was imaged on Confocal Leica SP8 microscope.

### Multiphoton microscopy

Second harmonic generation images of H&E sections were taken using a Zeiss Axio Examiner Z1 microscope with 20X water immersion objective (1.0 NA DIC [UV] VIS-IR) as described (186). The SHG signal was obtained using a band pass cube of 380–430nm. Images were taken with a Coherent Chameleon Verdi laser at 820 nm wavelength. Z-stack images were taken with a 1 μm interval.

## Western Blot

Lung tissue was harvested and flash frozen in liquid nitrogen. Frozen tissue was cut into 2mm pieces and ground in glass mortar and pestle in 1mL of lysis buffer TNES buffer (50 mM Tris pH 7.5, 100 mM NaCl, 2 mM EDTA, 1% Nonidet P-40, 1X Roche Complete Protease Inhibitors, 10 mM NaF, 1 mM NaVO<sub>4</sub>, 2 mM sodium pyrophosphate, and 2 mM  $\beta$ -glycerophosphate). Mixture was further homogenized with a sonicator. Lysate was centrifuged and supernatant was collected. Protein assay and western blot were performed as described (53). Primary antibody, diluted in either 5% BSA in TBST (vimentin R28 Cell signaling 1:1000) or 5% milk in TBST (tubulin Millipore MAB1864 1:20:000, GAPDH CST 1:30,000) was added to membrane overnight. Secondary antibodies were incubated at a concentration of 1:1000 in 5% milk in TBST for 1 hour.

## Cell Culture

H460 lung cancer cell line was subcultured in RPMI 1640 media supplemented with 10% FBS, 1% penicillin/streptomycin and 1% kanamycin. Human lung adenocarcinoma cancer-associated fibroblasts were purchased from Vitro Biopharma and subcultured in MSC Gro VitroPlus III, Low Serum media supplemented with 1% penicillin/streptomycin and 1% kanamycin. All cells were cultured in a humidified chamber at 37°C with 5% CO<sub>2</sub>. CAF cells were purchased from Vitro Biopharma (Golden, CO) in 2017. H460 cells were a lab stock originally purchased from ATCC (Manassas, VA).



### Stable Cell Line Generation

For the production of stable vimentin knock-down cancer-associated fibroblasts, pLKO.1 vector and vimentin shRNA virus described previously (53) was added to cells 1:2 in media with 8ug/mL polybrene three times. Cells expressing the constructs were selected using Puromycin 2ug/mL treatment.

### 3D Spheroid Invasion Assay

Spheroids of H460s, CAFs, and H460/CAF 50/50 co-cultures were generated as described (20). Spheroids were collected and resuspended in 2.0mg/mL MatriGel (VWR) in 35mm Dish with 14mm bottom well (Cellvis) and a coverslip was attached with Vaseline. After 45min incubation at 37°C, 2mL of media was added. Images were taken at 0 and 24 hours on Olympus IX51 microscope. Spheroid invasion was quantified using ImageJ (NIH). For 3D immunofluorescence, spheroids were formed as described above. Each well of a 96 well flat-bottomed plate (Corning) was coated with 8mg/mL MatriGel. Spheroids were collected and resuspended in 2.0mg/mL MatriGel. After 45 min incubation at 37°C, 100uL of media was added. Spheroids were allowed to invade for 48 hours.

### PCR

Tissue was collected from candidate pups prior to weaning. Genomic DNA was extracted using Alkaline Lysis Buffer at 100°C for 45 minutes. A 40mM Tris-HCL Neutralization Buffer was then added and samples were stored at -20°C. PCR was

performed using a GoTaq Flexi system from Promega. Samples were run on Biorad iCycler at recommended annealing temperatures.

### Image Analysis

H&E and IHC stained tissue samples were imaged on the Zeiss Axioplan 2 widefield microscope or whole slides were scanned into ImageScope software. Immunofluorescence images were taken on the Confocal Leica SP8. All images were analyzed with ImageJ and Photoshop Elements. CellProfiler was used for fluorescent image quantification. Imaris software was used for vim/FSP1 colocalization analysis where a mask was generated for each marker and then a colocalization mask was generated from this. The 2D histogram was generated in Imaris by removing background levels of each marker. Pearson's coefficient was generated from the histogram. Imaris was also used for CAF cell size analysis.

### Tumor Histology

Stromal and tumor compartments in *KLV* mouse were identified by a board certified thoracic pathologist. *KLV* model tumor grading was performed as described (154).

### Statistics

P-values of significance were obtained using a Fischer's exact test or unpaired t test when comparing two groups (ie *KLV*<sup>+/+</sup> vs *KLV*<sup>-/-</sup> or metastatic vs non-metastatic). Data with more than two groups were analyzed by one-way ANOVA followed by

Tukey's multiple comparisons test. Analysis of vimentin IHC in patient samples was performed using Wilcoxon Rank Sum test. Kaplan-Meier curves were analyzed by Mantel-Cox and Gehan-Breslow-Wilcoxon tests.

### 3.3 Results

#### Generation of a *Kras*<sup>G12D</sup>/*LKB1*<sup>fl/fl</sup>/*Vim*<sup>-/-</sup> GEMM (*KLV*<sup>-/-</sup>)

Metastasis is well characterized in the *LSL-Kras*<sup>G12D</sup>/*LKB1*<sup>fl/fl</sup> (*KLV*<sup>+/+</sup>) model (20, 21), where approximately 52% of mice that develop primary lung tumors at 8-10 weeks also develop metastasis to mediastinal lymph nodes at 12-16 weeks (20). A whole-body *vimentin*<sup>-/-</sup> mouse (180) was crossed to this *KLV*<sup>+/+</sup> mouse to test the hypothesis that vimentin is necessary for metastatic disease. Through this cross a novel *LSL-Kras*<sup>G12D</sup>,*LKB1*<sup>fl/fl</sup>,*Vim*<sup>-/-</sup> (*KLV*<sup>-/-</sup>) mouse was generated (Supplemental Figure 3-1A) that lacks vimentin expression throughout and has the *LSL-Kras*<sup>G12D</sup>,*LKB1*<sup>fl/fl</sup> conditionally mutated in the lungs via intranasal delivery of lentiviral Cre recombinase. Disruption of the vimentin allele and lack of protein expression in the *KLV*<sup>-/-</sup> mouse was validated by RT-PCR, western blotting, and immunofluorescence (Supplemental Figure 3-1B-D). Disruption of one vimentin allele in the heterozygous *KLV*<sup>+/-</sup> mouse did not greatly reduce vimentin protein expression (Supplemental Figure 3-1C,D). These results demonstrate the development of a novel *KLV*<sup>-/-</sup> GEMM to probe the role of vimentin in lung adenocarcinoma metastasis.

### ***KLV*<sup>+/+</sup> and *KLV*<sup>-/-</sup> mice have a similar primary tumor burden**

*KLV*<sup>+/+</sup> and *KLV*<sup>-/-</sup> were infected intranasally with Cre lentivirus and a comparison of tumor burden between the two genotypes (either at 25 weeks or before due to morbidity) revealed no significant differences in primary tumor initiation or growth (Table 3-I and Figure 3-1A). In both genotypes, 100% of primary tumors were lung adenocarcinomas with no significant difference in tumor incidence (Table 3-1). Both *KLV*<sup>+/+</sup> and *KLV*<sup>-/-</sup> mice generated primary lung tumors (Figure 3-1A) without a significant difference in lung weight (Figure 3-1B) or tumor multiplicity (number of tumor foci per H&E slice) (Figure 3-1C). Tumor histology was similar across genotypes with both *KLV*<sup>+/+</sup> and *KLV*<sup>-/-</sup> mice developing tumors with and without invasive fronts (Figure 1D). Proliferative index using Ki-67 staining was also not significantly different between the two genotypes (Figure 3-1E, F). Based on these data, we conclude that vimentin loss does not impact primary lung tumor initiation or growth.

A Kaplan-Meier curve to clinical symptoms shows that *KLV*<sup>-/-</sup> mice have decreased survival compared to *KLV*<sup>+/+</sup> (Supplemental Figure 3-2). Stratification of *KLV* mice by genotype and lung weight demonstrate that morbidity of *KLV*<sup>-/-</sup> mice is less dependent on tumor burden than in the *KLV*<sup>+/+</sup> mice. These data are consistent with previous work that demonstrate increased morbidity in the *vimentin*<sup>-/-</sup> background when a disease state is induced (187).

### **Vimentin null mice have reduced metastatic disease and less focal invasion**

The *KLV*<sup>+/+</sup> model develops robust primary lung tumors and metastasis to the mediastinal lymph node (20, 21). We leveraged this phenotype to investigate how the

vimentin loss affects the metastatic potential of *Kras/Lkb1* co-mutated lung adenocarcinomas. Vimentin loss in *KLV<sup>-/-</sup>* mice results in 54% less mediastinal lymph nodes metastasis compared to *KLV<sup>+/+</sup>* mice (Figure 3-2A, B). In mice with clinical symptoms (respiratory distress, weight loss, hunching), the vimentin loss was associated with significantly less metastatic disease to the draining lymph nodes compared to *KLV<sup>+/+</sup>* mice (Figure 3-2C). In addition to decreased incidence of lymph node metastasis, vimentin loss in the *KLV<sup>-/-</sup>* is associated with significantly less invasive foci than *KLV<sup>+/+</sup>* mice tumors as measured by the number of invasive fields (defined as a field with focal invasion) per mouse (Figure 3-2D). To assess the impact of vimentin loss on tumor progression, primary tumors of *KLV<sup>+/+</sup>* and *KLV<sup>-/-</sup>* were graded on a scale of 1 to 4 with grade 1 tumors classified as atypical adenomatous hyperplasia and grade 4 tumors demonstrating stromal reaction in addition to irregular mitoses and invasive borders along lymphatic vessels. Higher tumor grade are also associated with more invasive and metastatic tumors (154). Based on this analysis, we found that *KLV<sup>+/+</sup>* mice developed significantly more high grade tumors than *KLV<sup>-/-</sup>* mice (Figure 2E) further supporting the claim that vimentin loss reduces metastatic disease and tumor progression. Taken together, these data show that vimentin is required for efficient metastasis in *Kras/Lkb1* co-mutated lung adenocarcinoma.

### **Vimentin is required for collective invasion pack (CIP) formation**

To determine vimentin localization within the primary tumor, vimentin immunohistochemistry (IHC) was performed on *KLV<sup>+/+</sup>* primary tumor samples (Figure 3A). The vimentin antibody was validated for specificity by IHC in vimentin null tissue and by western blot (Supplemental Figure 3-3). To our surprise, in *KLV<sup>+/+</sup>* samples,

vimentin expression was absent in tumor cells but present in the stromal niche often surrounding tumor cells that appear to have budded off from the primary tumor. We previously termed these tumor cell histologies collective invasion packs (CIPs) (20). CIPs are surrounded by vimentin-positive, elongated stromal cells that resemble fibroblasts in morphology (Figure 3-3A).

CIPs are positive for the lung adenocarcinoma marker pro-SPC (10) (Figure 3-3B), indicating their type II pneumocyte origin, retain epithelial morphology (non-elongated), and express E-cadherin (20), while lacking vimentin protein expression (Figure 3-3A). This pattern suggests that tumor cells within CIPs retain homotypic cell contacts and are likely not undergoing a traditional EMT. CIPs range in size from 5-25 cells (Figure 3-3C) and are found within this range in *KLV<sup>+/+</sup>* and *KLV<sup>-/-</sup>* primary tumor samples. CIP density in each genotype was assessed and these data show that *KLV<sup>-/-</sup>* mice have significantly less CIPs per invasive field than *KLV<sup>+/+</sup>* mice overall (Figure 3-3D). When CIP density is stratified by tumor grade (Figure 3E), high grade *KLV<sup>-/-</sup>* tumors have significantly less CIPs than high grade *KLV<sup>+/+</sup>* tumors indicating that vimentin is required to maintain CIP density in invading tumors.

To determine the role of CIPs in tumor progression and metastasis, CIP density and invasive area was stratified by extent of disease or tumor stage. These data demonstrate that CIPs are found in both early (non-metastatic) and late (metastatic) stage *KLV* tumors (Figures 3-3F, G) with significantly higher CIP density and invasion in late stage tumors.

To probe CIP biology, immunofluorescence of extracellular matrix (ECM) components was performed. Fibronectin staining reveals that cancer cells themselves are

negative for fibronectin, but fibronectin is expressed in the regions surrounding emerging CIPs at the invasive front of the primary tumor in both *KLV<sup>+/+</sup>* and *KLV<sup>-/-</sup>* samples (Figure 3-3H, Supplemental Figure 3-4A). Interestingly, fibronectin expression is lost in CIPs farther away from the primary tumor, suggesting that fibronectin may only be important for early invasion events (Figure 3-3H).

Second harmonic generation imaging was performed to assess the collagen ECM which showed high levels of aligned collagen at the invasive front of the primary tumor and surrounding CIPs in the *KLV* models (Figure 3-3I, Supplemental Figure 3-4B). This aligned collagen persisted at metastatic lymph nodes, indicating that collagen alignment and secretion is maintained at the distant metastatic site (Figure 3-3I). To probe cancer invasion and EMT, immunofluorescence of TGF $\beta$ 1 ligand was performed in primary tumor samples (Supplemental Figure 3-4C). High expression was observed in areas of focal invasion at or near the primary tumor indicating TGF $\beta$ 1 is promoting cancer invasion and progression in the *KLV* models without inducing some canonical EMT markers.

### **Vimentin+ cancer-associated fibroblasts surround CIPs**

To characterize vimentin positive cells surrounding CIPs, FSP1 (Fibroblast Specific Protein 1) and alpha-Smooth Muscle Actin ( $\alpha$ -SMA) were used to mark cancer-associated fibroblasts (CAFs) (79). Dual labeling of vimentin and FSP1 in *KLV<sup>+/+</sup>* primary tumor samples demonstrates that vim+ stromal cells are also FSP1+ (Figure 3-4A). FSP1+/vim+ cells are randomly localized within the primary tumor (Figure 4A left) but surround CIPs at sites of focal invasion (Figure 3-4A right). Quantitative analysis of

FSP1<sup>+</sup>/vim<sup>+</sup> cells surrounding CIPs show co-localization between vimentin and FSP1 (Pearson coefficient = 0.59; Figure 4B). IHC of serial sections show that vim<sup>+</sup> cells are also  $\alpha$ -SMA<sup>+</sup> (Supplemental Figure 3-5A). These data strongly suggest that vim<sup>+</sup> cells are cancer-associated fibroblasts (CAFs). FSP1<sup>+</sup> CAFs are found at the invasive fronts of both *KLV*<sup>+/+</sup> and *KLV*<sup>-/-</sup> primary tumors (Supplemental Figure 3-5B); however, the significantly greater extent of focal invasion in *KLV*<sup>+/+</sup> tumors (Figure 3-3D) indicates increased CAF recruitment in this model.

Since many tumor-promoting components of the tumor microenvironment express vimentin, several members of the microenvironment were probed within the *KLV* models, including macrophages, inflammatory cells, and vascular cells. Immunofluorescence of tumor-associated macrophages (TAMs) with F4/80 in *KLV*<sup>+/+</sup> and *KLV*<sup>-/-</sup> primary tumor samples show no significant difference in macrophage recruitment (Supplemental Figure 6). IHC of a Pan T-cell marker (CD3) and endothelial marker (CD31) also demonstrated no difference in recruitment of these factors (Supplemental Figure 3-7A, B). Taken together, these data indicate vimentin loss does not impede the recruitment of vascular or inflammatory cells to the primary tumor microenvironment.

To determine the relationship between CAF recruitment and metastatic disease, the presence or absence of CAFs was stratified by genotype and metastatic phenotype. These results show that 100% of metastatic mice contained CAFs at the primary tumor site (Figure 4C) but less than 50% of non-metastatic mice had CAFs recruited to the primary tumor in both *KLV*<sup>+/+</sup> and *KLV*<sup>-/-</sup> genotypes. Vimentin IHC identified that CAFs are also found surrounding CIPs at the metastatic lymph nodes demonstrating that CAFs are important components of the tumor microenvironment at the secondary site (Figure 3-



4D) and perhaps travel with tumor cells to the lymph node. These data suggest that CAF recruitment contributes to tumor metastasis by promoting CIP formation and facilitating metastasis to the secondary site.

### **Vimentin regulates CAF invasion and stroma-cancer cell crosstalk.**

To probe the mechanisms of the heterotypic tumor cell-CAF interactions and CAF recruitment found in the *KLV* models, *in vitro* studies were performed. Stable knockdown of vimentin was achieved in human lung adenocarcinoma CAFs via shRNA (Figure 3-5A, B). CAFs lacking vimentin (shVIM19 and shVIM22) were found to be significantly smaller than pLKO.1 vector control (Figure 3-5C, D). To test the hypothesis that vimentin depletion inhibits CAF invasion in the *KLV* models, 3D spheroid invasion assays were performed with pLKO.1 and shVIM CAFs embedded in matrigel (Figure 5E). Results show that shVIM CAFs invaded significantly less than pLKO.1 CAFs (Figure 3-5F), supporting the hypothesis that CAF motility is impaired with loss of vimentin in the *KLV* models.

Co-culture 3D spheroid invasion assays were then performed to assess heterotypic cancer-cell-CAF interactions (Figure 3-5G). Invasion analysis revealed that the addition of CAFs to spheroids of H460s (lung adenocarcinoma cell line) decreases circularity, a surrogate for collective invasion branching (i.e. increased circularity means less collective invasion packs; Supplemental Figure 3-8). Co-culture spheroids with shVIM CAFs exhibit significantly higher circularity (decreased branching) compared to those with pLKO.1 CAFs (Figure 3-5H). These data suggest impairment in shVIM CAFs to drive collective invasion. Immunofluorescence of FSP1 and actin in co-culture spheroids

(Figure 3-5I) show that CAFs facilitate collective invasion by leading chains of H460s into the surrounding ECM. CAFs lacking vimentin expression lose the ability to lead cancer cells out of the spheroid as evidenced by the decrease in invasive branches with CAFs leading the chain (Figure 3-5H). Together, these data indicate that vimentin contributes to both homotypic and heterotypic collective invasion.

**Vimentin is expressed in cancer-associated fibroblasts of lung cancer patient CIPs which lack EMT in tumor cells.**

To analyze the clinical relevance of the CIP phenotype found in the *KLV* models, vimentin staining in human lung adenocarcinoma patients with varying genetic subtypes was performed to assess vimentin localization, invasive histology, and EMT (Figure 3-6A). A similar pattern to the *KLV*<sup>+/+</sup> mouse samples was observed in human tissues, where the vast majority of patient samples (25 of 26) expressed vimentin in the mesenchymal stroma and not within the collectively invading cancer cells (Figure 3-6A). Vimentin intensity was scored and was significantly higher in stromal cells compared to tumor cells across the majority of samples, independent of driver mutation (Figure 6B). Furthermore, there were no observable differences in vimentin stromal Q score (product of stain intensity and percent of vimentin-positive cells in stromal compartment) based upon genetic subtype (Supplemental Figure 3-8).

Since tumor cells lacked vimentin staining, the epithelial cell marker, E-cadherin, was used to further probe for evidence of EMT. Tumor cells within patient CIPs were E-cadherin positive (20) (Figure 3-6C) and pro-SPC positive (Figure 3-6D), which is also consistent with the data in the *KLV* model. Immunofluorescence of FSP1 was performed

to determine if patient CIPs are surrounded by CAFs similar to the *KLV* model. These data show an expression pattern consistent with the *KLV* model in which FSP1+ CAFs surround CIPs of tumor cells (Figure 3-6E). Taken together, these data suggest that in human lung adenocarcinoma samples tumor cells are not undergoing EMT but instead contain invasive CIPs surrounded by vim+/FSP+ CAFs.

To determine the clinical relevance of CIPs, CIP density was stratified by in human lung adenocarcinoma patient samples (Figure 3-6F, G). Stage 1 patients exhibit significantly higher CIP density than higher stage patients indicating an early dissemination of CIP and CAF invasion, though there are still CIPs present in late stage patients ( $p < 0.05$ ). Taken together, the formation of CIPs in early stage tumors supports an early dissemination model (188) in which metastatic seeds such as CIPs disseminate early during tumor progression.

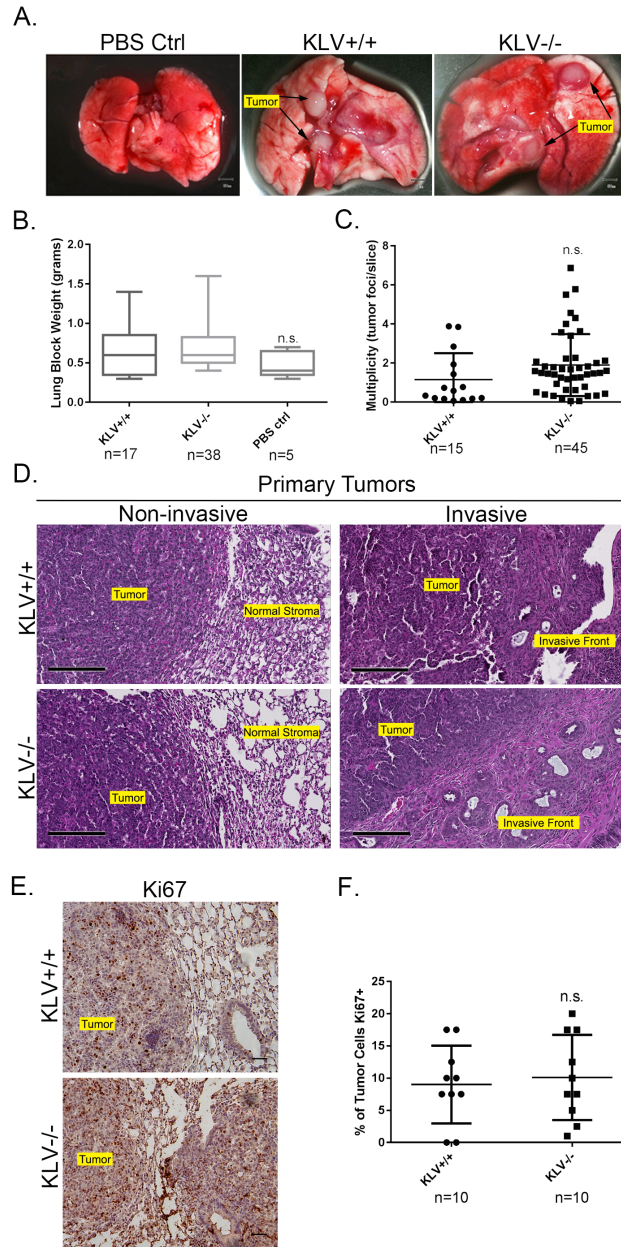


**Figure 3-1. KLV+/+ and KLV-/- mice have a similar primary tumor burden**

(A) Representative images of PBS control, *KLV+/+*, and *KLV-/-* lungs (scale=50mm). (B) Graphs showing weight of PBS control, *KLV+/+* and *KLV-/-* lungs. Statistical significance was determined by one-way ANOVA and Tukey’s multiple comparisons test ( $p < 0.05$ ). (C) Tumor multiplicity of *KLV+/+* and *KLV-/-* mice quantified as the number of tumor foci per H&E lung slice. Statistical significance was determined by unpaired t test ( $p < 0.05$ ). (D) Representative H&E sections of *KLV+/+* and *KLV-/-* primary tumors (scale = 200 $\mu$ m). (E) IHC of Ki67 in *KLV+/+* and *KLV-/-* primary tumors. (F) Quantification of percent of Ki67 positive tumor cells. Statistical significance was determined by unpaired t test ( $p < 0.05$ )

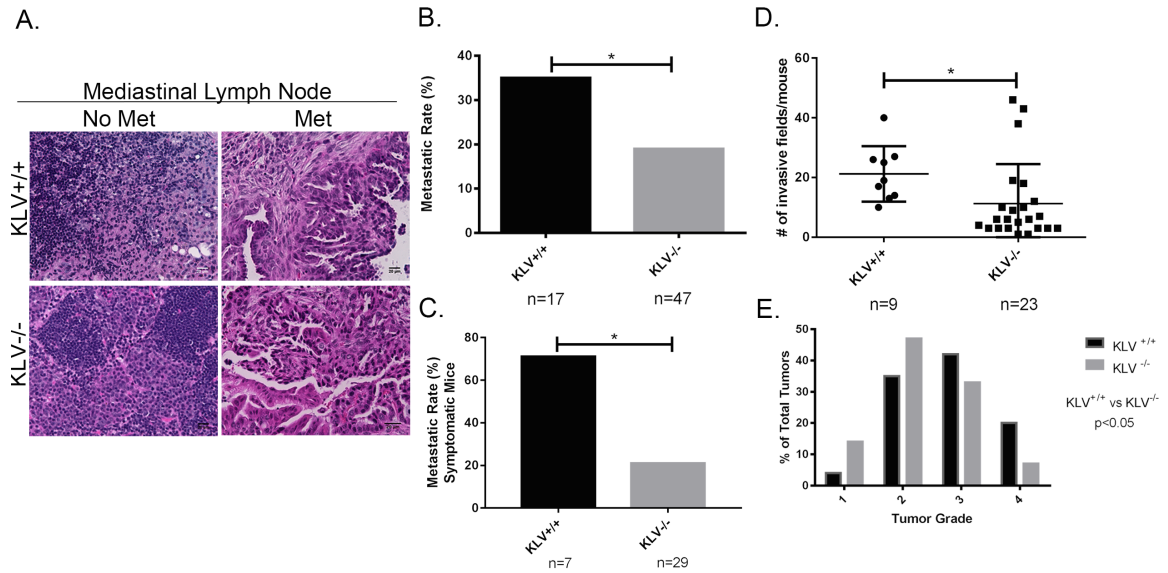


**Figure 3-2. Vimentin depletion inhibits invasion and metastasis.**

(A) Representative H&E images of lung draining lymph nodes of LV-CRE infected mice (scale= 20μm). (B) Metastatic incidence by *KLV* genotype. Statistical significance was determined by Fisher's exact test ( $p < 0.05$ ). (C) Metastatic incidence of mice sacrificed prior to 25-week endpoint due to lung cancer symptoms. Statistical significance was determined by Fisher's exact test ( $p < 0.05$ ). (D) Quantification of invasive fields per mouse by genotype. Statistical significance was determined by unpaired t test ( $p < 0.05$ ). (E) *KLV* tumor grading by genotype. Statistical significance was determined by Chi-square test ( $p < 0.05$ )

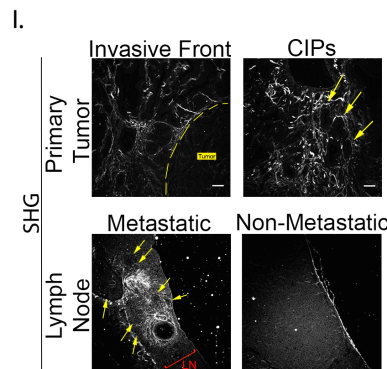
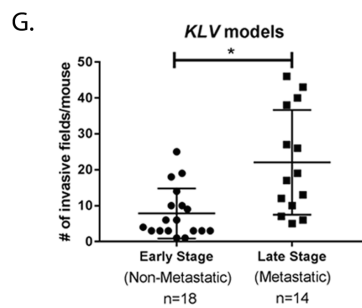
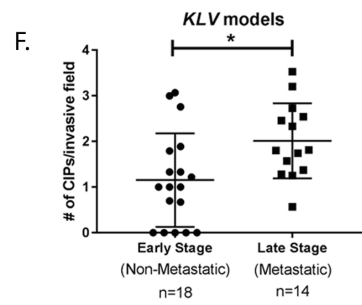
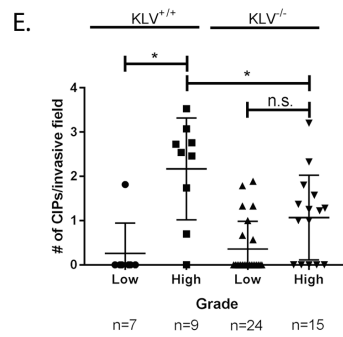
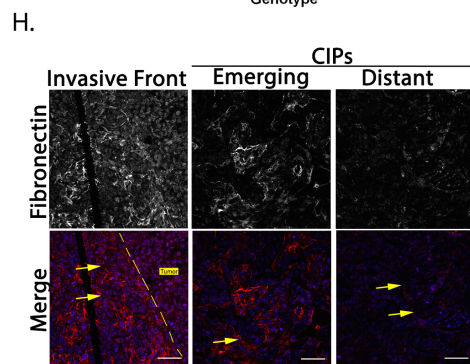
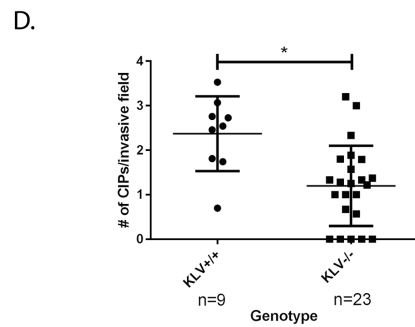
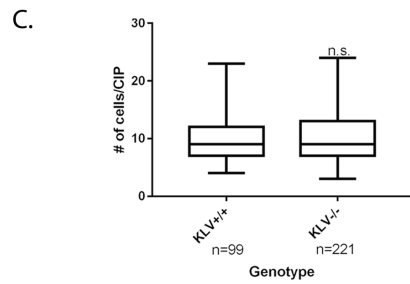
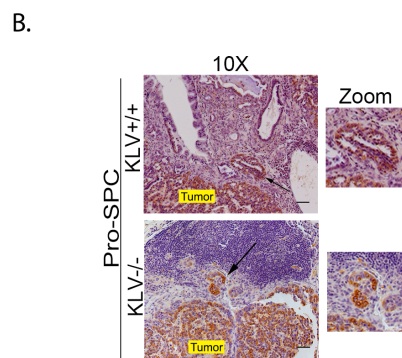
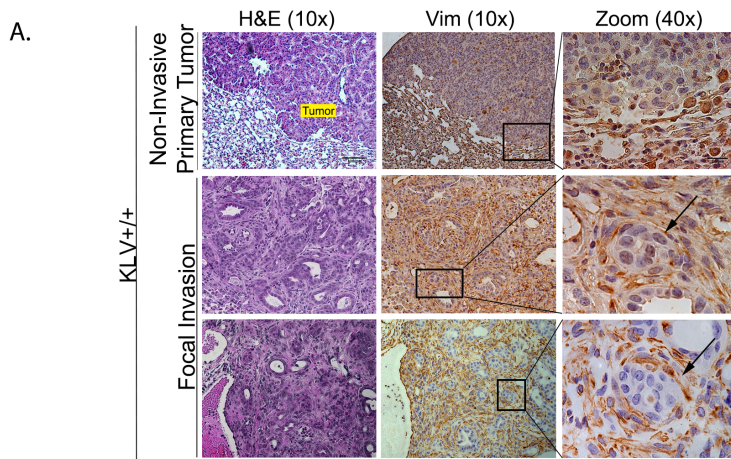


**Figure 3-3. Vimentin is required for collective invasion pack (CIP) formation.**

(A) Immunohistochemical staining of vimentin in *KLV*<sup>+/+</sup> and *KLV*<sup>-/-</sup> primary tumors with (10x scale = 100 $\mu$ m, 40x = 20 $\mu$ m). (B) Representative Pro-SPC stained sections of *KLV*<sup>+/+</sup> and *KLV*<sup>-/-</sup> primary tumors with CIPs marked by black arrows. (C) Quantification of the number of cells per CIP in both *KLV*<sup>+/+</sup> and *KLV*<sup>-/-</sup> mice. Statistical significance determined by unpaired t test ( $p < 0.05$ ). (D) Quantification of CIPs per invasive field in *KLV*<sup>+/+</sup> and *KLV*<sup>-/-</sup> mice. Statistical significance determined by unpaired t test ( $p < 0.05$ ). (E) CIPs per invasive field stratified by genotype and tumor grade. Statistical significance determined by ANOVA and Tukey's multiple comparisons test ( $p < 0.05$ ). (F) Quantification of CIPs per invasive field stratified by metastatic phenotype in *KLV* models ( $p < 0.05$ ). (G) Quantification of invasive fields by metastatic phenotype in *KLV* models. Statistical significance determined by unpaired t test ( $p < 0.05$ ). (H) Immunofluorescence of fibronectin in *KLV* primary tumor samples at the invasive front, emerging from the primary tumor, and at sites distant from the primary tumor. Yellow arrows mark CIPs with invasive front marked by dashed line (scale = 50 $\mu$ m). (I) Second harmonic generation imaging of collagen in *KLV* samples at the invasive front and surrounding CIPs in both primary tumor and metastatic lymph node. Yellow arrows mark CIPs with invasive front marked by dashed line (scale= 50  $\mu$ m).

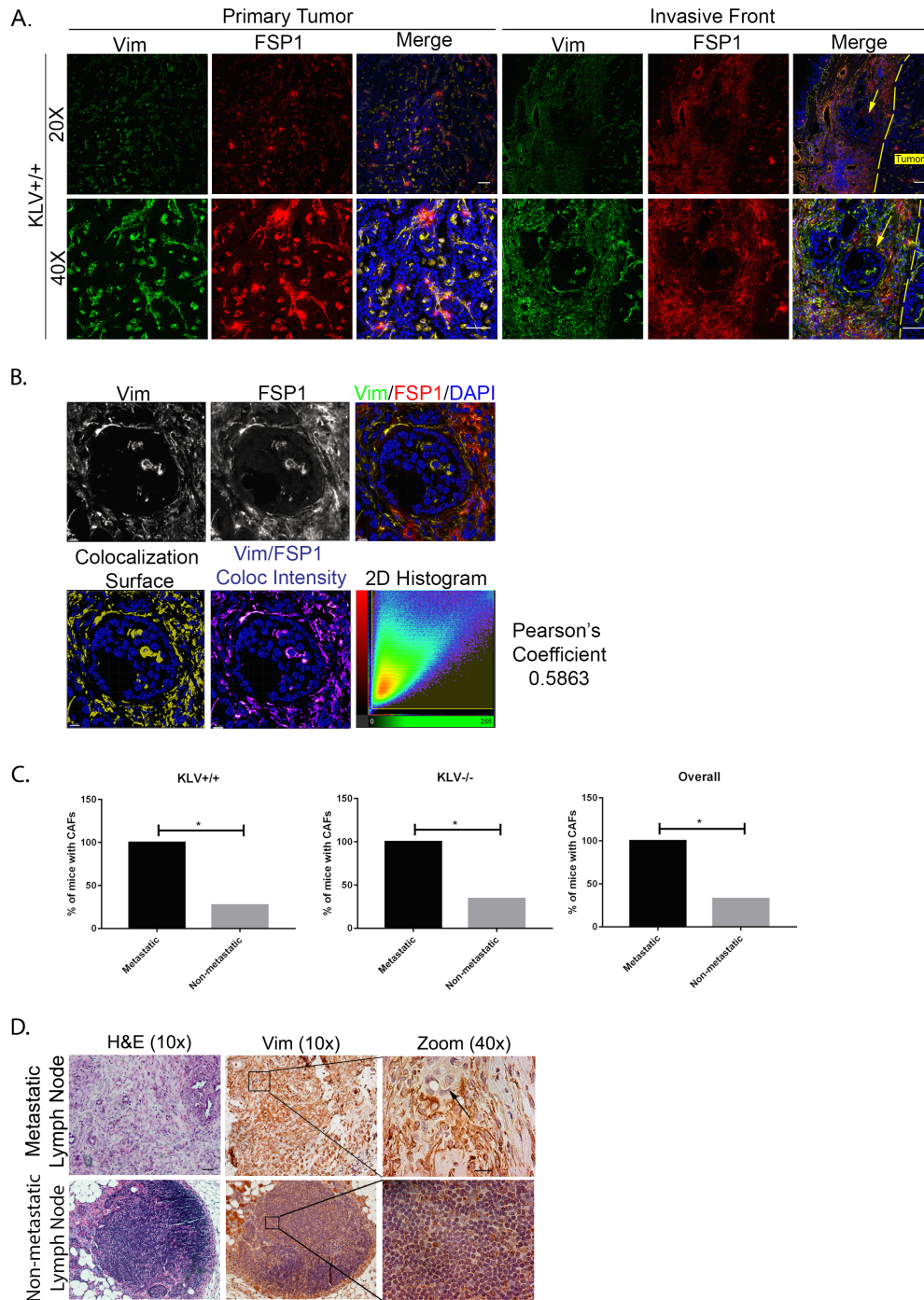


**Figure 3-4. Vimentin+ cancer-associated fibroblasts surround CIPs.**

(A) Immunofluorescence of vimentin (488) and FSP1 (555) on primary tumors of KLV+/+ mice (scale = 50 $\mu$ m). (B) Colocalization of vimentin and FSP1 staining (scale= 10 $\mu$ m). (C) Quantification of percent of mice of each genotype with CAFs stratified by metastatic or non-metastatic phenotypes. (D) Immunohistochemical staining of vimentin in the metastatic and non-metastatic lymph nodes (scale bars 10x= 100 $\mu$ m, 40x= 20 $\mu$ m)



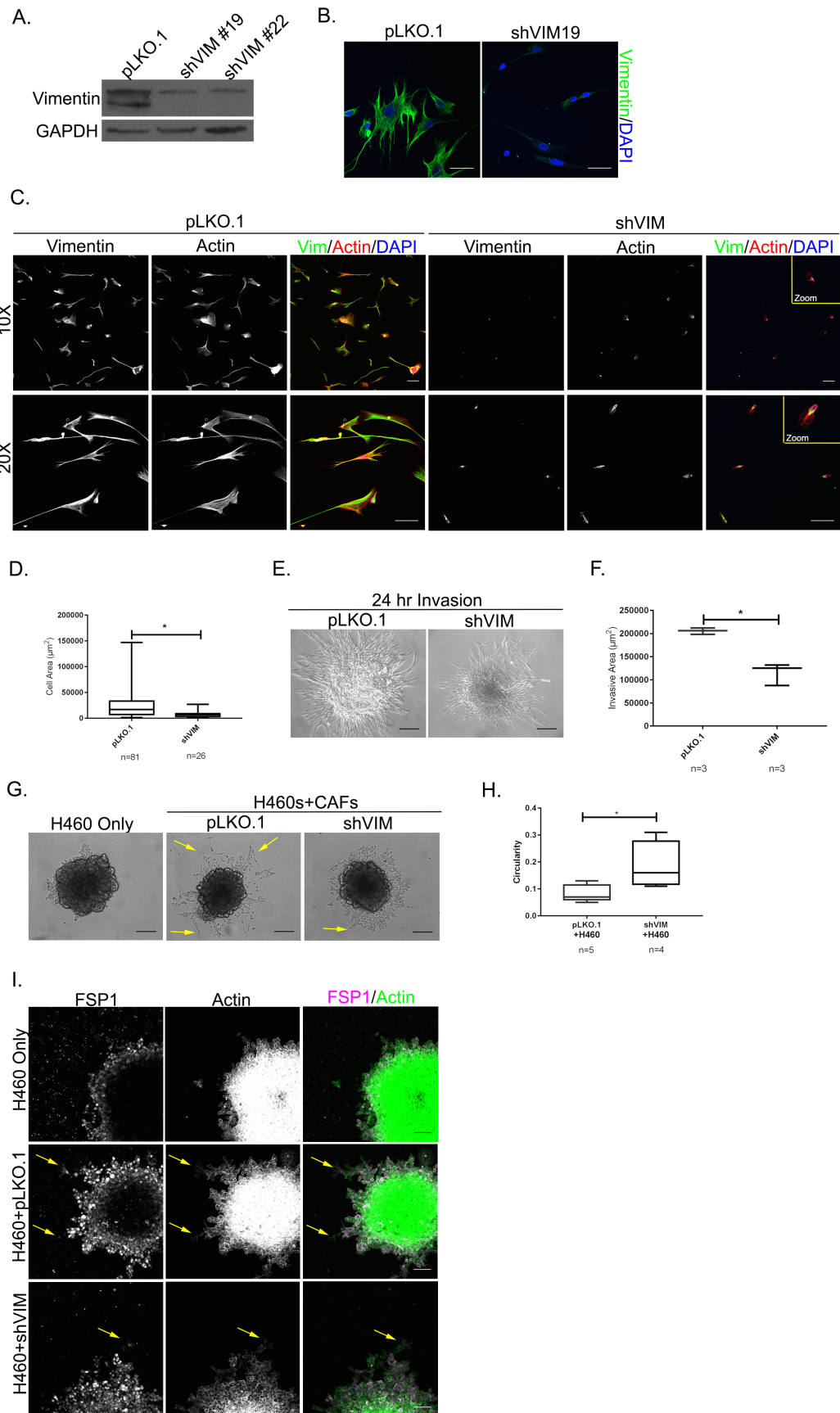


**Figure 3-5. Vimentin regulates CAF invasion and stroma-cancer cell crosstalk.**

(A) Western blot demonstrating generation of shVIM CAFs with two different shRNA clones. (B) Immunofluorescence of vimentin in pLKO.1 and shVIM19 CAFs (scale = 50 $\mu$ m). (C) Immunofluorescence of actin and vimentin in pLKO.1 and shVIM CAFs demonstrating cell size (10x scale= 100 $\mu$ m, 20x scale= 100 $\mu$ m). (D) Quantification of cell area of pLKO.1 and shVIM CAFs. Significance determined by unpaired t test ( $p < 0.05$ ). (E) Representative images of spheroid invasion assay with pLKO.1 and shVIM CAFs in matrigel (scale = 100 $\mu$ m). (F) Quantification of invasive area in spheroid invasion assay. Significance determined by unpaired t test ( $p < 0.05$ ). (G) Representative images of coculture spheroid invasion assay with H460 lung cancer line alone or in combination with pLKO.1 or shVIM CAFs (scale = 100 $\mu$ m). (H) Circularity of invasive areas in coculture spheroids with pLKO.1 or shVIM CAFs. Value of 1= perfect circle. Significance determined by unpaired t test ( $p < 0.05$ ). (I) Representative images of immunofluorescence of FSP1 and phalloidin in coculture spheroids. Yellow arrows mark FSP1+ CAFs leading invasive chains of H460s (scale = 100 $\mu$ m).

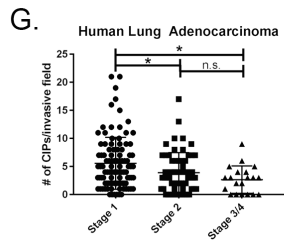
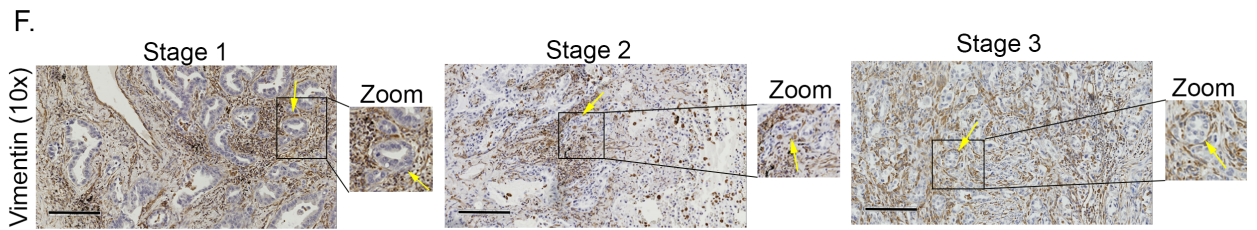
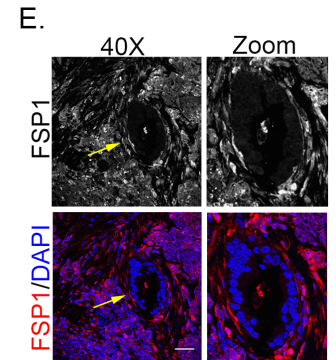
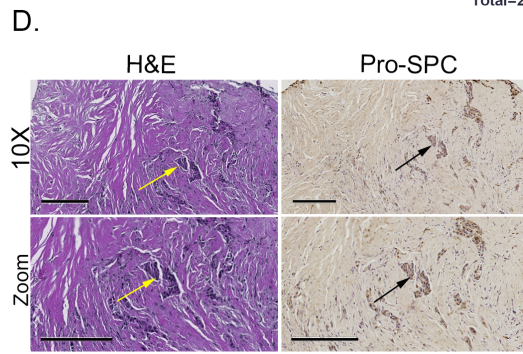
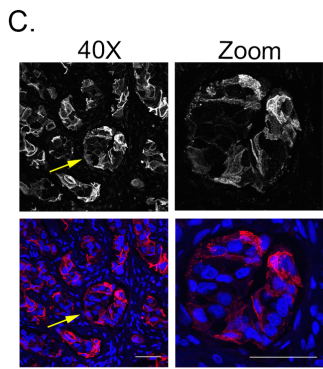
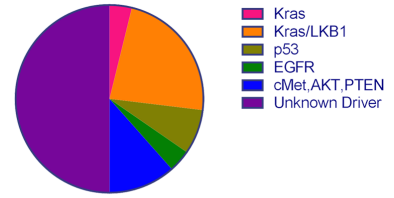
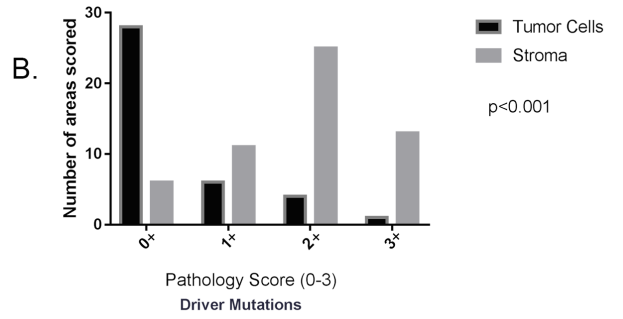
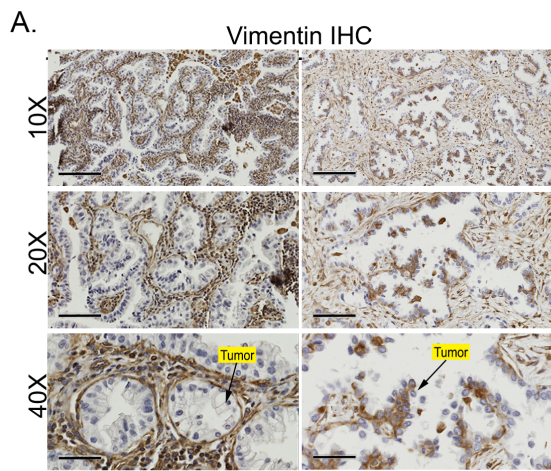


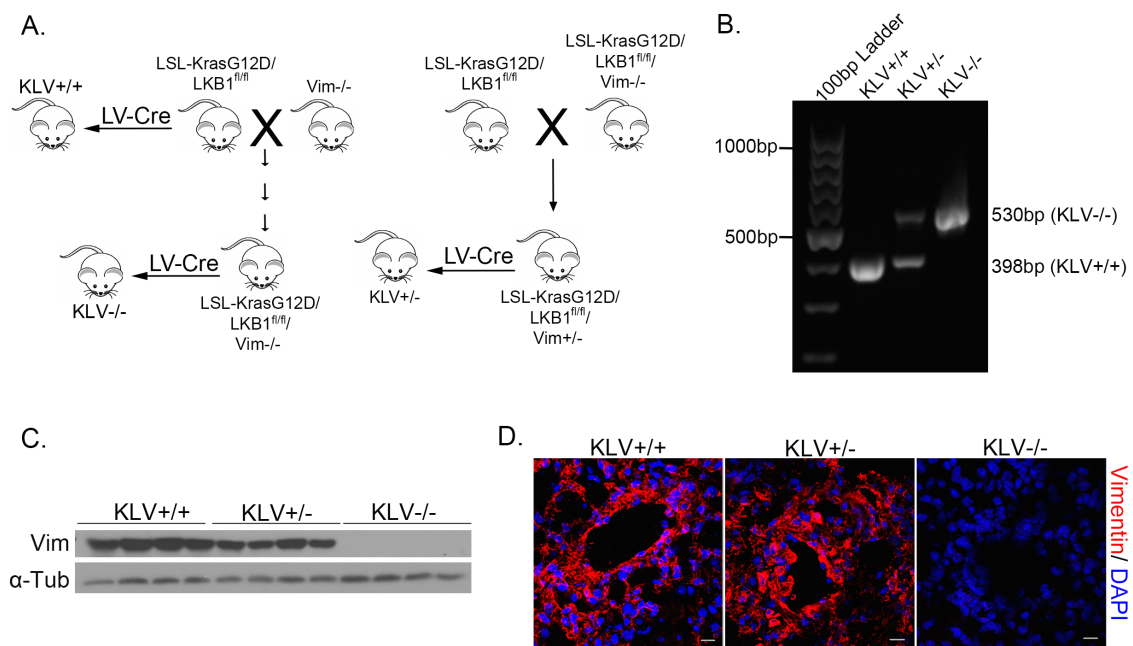
**Figure 3-6. Vimentin is expressed in cancer-associated fibroblasts of lung cancer patient CIPs, which lack EMT in tumor cells.**

(A) Representative images of patient primary tumor samples stained for vimentin by immunohistochemistry (scale bars 10x = 200 $\mu$ m, 20x = 100 $\mu$ m, 40x = 50 $\mu$ m). (B) Quantification of vimentin staining in tumor and stromal compartments. Pie chart of driver mutations in patient samples stained for vimentin. Statistical analysis was conducted using SAS Version 9.4. For the ordinal variable, frequency and average rank are calculated and presented. The univariate association of staining and different group, i.e., tumor cell and stroma was detected by Wilcoxon Rank Sum test. (C) Representative images of E-cadherin immunofluorescence of human lung adenocarcinoma sample marking collective invasion packs of tumor cells (40x= 50 $\mu$ m). (D) H&E and SPC staining of adenocarcinoma samples. CIPs marked with arrows (scale= 200 $\mu$ m). (E) Immunofluorescence of FSP1 on Kras/LKB1 patient sample. CIP marked with an arrow (scale = 50 $\mu$ m). (F) Representative images of human lung adenocarcinoma samples stained for vimentin at stages 1-3. (G) CIPs per invasive field by stage in human lung adenocarcinoma samples. Statistical significance determined by ANOVA with Tukey's multiple comparisons test ( $p < 0.05$ )

## Chapter 3 Supplemental Figures

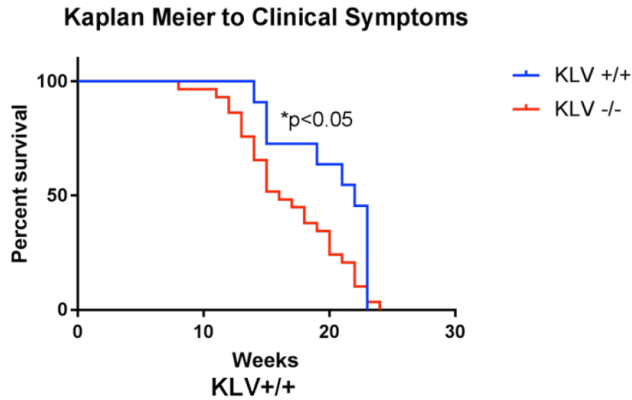
Genotype	Primary Tumor Rate	Adenocarcinoma Histology
$KLV^{+/+}$	17/26 (66%)	17/17 (100%)
$KLV^{-/-}$	47/70 (67%)	47/47 (100%)

Table 3-1. Infection rate and histology of lentiviral-Cre treated mice of both  $KLV^{+/+}$  and  $KLV^{-/-}$  mice

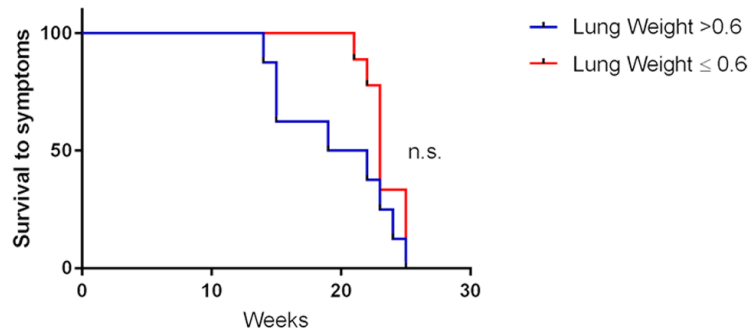


**Supplemental Figure 3-1. Generation of a *LSL-KrasG12D/LKB1fl/fl/Vim-/-* GEMM (*KLV-/-*).** (A) Breeding scheme used to generate *KLV-/-* and *KLV+/-* mice. (B) PCR genotyping results showing disrupted alleles in *KLV+/-* and *KLV-/-* mice. (C) Western blot showing vimentin expression in the *KLV+/+*, *KLV+/-*, and *KLV-/-* mice. (D) Immunofluorescence of vimentin (red) in *KLV+/+*, *KLV+/-*, *KLV-/-* mice (scale=20 $\mu$ m).

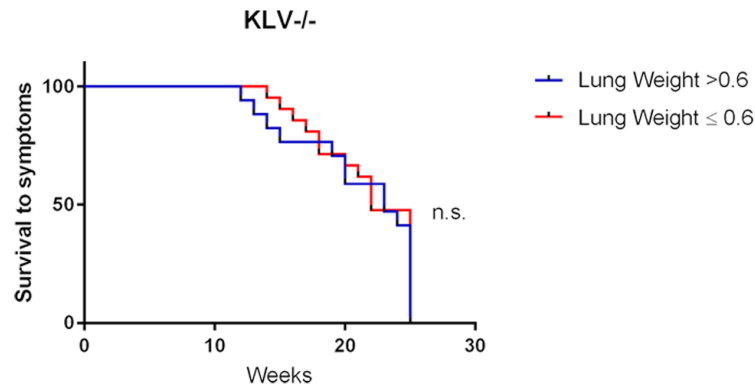
A.



B.

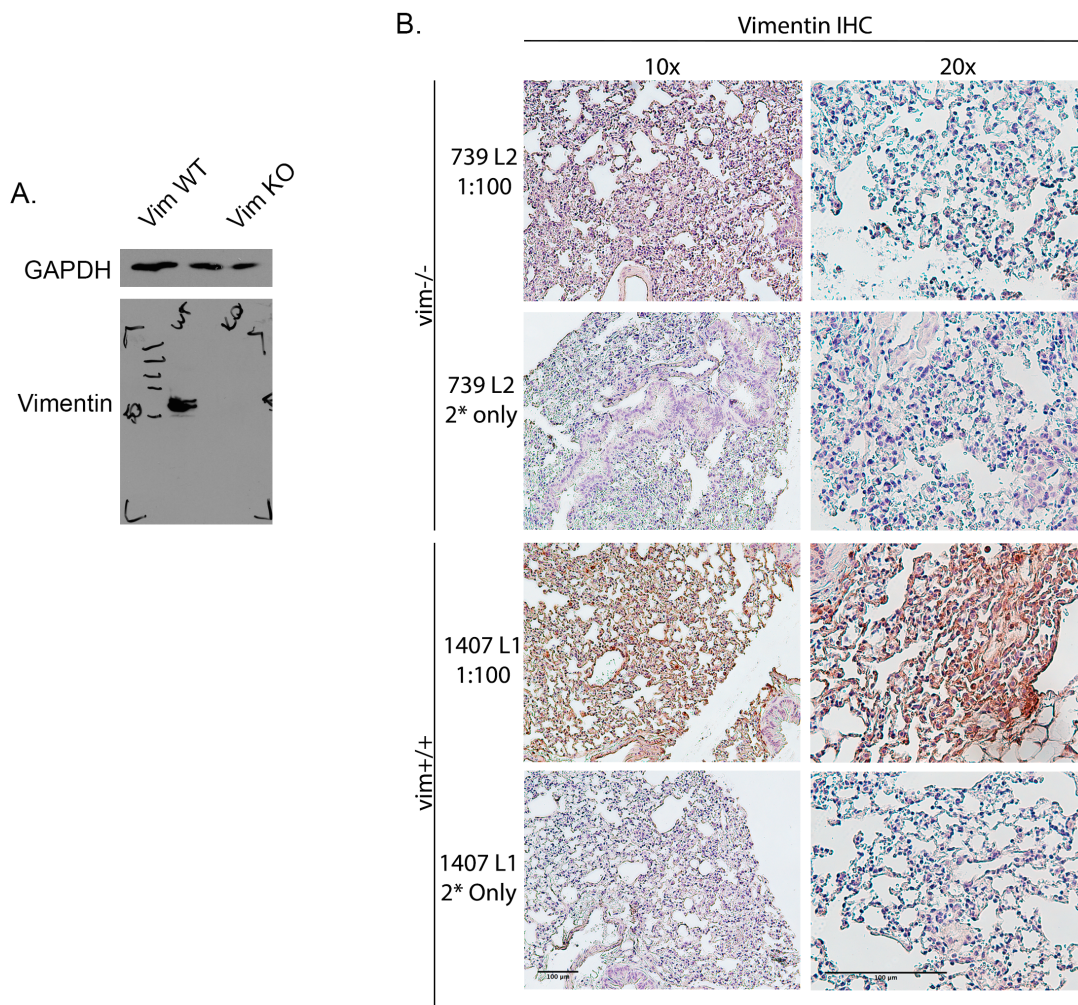


C.

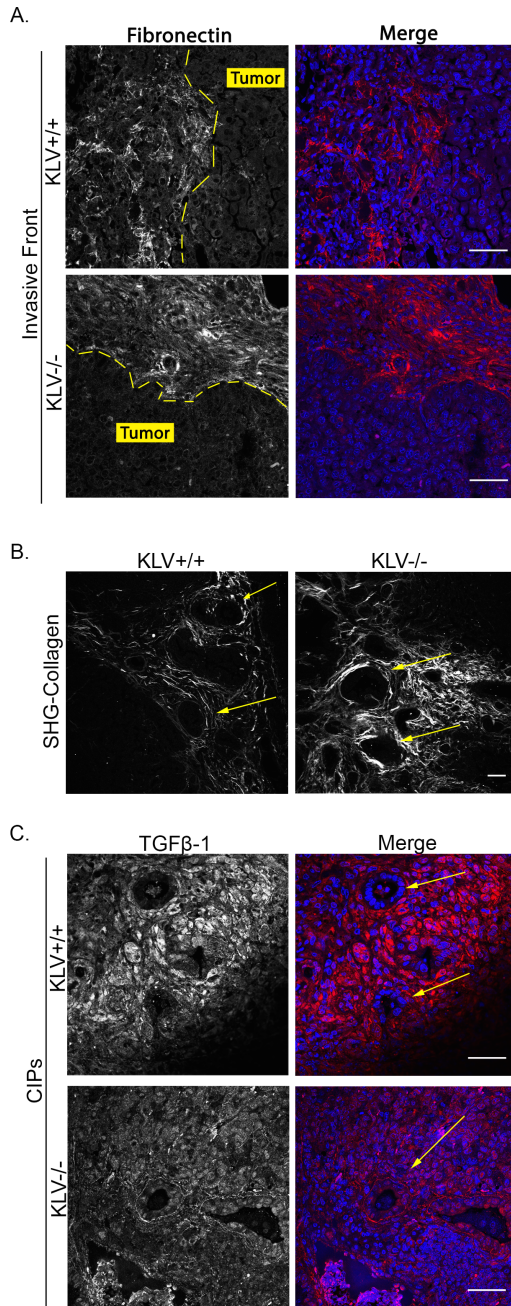


**Supplemental Figure 3-2. KLV model survival analysis** (A) Kaplan Meier to Clinical Symptoms of *KLV*<sup>+/+</sup> and *KLV*<sup>-/-</sup> mice. *KLV*<sup>+/+</sup> median survival was 22 weeks and *KLV*<sup>-/-</sup> median survival was 16 weeks. (B) Kaplan-Meier to clinical symptoms of *KLV*<sup>+/+</sup> and *KLV*<sup>-/-</sup> mice stratified by lung weight. Lung blocks less than 0.6g were below average (0.6g) and lung blocks 0.6g or greater were considered to be average or above average. Statistical significance determined by Mantel-Cox and Gehan-Breslow-Wilcoxon tests.



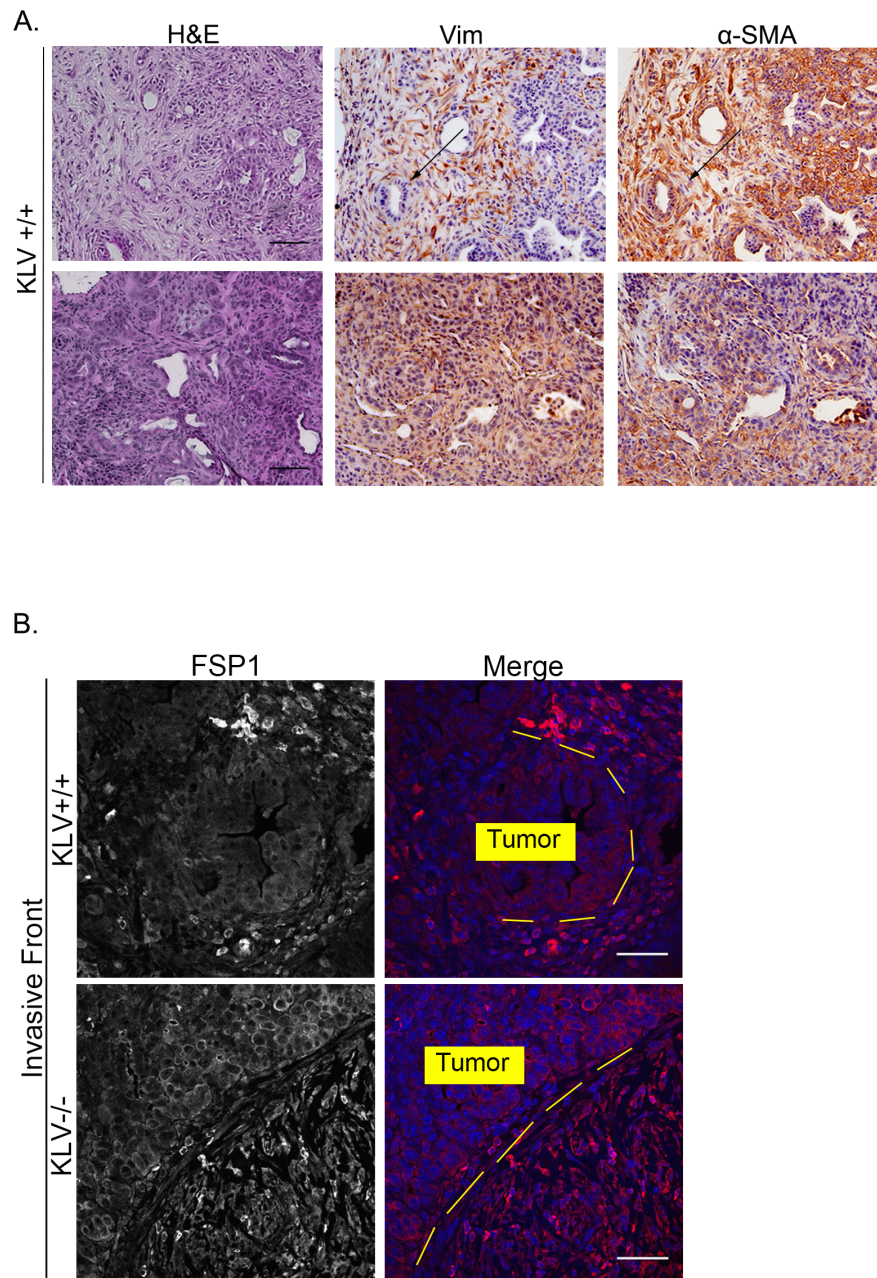


**Supplemental Figure 3-3. Vimentin antibody validation.** (A) Western blot of vimentin WT and KO cells. (B) Immunohistochemistry of vimentin WT and KO lung tissue. Scale bars 100 $\mu$ m.

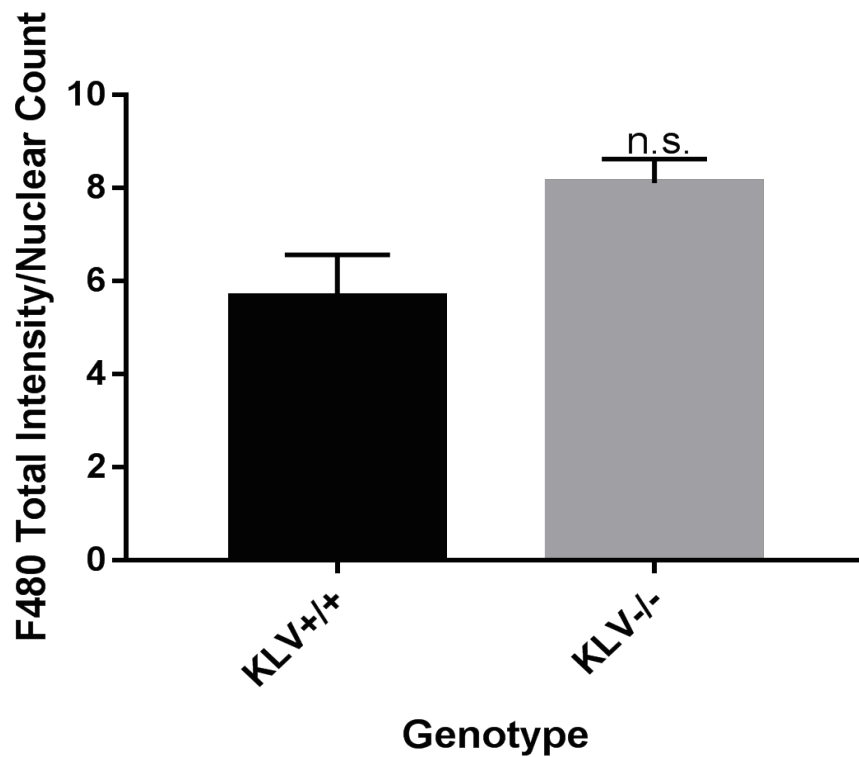


**Supplemental Figure 3-4. CIP biology is similar in both *KLV+/+* and *KLV-/-* tumors.**

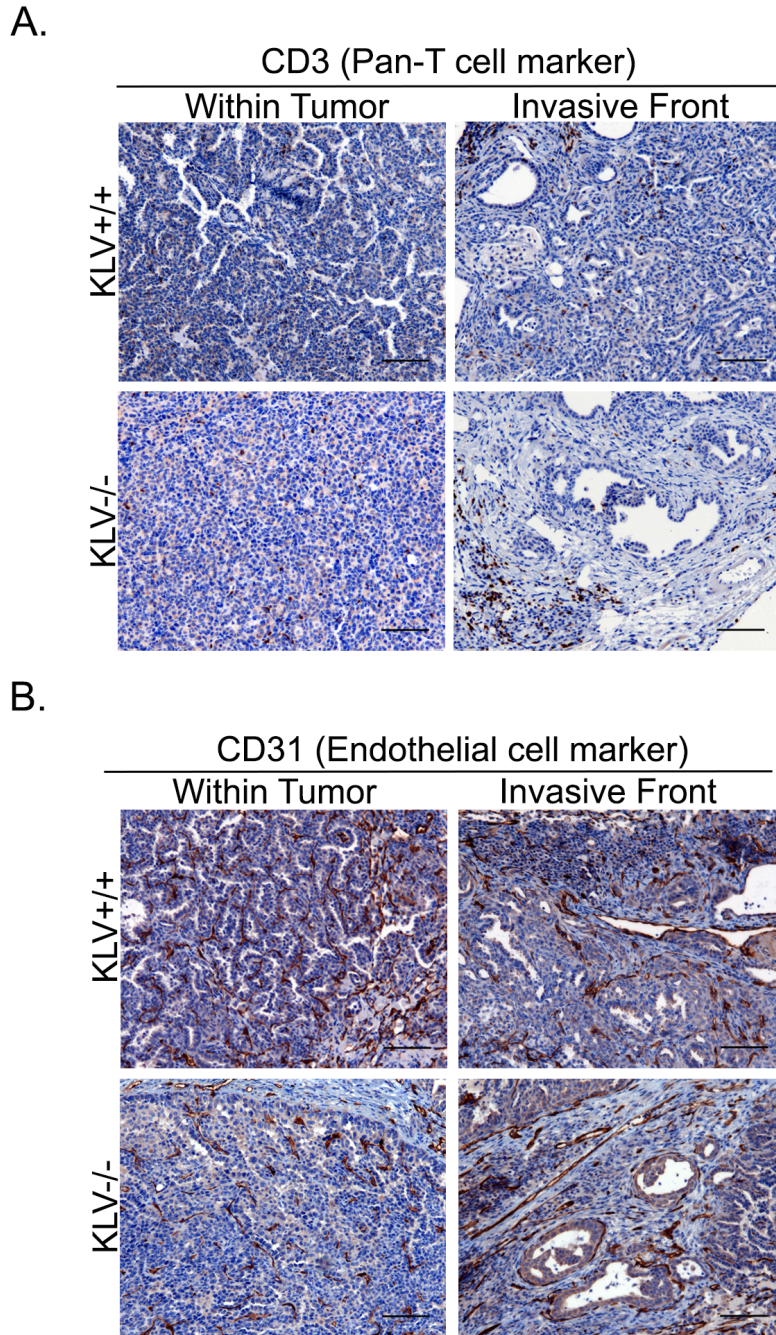
(A) Immunofluorescence of fibronectin shows secretion at the invasive front of both *KLV+/+* and *KLV-/-* primary tumors. (scale= 50μm). (B) Second Harmonic Generation shows collagen surrounding CIPs in both *KLV+/+* and *KLV-/-* samples (scale= 50μm). (C) Immunofluorescence of TGFβ-1 shows secretion in both *KLV+/+* and *KLV-/-* samples (scale= 50μm).



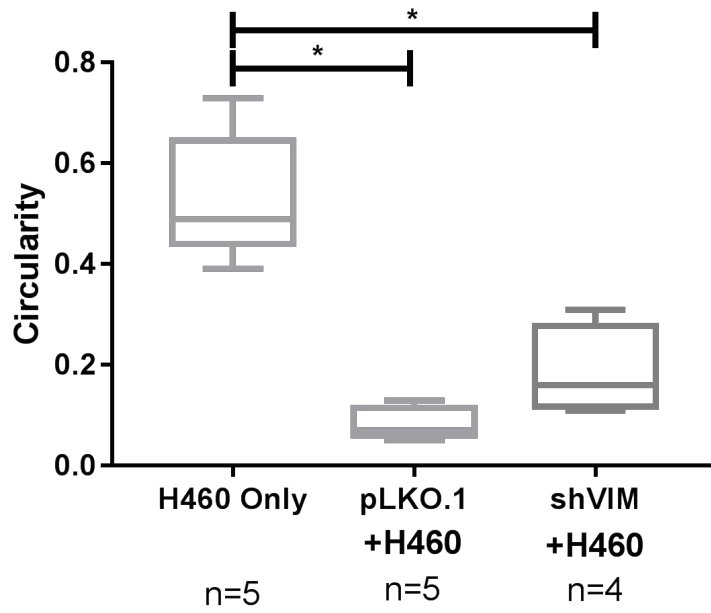
**Supplemental Figure 3-5. CAFs are present at the invasive front** (A) IHC of serial sections showing *KLV*<sup>+/+</sup> CAFs express both vimentin and  $\alpha$ -Smooth Muscle Actin. Black arrows indicate CIPs (10x scale= 50 $\mu$ m). (B) Immunofluorescence of FSP1 shows CAFs are present in both *KLV*<sup>+/+</sup> and *KLV*<sup>-/-</sup> invasive fronts (yellow dash line, scale= 50 $\mu$ m).



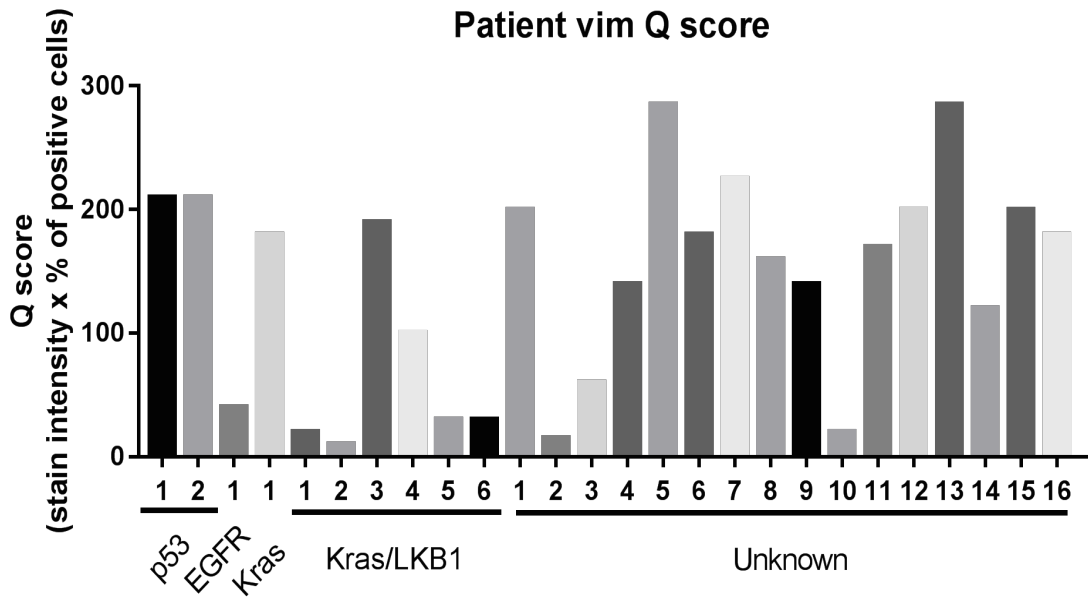
**Supplemental Figure 3-6. Macrophage recruitment is similar in both *KLV* models,** Quantification of macrophages in *KLV*<sup>+/+</sup> (n=2) and *KLV*<sup>-/-</sup> (n=2) mice by F480 immunofluorescence. Graph shows mean +/- standard deviation. Significance determined by unpaired t-test



**Supplemental Figure 3-7. Probing members of the tumor microenvironment.** (A) Immunohistochemistry for CD3 (Pan-T cell marker) shows no difference in T cell recruitment between KLV genotypes. (B) Immunohistochemistry for CD31 (Endothelial cell marker) shows no difference in vasculature between KLV genotypes.



**Supplemental Figure 3-8. Circularity of invasive areas in 3D spheroid assay.** Statistical significance determined by one-way ANOVA and multiple comparison test. (p<0.05)



**Supplemental Figure 3-9. Vimentin pathology Q score (staining intensity X percent of positive cells)**

### 3.4 Discussion

Vimentin expression has historically correlated with increased metastatic potential across numerous solid tumor types (116, 189); however, a functional role for vimentin in cancer progression has yet to be elucidated. Data from the *KLV*<sup>-/-</sup> GEMM show that vimentin is required for metastasis and progression but not primary tumor formation, whereby *KLV*<sup>-/-</sup> mice had less mediastinal lymph nodes metastasis, less invasive foci, and lower grade tumors compared to their *KLV*<sup>+/+</sup> counterparts (Figures 3-1 and 3-2); therefore, this supports a model that vimentin is more than an EMT biomarker and plays a functional role in lung adenocarcinoma invasion and metastasis.

EMT has been the canonical mechanism (38) for how cancer cells lose their epithelial morphology (174), invade through the basement membrane, and navigate the surrounding microenvironment (173, 190); however, this model is challenged by studies showing a more epithelial and collective-based migration by tumor cell clusters or packs (20, 191). The data presented here support the concept that a classical EMT does not occur in the majority of lung adenocarcinoma patients or in the lung adenocarcinoma *KLV* GEMM, but rather cancer cells undergo epithelial-like collective invasion and are surrounded by vim+/FSP1+ CAFs (Figures 3-3 and 3-4). Across 96% of lung adenocarcinoma patient samples tested (n=26), independent of driver mutation, vimentin was expressed in CAFs surrounding epithelial CIPs and only rarely in the tumor cells (Figure 6). Similarly, vimentin was not expressed within the tumor cells of the *KLV*<sup>+/+</sup> GEMM, and only in the CAFs surrounding collective invasion packs at the primary tumor site and at secondary metastatic lymph nodes (Figure 3-3 and 3-4). This supports



the concept that malignant cancer cells are not undergoing EMT but partnering with vim+/FSP1+ CAFs to potentially co-metastasize to a secondary site (64). This finding is consistent with studies demonstrating that clusters of circulating tumor cells have a metastatic potential up to 50 times higher than that of single circulating tumor cells (60), suggesting that tumor cell cooperativity can lead to greater metastatic success. Furthermore, these heterotypic CAF-CIP clusters are enriched in early stage lung adenocarcinoma patient samples (Figure 6), indicating potential early dissemination (188, 192) of metastatic seeding.

Investigation of the role of vimentin within CAFs in homotypic and heterotypic cell cultures demonstrates that vimentin drives not only CAF invasion, but also the formation and maintenance of heterotypic collective invasion chains (Figure 5). We show that the ability of vimentin-depleted CAFs to form heterotypic invasive chains is significantly impaired compared to their wild-type counterparts. These data suggest that intact vimentin function is important for heterotypic collective invasion and would be consistent with impaired CIP formation in the *KLV<sup>-/-</sup>* mice.

Taken together, our data support a model in which vimentin is required for lung cancer invasion and metastasis by facilitating CIP formation via regulation of CAF invasion and function. This supports the claim that there are early stage, epithelial and collective modes of metastasis that drive cellular escape from the primary tumor and require vimentin-positive CAFs.

## **Chapter 4: Discussion of Dissertation**

## 4. Discussion of Dissertation

### 4.1. Vimentin is identified as a key player in lung cancer invasion and metastasis

Tumors are opportunistic. When a tumor has depleted all of the resources in the primary organ it must find a new source of oxygen and nutrients at a secondary site. The tumor will use whatever means necessary to escape the hypoxic tumor microenvironment in search of a chance at survival. This metastatic process accounts for 90% of cancer-related deaths; however, the exact mechanisms by which cancer cells escape the primary tumor and colonize secondary organs remain poorly understood. As the canonical epithelial to mesenchymal transition (EMT) continues to be investigated (177), alternative models of tumor cell escape, such as collective invasion, are gaining support (47, 193).

The data presented in this thesis explore functional roles for a canonical EMT marker, vimentin, in cancer cell invasion and metastasis. Though there are extensive studies demonstrating a correlation between vimentin expression and metastatic potential (116, 189) as well as mesenchymal cell morphology (130), the functional role of vimentin within these contexts has been severely understudied.

Our initial findings, presented in Chapter 2, propose a model in which vimentin enters focal adhesion sites to promote focal adhesion assembly and stability via VAV2-Rac1-FAK signaling in lung cancer cell lines. This was the catalyst for investigating whether vimentin is necessary for metastasis *in vivo* in the context of the *Kras/LKB1* lung cancer metastasis mouse model. These results, presented in Chapter 3, identified that vimentin is necessary for metastasis to occur and revealed a shift in vimentin function

and expression, within the GEMM, from cancer cells to the tumor microenvironment. Taken together, these data demonstrate that vimentin is not only a biomarker of cancer metastasis but also a key player in the early invasive steps of the metastatic cascade.

#### **4.2. A novel mechanism of vimentin-mediated cell adhesion *in vitro***

Identification of a cell adhesion pathway dependent on vimentin provided mechanistic insight into the role of vimentin as a signaling hub. The work presented in this dissertation built upon several seminal papers in the intermediate filament field that demonstrated vimentin is necessary in cell morphology, signaling, adhesion, and motility (127, 129, 130). Our work identifies vimentin as an upstream mediator of the focal adhesion signaling within lung cancer cells. We confirmed that vimentin filaments and squiggles directly enter focal adhesion sites (168). Once at the focal adhesion, vimentin facilitates EGFR-mediated activation of VAV2 at phosphorylation sites Y142 and Y172. Activated VAV2 acts as a guanine nucleotide exchange factor (GEF) for Rac1. Upon activation, Rac1 promotes FAK autophosphorylation and activation. Within this signaling pathway vimentin not only facilitates activation of VAV2, but also stabilizes an autophosphorylated pY397-FAK to strengthen cell adhesion.

This work provided mechanistic insight into the role of vimentin within motile lung cancer cells. Further, it led to the development of subsequent *in vitro* and *in vivo* projects to advance vimentin as a key player in cancer cell invasion and metastasis.

Others have shown that vimentin assembly is mediated by phosphorylation at key serine residues along the head and tail domains of the protein (124). We began exploring the role of specific serine sites in the vimentin head domain (S6, S38, S56, and S72)

using phospho-mutant constructs. These early studies revealed that mutations at each serine site did generate distinct vimentin filament morphology (data not shown).

The central question that remained, however, was whether vimentin exhibited a functional role within lung cancer metastasis *in vivo*. Extensive correlative studies associating vimentin with metastatic disease (189) and our own findings, described above, led to the development of a lung cancer metastasis mouse model that lacked vimentin.

#### **4.3. Vimentin is necessary for lung cancer metastasis *in vivo***

In order to probe whether vimentin is necessary for metastasis to occur, we developed a novel genetically engineered mouse model (GEMM): *LSL-Kras<sup>G12D</sup>, LKBI<sup>fl/fl</sup>, Vim<sup>-/-</sup> (KLV<sup>-/-</sup>)*. The metastatic rate of the *KLV<sup>-/-</sup>* mouse was significantly lower than that of the *KLV<sup>+/+</sup>* mouse. However, tumor burden was not impacted by vimentin depletion. These data established that vimentin is necessary for metastasis in a lung cancer GEMM.

Histological analysis of the primary tumors in the *KLV* models demonstrate that mice lacking vimentin not only exhibited a reduced metastatic rate but also developed less aggressive primary tumors with smaller areas of focal invasion marked by less stromal involvement. These data suggest that vimentin is important for the early invasive steps of the metastatic cascade.

#### **4.4. Lung adenocarcinoma metastasis occurs via vimentin-mediated collective invasion**

Based on our findings, published in *Havel et al.*, we hypothesized that vimentin would promote metastasis by inducing cancer cell motility via focal adhesion signaling. Interestingly, immunohistochemical studies of our *KLV<sup>+/+</sup>* model revealed that vimentin is predominantly expressed in the tumor microenvironment and not the cancer cells. We demonstrate that while vimentin is expressed in many components of the tumor microenvironment, lack of vimentin in the *KLV<sup>-/-</sup>* model most significantly impacted recruitment of cancer-associated fibroblasts (CAFs) as marked by a significant reduction in focal invasion in *KLV<sup>-/-</sup>* mice. Therefore, instead of a canonical EMT, we found that cancer-associated fibroblasts (CAFs) form heterotypic cell clusters with cancer cells termed “CIPs” (collective invasion packs). CIPs maintain their epithelial morphology and markers including e-cadherin and Pro-SPC (20). We demonstrate that CIP frequency and metastatic rates significantly increased with vimentin expression in the KLV models indicating that vimentin is instrumental for CIP formation, cancer invasion, and metastasis.

We validated the immunoprofile of the heterotypic CAF-CIP clusters in patient lung adenocarcinoma samples from clinical collaborators. In 96% of lung adenocarcinoma samples tested, vimentin expression was found predominantly in the stromal compartment, which we show to be positively marked by the CAF marker, FSP1. Consistent with the KLV models, we demonstrate that CIPs in human lung adenocarcinoma tissue samples are positive for e-cadherin and Pro-SPC. This immunoprofile was found to be independent of genetic drivers as the samples tested had a

wide variety of genetic backgrounds. Together these data indicate that our *KLV* models translate histologically to clinical samples. Further, the predominant mode of invasion and metastasis within lung adenocarcinoma is not EMT but heterotypic collective invasion.

To model heterotypic interactions in collective invasion, we performed homotypic and heterotypic spheroid invasion assays *in vitro* with CAFs and lung cancer cells. We demonstrate through these studies that vimentin depletion in CAFs impairs their invasive functions in both CAF only and co-culture spheroid experiments. CAFs expressing shRNA for vimentin exhibited significantly less invasion into an extracellular matrix than pLKO.1 isogenic control cells. Co-culture invasion experiments performed with CAFs and lung cancer cells demonstrate impairment in the ability of CAFs to lead cancer cells out of the spheroid in invasive chains upon loss of vimentin expression. These data suggest that vimentin is a key component of proper CAF function. Our proposed model is outlined in Figure 4-1.

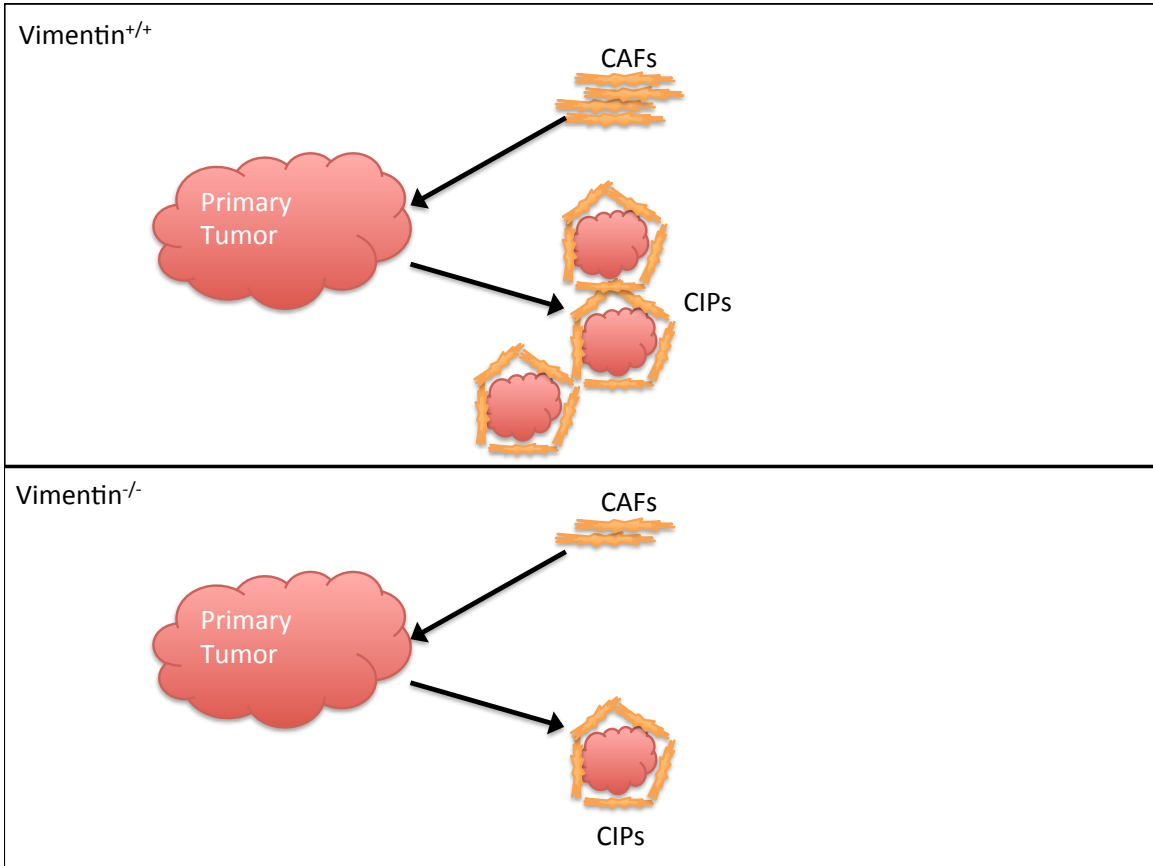


**Figure 4-1. Proposed model of vimentin-dependent CAF/CIP interactions.** CAFs wild type for vimentin have fully functional motility machinery that allow them to be recruited to the primary tumor quickly and form many CIPs that result in lymph node metastasis. Loss of vimentin inhibits CAF motility resulting in generation of fewer CIPs



#### 4.5. Context-dependent roles for vimentin

Marked by the release of the seminal review by Hanahan and Weinberg on the cancer hallmarks, the scientific community's approach to cancer research has shifted from away from a reductionist view in which cancer biology is completely dependent on the oncogenes and tumor suppressors expressed by cancer cells. Instead, heterotypic cell biology approaches reveal that there are many factors within the tumor microenvironment that determine the phenotype and fate of a tumor. The work presented in this dissertation supports that tumor cell context is an important factor in determining invasive behavior.

Our findings described in Chapter 2 demonstrate a functional role for vimentin within lung cancer cell biology using predominantly *in vitro* approaches. Through this work we show that vimentin modulates focal adhesion signaling by acting as a scaffold for proteins at the leading edge of motile cells. While these data were the basis of the development of the *KLV<sup>-/-</sup>* mouse, our *in vivo* project demonstrated that within a tissue context, the role of vimentin shifts from cancer cells to the tumor microenvironment. The juxtaposition of these two projects shows that while the role of vimentin is context dependent, all work presented in this dissertation support that vimentin is an active mediator of cancer cell invasion and metastasis.

In addition, our findings highlight the importance of testing hypotheses in multiple experimental model systems. As our understanding of cancer continues to develop, it is critical to take into account all potential variables mediating cancer formation, progression, and metastasis. By using a multi-pronged approach to

investigating vimentin function in lung cancer invasion and metastasis, we are better able to provide insight into how vimentin contributes to the metastatic cascade.

#### **4.6. Postulated mechanisms of vimentin-mediated stroma-cancer cell crosstalk**

Across cancer types and cell populations, the fact that remains constant is that vimentin regulates intrinsic motile and invasive phenotypes (130, 132, 194). However, the ability of vimentin to mediate cell-cell communication remains to be understood. Previous studies have shown that vimentin interacts with several cell surface proteins including integrins, plectins, and FAK (168, 195, 196). Vimentin could contribute to heterotypic crosstalk by regulating the localization of proteins at cell-cell junctions. As our work shows, presence of vimentin in focal adhesion sites strengthens the stability of the adhesions by providing a signaling scaffold for proteins at the leading edge of motile cells. Within heterotypic cell junctions vimentin could act as a signaling hub, supporting cell-cell contacts as a means of preserving the structural integrity of the tissue. Tumor stiffness has been shown to modulate tumor progression (197). Intermediate filaments, including vimentin, were first identified as important components in the preservation of cellular architecture and integrity (198). Vimentin could be maintaining cellular architecture and stiffness by both intracellular and intercellular structural regulation. Within a vimentin-expressing cell, vimentin filaments extend throughout the cell to protect the nucleus and cytoplasm from shear forces (199). In addition, vimentin could facilitate cells to maintain intercellular contacts as a way to further stabilize the vimentin-expressing cell as well as the tissue at large.

#### **4.7. Future directions and translational implications**

Understanding cancer metastasis is key to improving patient outcomes across solid tumor types and converting cancer from a death sentence to a chronic disease. As we gain more information regarding the complexities of tumors, including their microenvironment, it is important to revisit early theories on cancer progression and test their rigor in new models. Our work brings to the forefront the importance of the tumor microenvironment and how cell context can determine expression and function of key proteins that contribute to tumor progression.

The work presented in this dissertation advanced the understanding of how lung cancer metastasis is regulated. Specifically, we identified vimentin as mediating lung cancer cell invasion and metastasis. Since vimentin is upregulated in metastatic tumors across solid tumor types, the findings presented here could have major impacts for large numbers of cancer patients. The importance of vimentin at the early invasive steps of the metastatic cascade provides a therapeutic opportunity for targeting cancer cell invasion that could promote the conversion of cancer from a death sentence to a chronic disease. One promising natural compound, withaferin A, has been shown to disrupt vimentin filaments and inhibit EMT in breast cancer (200, 201). Future works stemming from these studies will likely include optimizing vimentin inhibition therapeutically in metastatic disease models.

Identification of vimentin as a signaling hub at the leading edge of motile cells directs us to consider what other signaling networks might be supported by vimentin, or other intermediate filaments. Further investigation into signaling complexes found in

vimentin-positive cells may reveal the importance of ubiquitous vimentin expression across tissue types.

Future directions from this work would also include further investigation of the importance of vimentin expression in the tumor microenvironment. We show here that CAFs provide the greatest contribution to cancer metastasis in our GEMM model via vimentin expression. However, as we show, context is critical in cancer models. In other cancer types and models vimentin may be more predominant in other microenvironmental factors, such as macrophages. Intermediate filaments have been understudied for so long that it is important to fully investigate their impacts in multiple disease models.

Overall, the work presented in this dissertation provides a foundation for understanding lung cancer metastasis. Through the analysis of *in vitro* and *in vivo* models as well as patient samples, the importance of vimentin as a modulator of cancer metastasis was revealed. The prevalence of vimentin overexpression in metastasis across solid tumor types emphasizes the importance of this study as broadly applicable to our understanding of cancer.

## References

1. Siegel RL, Miller KD, Jemal A. Cancer Statistics, 2017. *CA Cancer J Clin.* 2017 Jan;67(1):7-30.
2. Popper HH. Progression and metastasis of lung cancer. *Cancer metastasis reviews.* 2016 Mar;35(1):75-91.
3. Weigelt B, Peterse JL, van 't Veer LJ. Breast cancer metastasis: markers and models. *Nat Rev Cancer.* 2005 Aug;5(8):591-602.
4. Herbst RS, Heymach JV, Lippman SM. Lung Cancer. *New England Journal of Medicine.* 2008;359(13):1367-80.
5. Pao W, Hutchinson KE. Chipping away at the lung cancer genome. *Nat Med.* 2012 Mar;18(3):349-51.
6. Gurda GT, Zhang L, Wang Y, Chen L, Geddes S, Cho WC, et al. Utility of five commonly used immunohistochemical markers TTF-1, Napsin A, CK7, CK5/6 and P63 in primary and metastatic adenocarcinoma and squamous cell carcinoma of the lung: a retrospective study of 246 fine needle aspiration cases. *Clinical and translational medicine.* 2015;4:16.
7. Hirsch FR, Spreafico A, Novello S, Wood MD, Simms L, Papotti M. The prognostic and predictive role of histology in advanced non-small cell lung cancer: a literature review. *Journal of thoracic oncology : official publication of the International Association for the Study of Lung Cancer.* 2008 Dec;3(12):1468-81.
8. PDQ Adult Treatment Editorial Board. Non-Small Cell Lung Cancer Treatment (PDQ®): Health Professional Version.
9. Sica G, Yoshizawa A, Sima CS, Azzoli CG, Downey RJ, Rusch VW, et al. A grading system of lung adenocarcinomas based on histologic pattern is predictive of disease recurrence in stage I tumors. *The American journal of surgical pathology.* 2010 Aug;34(8):1155-62.
10. Mao P, Wu S, Li J, Fu W, He W, Liu X, et al. Human alveolar epithelial type II cells in primary culture. *Physiological reports.* 2015 Feb 01;3(2).
11. Rekhman N, Ang DC, Sima CS, Travis WD, Moreira AL. Immunohistochemical algorithm for differentiation of lung adenocarcinoma and squamous cell carcinoma based on large series of whole-tissue sections with validation in small specimens. *Mod Pathol.* 2011 Oct;24(10):1348-59.
12. Pao W, Girard N. New driver mutations in non-small-cell lung cancer. *The Lancet Oncology.* 2011 Feb;12(2):175-80.
13. The Cancer Genome Atlas Research N. Comprehensive molecular profiling of lung adenocarcinoma. *Nature.* 2014 07/31/print;511(7511):543-50.
14. Forbes SA, Bindal N, Bamford S, Cole C, Kok CY, Beare D, et al. COSMIC: mining complete cancer genomes in the Catalogue of Somatic Mutations in Cancer. *Nucleic acids research.* 2011 Jan;39(Database issue):D945-50.
15. Garassino MC, Marabese M, Rusconi P, Rulli E, Martelli O, Farina G, et al. Different types of K-Ras mutations could affect drug sensitivity and tumour behaviour in non-small-cell lung cancer. *Annals of oncology : official journal of the European Society for Medical Oncology.* 2011 Jan;22(1):235-7.
16. Hanahan D, Weinberg RA. Hallmarks of cancer: the next generation. *Cell.* 2011 Mar 04;144(5):646-74.

17. Johnson L, Mercer K, Greenbaum D, Bronson RT, Crowley D, Tuveson DA, et al. Somatic activation of the K-ras oncogene causes early onset lung cancer in mice. *Nature*. 2001 Apr 26;410(6832):1111-6.
18. Sanchez-Cespedes M, Parrella P, Esteller M, Nomoto S, Trink B, Engles JM, et al. Inactivation of LKB1/STK11 is a common event in adenocarcinomas of the lung. *Cancer research*. 2002 Jul 01;62(13):3659-62.
19. Ding L, Getz G, Wheeler DA, Mardis ER, McLellan MD, Cibulskis K, et al. Somatic mutations affect key pathways in lung adenocarcinoma. *Nature*. 2008 Oct 23;455(7216):1069-75.
20. Gilbert-Ross M, Konen J, Koo J, Shupe J, Robinson BS, Wiles WGt, et al. Targeting adhesion signaling in KRAS, LKB1 mutant lung adenocarcinoma. *JCI insight*. 2017 Mar 09;2(5):e90487.
21. Ji H, Ramsey MR, Hayes DN, Fan C, McNamara K, Kozlowski P, et al. LKB1 modulates lung cancer differentiation and metastasis. *Nature*. 2007 Aug 16;448(7155):807-10.
22. Carretero J, Shimamura T, Rikova K, Jackson AL, Wilkerson MD, Borgman CL, et al. Integrative genomic and proteomic analyses identify targets for Lkb1-deficient metastatic lung tumors. *Cancer cell*. 2010 Jun 15;17(6):547-59.
23. Kottakis F, Nicolay BN, Roumane A, Karnik R, Gu H, Nagle JM, et al. LKB1 loss links serine metabolism to DNA methylation and tumorigenesis. *Nature*. 2016 Nov 17;539(7629):390-5.
24. Shackelford DB, Abt E, Gerken L, Vasquez DS, Seki A, Leblanc M, et al. LKB1 inactivation dictates therapeutic response of non-small cell lung cancer to the metabolism drug phenformin. *Cancer cell*. 2013 Feb 11;23(2):143-58.
25. Neal JW. The SATURN trial: the value of maintenance erlotinib in patients with non-small-cell lung cancer. *Future oncology (London, England)*. 2010 Dec;6(12):1827-32.
26. Rami-Porta R, Asamura H, Travis WD, Rusch VW. Lung cancer - major changes in the American Joint Committee on Cancer eighth edition cancer staging manual. *CA Cancer J Clin*. 2017 Mar;67(2):138-55.
27. Scagliotti GV, Parikh P, von Pawel J, Biesma B, Vansteenkiste J, Manegold C, et al. Phase III study comparing cisplatin plus gemcitabine with cisplatin plus pemetrexed in chemotherapy-naive patients with advanced-stage non-small-cell lung cancer. *Journal of clinical oncology : official journal of the American Society of Clinical Oncology*. 2008 Jul 20;26(21):3543-51.
28. Chen Z, Cheng K, Walton Z, Wang Y, Ebi H, Shimamura T, et al. A murine lung cancer co-clinical trial identifies genetic modifiers of therapeutic response. *Nature*. 2012 Mar 18;483(7391):613-7.
29. Brahmer J, Reckamp KL, Baas P, Crino L, Eberhardt WE, Poddubskaya E, et al. Nivolumab versus Docetaxel in Advanced Squamous-Cell Non-Small-Cell Lung Cancer. *The New England journal of medicine*. 2015 Jul 09;373(2):123-35.
30. Borghaei H, Paz-Ares L, Horn L, Spigel DR, Steins M, Ready NE, et al. Nivolumab versus Docetaxel in Advanced Nonsquamous Non-Small-Cell Lung Cancer. *The New England journal of medicine*. 2015 Oct 22;373(17):1627-39.

31. Garon EB, Rizvi NA, Hui R, Leighl N, Balmanoukian AS, Eder JP, et al. Pembrolizumab for the treatment of non-small-cell lung cancer. *The New England journal of medicine*. 2015 May 21;372(21):2018-28.
32. Zijlstra A, Mellor R, Panzarella G, Aimes RT, Hooper JD, Marchenko ND, et al. A quantitative analysis of rate-limiting steps in the metastatic cascade using human-specific real-time polymerase chain reaction. *Cancer research*. 2002 Dec 01;62(23):7083-92.
33. Friedl P, Wolf K. Tumour-cell invasion and migration: diversity and escape mechanisms. *Nat Rev Cancer*. 2003 May;3(5):362-74.
34. Lamouille S, Xu J, Derynck R. Molecular mechanisms of epithelial-mesenchymal transition. *Nature reviews Molecular cell biology*. 2014 Mar;15(3):178-96.
35. Serrano-Gomez SJ, Maziveyi M, Alahari SK. Regulation of epithelial-mesenchymal transition through epigenetic and post-translational modifications. *Molecular cancer*. 2016 Feb 24;15:18.
36. Kalluri R, Weinberg RA. The basics of epithelial-mesenchymal transition. *The Journal of clinical investigation*. 2009 Jun;119(6):1420-8.
37. Chaffer CL, San Juan BP, Lim E, Weinberg RA. EMT, cell plasticity and metastasis. *Cancer metastasis reviews*. 2016 Dec;35(4):645-54.
38. Thiery JP. Epithelial-mesenchymal transitions in tumour progression. *Nat Rev Cancer*. 2002 Jun;2(6):442-54.
39. Yao D, Dai C, Peng S. Mechanism of the mesenchymal-epithelial transition and its relationship with metastatic tumor formation. *Mol Cancer Res*. 2011 Dec;9(12):1608-20.
40. Puisieux A, Brabletz T, Caramel J. Oncogenic roles of EMT-inducing transcription factors. *Nat Cell Biol*. 2014 Jun;16(6):488-94.
41. Cicchini C, Laudadio I, Citarella F, Corazzari M, Steindler C, Conigliaro A, et al. TGFbeta-induced EMT requires focal adhesion kinase (FAK) signaling. *Experimental cell research*. 2008 Jan 01;314(1):143-52.
42. Lauffenburger DA, Horwitz AF. Cell migration: a physically integrated molecular process. *Cell*. 1996 Feb 09;84(3):359-69.
43. Gialeli C, Theocharis AD, Karamanos NK. Roles of matrix metalloproteinases in cancer progression and their pharmacological targeting. *The FEBS journal*. 2011 Jan;278(1):16-27.
44. Krakhmal NV, Zavyalova MV, Denisov EV, Vtorushin SV, Perelmuter VM. Cancer Invasion: Patterns and Mechanisms. *Acta naturae*. 2015 Apr-Jun;7(2):17-28.
45. Friedl P, Locker J, Sahai E, Segall JE. Classifying collective cancer cell invasion. *Nat Cell Biol*. 2012 Aug;14(8):777-83.
46. Friedl P, Gilmour D. Collective cell migration in morphogenesis, regeneration and cancer. *Nature reviews Molecular cell biology*. 2009 Jul;10(7):445-57.
47. Konen J, Summerbell E, Dwivedi B, Galior K, Hou Y, Rusnak L, et al. Image-guided genomics of phenotypically heterogeneous populations reveals vascular signaling during symbiotic collective cancer invasion. *Nature Communications*. 2017 In Press.



48. Schlaepfer DD, Mitra SK, Ilic D. Control of motile and invasive cell phenotypes by focal adhesion kinase. *Biochimica et biophysica acta*. 2004 Jul 05;1692(2-3):77-102.
49. Truong H, Danen EH. Integrin switching modulates adhesion dynamics and cell migration. *Cell adhesion & migration*. 2009 Apr-Jun;3(2):179-81.
50. van der Flier A, Sonnenberg A. Function and interactions of integrins. *Cell and tissue research*. 2001 Sep;305(3):285-98.
51. Michael KE, Dumbauld DW, Burns KL, Hanks SK, Garcia AJ. Focal adhesion kinase modulates cell adhesion strengthening via integrin activation. *Molecular biology of the cell*. 2009 May;20(9):2508-19.
52. Burridge K, Fath K, Kelly T, Nuckolls G, Turner C. Focal adhesions: transmembrane junctions between the extracellular matrix and the cytoskeleton. *Annual review of cell biology*. 1988;4:487-525.
53. Havel LS, Kline ER, Salgueiro AM, Marcus AI. Vimentin regulates lung cancer cell adhesion through a VAV2-Rac1 pathway to control focal adhesion kinase activity. *Oncogene*. 2015 Apr 09;34(15):1979-90.
54. Owens LV, Xu L, Craven RJ, Dent GA, Weiner TM, Kornberg L, et al. Overexpression of the focal adhesion kinase (p125FAK) in invasive human tumors. *Cancer research*. 1995 Jul 01;55(13):2752-5.
55. McLean GW, Carragher NO, Avizienyte E, Evans J, Brunton VG, Frame MC. The role of focal-adhesion kinase in cancer - a new therapeutic opportunity. *Nat Rev Cancer*. 2005 Jul;5(7):505-15.
56. Reymond N, d'Agua BB, Ridley AJ. Crossing the endothelial barrier during metastasis. *Nat Rev Cancer*. 2013 Dec;13(12):858-70.
57. Anderberg C, Cunha SI, Zhai Z, Cortez E, Pardali E, Johnson JR, et al. Deficiency for endoglin in tumor vasculature weakens the endothelial barrier to metastatic dissemination. *The Journal of experimental medicine*. 2013 Mar 11;210(3):563-79.
58. Joosse SA, Gorges TM, Pantel K. Biology, detection, and clinical implications of circulating tumor cells. *EMBO molecular medicine*. 2015 Jan;7(1):1-11.
59. Molnar B, Ladanyi A, Tanko L, Sreter L, Tulassay Z. Circulating tumor cell clusters in the peripheral blood of colorectal cancer patients. *Clinical cancer research : an official journal of the American Association for Cancer Research*. 2001 Dec;7(12):4080-5.
60. Aceto N, Bardia A, Miyamoto DT, Donaldson MC, Wittner BS, Spencer JA, et al. Circulating tumor cell clusters are oligoclonal precursors of breast cancer metastasis. *Cell*. 2014 Aug 28;158(5):1110-22.
61. Fabisiwicz A, Grzybowska E. CTC clusters in cancer progression and metastasis. *Medical oncology (Northwood, London, England)*. 2017 Jan;34(1):12.
62. Suo Y, Xie C, Zhu X, Fan Z, Yang Z, He H, et al. Proportion of circulating tumor cell clusters increases during cancer metastasis. *Cytometry Part A : the journal of the International Society for Analytical Cytology*. 2016 Dec 23.
63. Nash GF, Turner LF, Scully MF, Kakkar AK. Platelets and cancer. *The Lancet Oncology*. 2002 Jul;3(7):425-30.
64. Duda DG, Duyverman AM, Kohno M, Snuderl M, Steller EJ, Fukumura D, et al. Malignant cells facilitate lung metastasis by bringing their own soil. *Proceedings of*

- the National Academy of Sciences of the United States of America. 2010 Dec 14;107(50):21677-82.
65. Chatterjee S, Behnam Azad B, Nimmagadda S. The intricate role of CXCR4 in cancer. *Advances in cancer research*. 2014;124:31-82.
  66. Ganju RK, Brubaker SA, Meyer J, Dutt P, Yang Y, Qin S, et al. The alpha-chemokine, stromal cell-derived factor-1alpha, binds to the transmembrane G-protein-coupled CXCR-4 receptor and activates multiple signal transduction pathways. *The Journal of biological chemistry*. 1998 Sep 04;273(36):23169-75.
  67. Massague J, Obenauf AC. Metastatic colonization by circulating tumour cells. *Nature*. 2016 Jan 21;529(7586):298-306.
  68. Chambers AF, Groom AC, MacDonald IC. Dissemination and growth of cancer cells in metastatic sites. *Nat Rev Cancer*. 2002 Aug;2(8):563-72.
  69. Minn AJ, Gupta GP, Siegel PM, Bos PD, Shu W, Giri DD, et al. Genes that mediate breast cancer metastasis to lung. *Nature*. 2005 Jul 28;436(7050):518-24.
  70. Schumacher D, Strilic B, Sivaraj KK, Wettschureck N, Offermanns S. Platelet-derived nucleotides promote tumor-cell transendothelial migration and metastasis via P2Y2 receptor. *Cancer cell*. 2013 Jul 08;24(1):130-7.
  71. Sevenich L, Bowman RL, Mason SD, Quail DF, Rapaport F, Elie BT, et al. Analysis of tumour- and stroma-supplied proteolytic networks reveals a brain-metastasis-promoting role for cathepsin S. *Nat Cell Biol*. 2014 Sep;16(9):876-88.
  72. Hart IR, Fidler IJ. Role of organ selectivity in the determination of metastatic patterns of B16 melanoma. *Cancer research*. 1980 Jul;40(7):2281-7.
  73. Fidler IJ. The pathogenesis of cancer metastasis: the 'seed and soil' hypothesis revisited. *Nat Rev Cancer*. 2003 Jun;3(6):453-8.
  74. Hanahan D, Weinberg RA. The hallmarks of cancer. *Cell*. 2000 Jan 07;100(1):57-70.
  75. Chen F, Zhuang X, Lin L, Yu P, Wang Y, Shi Y, et al. New horizons in tumor microenvironment biology: challenges and opportunities. *BMC medicine*. 2015 Mar 05;13:45.
  76. Xie HY, Shao ZM, Li DQ. Tumor microenvironment: driving forces and potential therapeutic targets for breast cancer metastasis. *Chinese journal of cancer*. 2017 Mar 29;36(1):36.
  77. Pantel K, Alix-Panabieres C. Tumour microenvironment: informing on minimal residual disease in solid tumours. *Nature reviews Clinical oncology*. 2017 Jun;14(6):325-6.
  78. Johansson M, Denardo DG, Coussens LM. Polarized immune responses differentially regulate cancer development. *Immunological reviews*. 2008 Apr;222:145-54.
  79. Augsten M. Cancer-associated fibroblasts as another polarized cell type of the tumor microenvironment. *Front Oncol*. 2014;4:62.
  80. Li H, Fan X, Houghton J. Tumor microenvironment: the role of the tumor stroma in cancer. *Journal of cellular biochemistry*. 2007 Jul 01;101(4):805-15.
  81. Kidd S, Spaeth E, Watson K, Burks J, Lu H, Klopp A, et al. Origins of the tumor microenvironment: quantitative assessment of adipose-derived and bone marrow-derived stroma. *PLoS One*. 2012;7(2):e30563.

82. Subramaniam KS, Tham ST, Mohamed Z, Woo YL, Mat Adenan NA, Chung I. Cancer-associated fibroblasts promote proliferation of endometrial cancer cells. *PLoS One*. 2013;8(7):e68923.
83. Jia CC, Wang TT, Liu W, Fu BS, Hua X, Wang GY, et al. Cancer-associated fibroblasts from hepatocellular carcinoma promote malignant cell proliferation by HGF secretion. *PLoS One*. 2013;8(5):e63243.
84. Brabletz T, Jung A, Reu S, Porzner M, Hlubek F, Kunz-Schughart LA, et al. Variable beta-catenin expression in colorectal cancers indicates tumor progression driven by the tumor environment. *Proceedings of the National Academy of Sciences of the United States of America*. 2001 Aug 28;98(18):10356-61.
85. Henriksson ML, Edin S, Dahlin AM, Oldenborg PA, Oberg A, Van Guelpen B, et al. Colorectal cancer cells activate adjacent fibroblasts resulting in FGF1/FGFR3 signaling and increased invasion. *The American journal of pathology*. 2011 Mar;178(3):1387-94.
86. Strell C, Rundqvist H, Ostman A. Fibroblasts--a key host cell type in tumor initiation, progression, and metastasis. *Uppsala journal of medical sciences*. 2012 May;117(2):187-95.
87. Chang HY, Sneddon JB, Alizadeh AA, Sood R, West RB, Montgomery K, et al. Gene expression signature of fibroblast serum response predicts human cancer progression: similarities between tumors and wounds. *PLoS biology*. 2004 Feb;2(2):E7.
88. Chen WJ, Ho CC, Chang YL, Chen HY, Lin CA, Ling TY, et al. Cancer-associated fibroblasts regulate the plasticity of lung cancer stemness via paracrine signalling. *Nat Commun*. 2014 Mar 25;5:3472.
89. Green JL, La J, Yum KW, Desai P, Rodewald LW, Zhang X, et al. Paracrine Wnt signaling both promotes and inhibits human breast tumor growth. *Proceedings of the National Academy of Sciences of the United States of America*. 2013 Apr 23;110(17):6991-6.
90. Chang PH, Hwang-Verslues WW, Chang YC, Chen CC, Hsiao M, Jeng YM, et al. Activation of Robo1 signaling of breast cancer cells by Slit2 from stromal fibroblast restrains tumorigenesis via blocking PI3K/Akt/beta-catenin pathway. *Cancer research*. 2012 Sep 15;72(18):4652-61.
91. Mace TA, Ameen Z, Collins A, Wojcik S, Mair M, Young GS, et al. Pancreatic cancer-associated stellate cells promote differentiation of myeloid-derived suppressor cells in a STAT3-dependent manner. *Cancer research*. 2013 May 15;73(10):3007-18.
92. Comito G, Giannoni E, Segura CP, Barcellos-de-Souza P, Raspollini MR, Baroni G, et al. Cancer-associated fibroblasts and M2-polarized macrophages synergize during prostate carcinoma progression. *Oncogene*. 2014 May 08;33(19):2423-31.
93. Hanahan D, Coussens LM. Accessories to the crime: functions of cells recruited to the tumor microenvironment. *Cancer cell*. 2012 Mar 20;21(3):309-22.
94. Tlsty TD, Coussens LM. Tumor stroma and regulation of cancer development. *Annual review of pathology*. 2006;1:119-50.
95. Balkwill F, Charles KA, Mantovani A. Smoldering and polarized inflammation in the initiation and promotion of malignant disease. *Cancer cell*. 2005 Mar;7(3):211-7.

96. Samples J, Willis M, Klauber-Demore N. Targeting angiogenesis and the tumor microenvironment. *Surgical oncology clinics of North America*. 2013 Oct;22(4):629-39.
97. Patan S. Vasculogenesis and angiogenesis. *Cancer treatment and research*. 2004;117:3-32.
98. Tang HS, Feng YJ, Yao LQ. Angiogenesis, vasculogenesis, and vasculogenic mimicry in ovarian cancer. *International journal of gynecological cancer : official journal of the International Gynecological Cancer Society*. 2009 May;19(4):605-10.
99. Baeriswyl V, Christofori G. The angiogenic switch in carcinogenesis. *Seminars in cancer biology*. 2009 Oct;19(5):329-37.
100. Bielenberg DR, Zetter BR. The Contribution of Angiogenesis to the Process of Metastasis. *Cancer journal (Sudbury, Mass)*. 2015 Jul-Aug;21(4):267-73.
101. Kessenbrock K, Plaks V, Werb Z. Matrix metalloproteinases: regulators of the tumor microenvironment. *Cell*. 2010 Apr 02;141(1):52-67.
102. Pirila E, Ramamurthy NS, Sorsa T, Salo T, Hietanen J, Maisi P. Gelatinase A (MMP-2), collagenase-2 (MMP-8), and laminin-5 gamma2-chain expression in murine inflammatory bowel disease (ulcerative colitis). *Digestive diseases and sciences*. 2003 Jan;48(1):93-8.
103. Kashiwagi S, Izumi Y, Gohongi T, Demou ZN, Xu L, Huang PL, et al. NO mediates mural cell recruitment and vessel morphogenesis in murine melanomas and tissue-engineered blood vessels. *The Journal of clinical investigation*. 2005 Jul;115(7):1816-27.
104. Yang J, Weinberg RA. Epithelial-mesenchymal transition: at the crossroads of development and tumor metastasis. *Developmental cell*. 2008 Jun;14(6):818-29.
105. Heerboth S, Housman G, Leary M, Longacre M, Byler S, Lapinska K, et al. EMT and tumor metastasis. *Clinical and translational medicine*. 2015;4:6.
106. Son H, Moon A. Epithelial-mesenchymal Transition and Cell Invasion. *Toxicological research*. 2010 Dec;26(4):245-52.
107. Mutlu N, Turkeri L, Emerk K. Analytical and clinical evaluation of a new urinary tumor marker: bladder tumor fibronectin in diagnosis and follow-up of bladder cancer. *Clinical chemistry and laboratory medicine*. 2003 Aug;41(8):1069-74.
108. Nakashima T, Huang C, Liu D, Kameyama K, Masuya D, Kobayashi S, et al. Neural-cadherin expression associated with angiogenesis in non-small-cell lung cancer patients. *British journal of cancer*. 2003 Jun 02;88(11):1727-33.
109. Al-Saad S, Al-Shibli K, Donnem T, Persson M, Bremnes RM, Busund LT. The prognostic impact of NF-kappaB p105, vimentin, E-cadherin and Par6 expression in epithelial and stromal compartment in non-small-cell lung cancer. *British journal of cancer*. 2008 Nov 04;99(9):1476-83.
110. Zhao J, Dong D, Sun L, Zhang G, Sun L. Prognostic significance of the epithelial-to-mesenchymal transition markers e-cadherin, vimentin and twist in bladder cancer. *International braz j urol : official journal of the Brazilian Society of Urology*. 2014 Mar-Apr;40(2):179-89.
111. Han JY, Kim HS, Lee SH, Park WS, Lee JY, Yoo NJ. Immunohistochemical expression of integrins and extracellular matrix proteins in non-small cell lung

- cancer: correlation with lymph node metastasis. *Lung cancer* (Amsterdam, Netherlands). 2003 Jul;41(1):65-70.
112. Nagi C, Guttman M, Jaffer S, Qiao R, Keren R, Triana A, et al. N-cadherin expression in breast cancer: correlation with an aggressive histologic variant--invasive micropapillary carcinoma. *Breast cancer research and treatment*. 2005 Dec;94(3):225-35.
113. Thomas PA, Kirschmann DA, Cerhan JR, Folberg R, Seftor EA, Sellers TA, et al. Association between keratin and vimentin expression, malignant phenotype, and survival in postmenopausal breast cancer patients. *Clinical cancer research : an official journal of the American Association for Cancer Research*. 1999 Oct;5(10):2698-703.
114. Wu M, Bai X, Xu G, Wei J, Zhu T, Zhang Y, et al. Proteome analysis of human androgen-independent prostate cancer cell lines: variable metastatic potentials correlated with vimentin expression. *Proteomics*. 2007 Jun;7(12):1973-83.
115. Sun B, Zhang S, Zhang D, Li Y, Zhao X, Luo Y, et al. Identification of metastasis-related proteins and their clinical relevance to triple-negative human breast cancer. *Clinical cancer research : an official journal of the American Association for Cancer Research*. 2008 Nov 01;14(21):7050-9.
116. Dauphin M, Barbe C, Lemaire S, Nawrocki-Raby B, Lagonotte E, Delepine G, et al. Vimentin expression predicts the occurrence of metastases in non small cell lung carcinomas. *Lung cancer* (Amsterdam, Netherlands). 2013 Jul;81(1):117-22.
117. Zhang H, Liu J, Yue D, Gao L, Wang D, Zhang H, et al. Clinical significance of E-cadherin, beta-catenin, vimentin and S100A4 expression in completely resected squamous cell lung carcinoma. *Journal of clinical pathology*. 2013 Nov;66(11):937-45.
118. Fuchs E, Cleveland DW. A structural scaffolding of intermediate filaments in health and disease. *Science*. 1998 Jan 23;279(5350):514-9.
119. Goldman RD, Cleland MM, Murthy SN, Mahammad S, Kuczmarski ER. Inroads into the structure and function of intermediate filament networks. *Journal of structural biology*. 2012 Jan;177(1):14-23.
120. Chang L, Barlan K, Chou YH, Grin B, Lakonishok M, Serpinskaya AS, et al. The dynamic properties of intermediate filaments during organelle transport. *Journal of cell science*. 2009 Aug 15;122(Pt 16):2914-23.
121. Omary MB, Coulombe PA, McLean WH. Intermediate filament proteins and their associated diseases. *The New England journal of medicine*. 2004 Nov 11;351(20):2087-100.
122. Eriksson JE, Dechat T, Grin B, Helfand B, Mendez M, Pallari HM, et al. Introducing intermediate filaments: from discovery to disease. *The Journal of clinical investigation*. 2009 Jul;119(7):1763-71.
123. Herrmann H, Aebi U. Intermediate filaments: molecular structure, assembly mechanism, and integration into functionally distinct intracellular Scaffolds. *Annual review of biochemistry*. 2004;73:749-89.
124. Eriksson JE, He T, Trejo-Skalli AV, Harmala-Brasken AS, Hellman J, Chou YH, et al. Specific in vivo phosphorylation sites determine the assembly dynamics of vimentin intermediate filaments. *Journal of cell science*. 2004 Feb 29;117(Pt 6):919-32.

125. Li QF, Spinelli AM, Wang R, Anfinogenova Y, Singer HA, Tang DD. Critical role of vimentin phosphorylation at Ser-56 by p21-activated kinase in vimentin cytoskeleton signaling. *The Journal of biological chemistry*. 2006 Nov 10;281(45):34716-24.
126. Chou YH, Flitney FW, Chang L, Mendez M, Grin B, Goldman RD. The motility and dynamic properties of intermediate filaments and their constituent proteins. *Experimental cell research*. 2007 Jun 10;313(10):2236-43.
127. Helfand BT, Mendez MG, Murthy SN, Shumaker DK, Grin B, Mahammad S, et al. Vimentin organization modulates the formation of lamellipodia. *Molecular biology of the cell*. 2011 Apr 15;22(8):1274-89.
128. Chung BM, Rotty JD, Coulombe PA. Networking galore: intermediate filaments and cell migration. *Current opinion in cell biology*. 2013 Oct;25(5):600-12.
129. Ivaska J, Pallari HM, Nevo J, Eriksson JE. Novel functions of vimentin in cell adhesion, migration, and signaling. *Experimental cell research*. 2007 Jun 10;313(10):2050-62.
130. Mendez MG, Kojima S, Goldman RD. Vimentin induces changes in cell shape, motility, and adhesion during the epithelial to mesenchymal transition. *FASEB journal : official publication of the Federation of American Societies for Experimental Biology*. 2010 Jun;24(6):1838-51.
131. Tzivion G, Luo ZJ, Avruch J. Calyculin A-induced vimentin phosphorylation sequesters 14-3-3 and displaces other 14-3-3 partners in vivo. *The Journal of biological chemistry*. 2000 Sep 22;275(38):29772-8.
132. Zhu QS, Rosenblatt K, Huang KL, Lahat G, Brobey R, Bolshakov S, et al. Vimentin is a novel AKT1 target mediating motility and invasion. *Oncogene*. 2011 Jan 27;30(4):457-70.
133. Berghmans S, Jette C, Langenau D, Hsu K, Stewart R, Look T, et al. Making waves in cancer research: new models in the zebrafish. *BioTechniques*. 2005 Aug;39(2):227-37.
134. Blouin S, Basle MF, Chappard D. Rat models of bone metastases. *Clinical & experimental metastasis*. 2005;22(8):605-14.
135. Khanna C, Hunter K. Modeling metastasis in vivo. *Carcinogenesis*. 2005 Mar;26(3):513-23.
136. Chambers AF, Naumov GN, Varghese HJ, Nadkarni KV, MacDonald IC, Groom AC. Critical steps in hematogenous metastasis: an overview. *Surgical oncology clinics of North America*. 2001 Apr;10(2):243-55, vii.
137. Saxena M, Christofori G. Rebuilding cancer metastasis in the mouse. *Molecular oncology*. 2013 Apr;7(2):283-96.
138. Francia G, Cruz-Munoz W, Man S, Xu P, Kerbel RS. Mouse models of advanced spontaneous metastasis for experimental therapeutics. *Nat Rev Cancer*. 2011 Feb;11(2):135-41.
139. Wilmanns C, Fan D, O'Brian CA, Bucana CD, Fidler IJ. Orthotopic and ectopic organ environments differentially influence the sensitivity of murine colon carcinoma cells to doxorubicin and 5-fluorouracil. *International journal of cancer*. 1992 Aug 19;52(1):98-104.
140. Cespedes MV, Casanova I, Parreno M, Manges R. Mouse models in oncogenesis and cancer therapy. *Clinical & translational oncology : official*

- publication of the Federation of Spanish Oncology Societies and of the National Cancer Institute of Mexico. 2006 May;8(5):318-29.
141. Bibby MC. Orthotopic models of cancer for preclinical drug evaluation: advantages and disadvantages. *European journal of cancer (Oxford, England : 1990)*. 2004 Apr;40(6):852-7.
  142. Khanna C, Prehn J, Yeung C, Caylor J, Tsokos M, Helman L. An orthotopic model of murine osteosarcoma with clonally related variants differing in pulmonary metastatic potential. *Clinical & experimental metastasis*. 2000;18(3):261-71.
  143. Fantozzi A, Christofori G. Mouse models of breast cancer metastasis. *Breast cancer research : BCR*. 2006;8(4):212.
  144. Jonkers J, Derksen PW. Modeling metastatic breast cancer in mice. *Journal of mammary gland biology and neoplasia*. 2007 Sep;12(2-3):191-203.
  145. Kuperwasser C, Chavarria T, Wu M, Magrane G, Gray JW, Carey L, et al. Reconstruction of functionally normal and malignant human breast tissues in mice. *Proceedings of the National Academy of Sciences of the United States of America*. 2004 Apr 06;101(14):4966-71.
  146. Becher OJ, Holland EC. Genetically engineered models have advantages over xenografts for preclinical studies. *Cancer research*. 2006 Apr 01;66(7):3355-8, discussion 8-9.
  147. Firestone B. The challenge of selecting the 'right' in vivo oncology pharmacology model. *Current opinion in pharmacology*. 2010 Aug;10(4):391-6.
  148. Frese KK, Tuveson DA. Maximizing mouse cancer models. *Nat Rev Cancer*. 2007 Sep;7(9):645-58.
  149. Maddison K, Clarke AR. New approaches for modelling cancer mechanisms in the mouse. *The Journal of pathology*. 2005 Jan;205(2):181-93.
  150. Richmond A, Su Y. Mouse xenograft models vs GEM models for human cancer therapeutics. *Disease models & mechanisms*. 2008 Sep-Oct;1(2-3):78-82.
  151. Gopinathan A, Morton JP, Jodrell DI, Sansom OJ. GEMMs as preclinical models for testing pancreatic cancer therapies. *Disease models & mechanisms*. 2015 Oct 01;8(10):1185-200.
  152. Weiser-Evans MC, Wang XQ, Amin J, Van Putten V, Choudhary R, Winn RA, et al. Depletion of cytosolic phospholipase A2 in bone marrow-derived macrophages protects against lung cancer progression and metastasis. *Cancer research*. 2009 Mar 01;69(5):1733-8.
  153. Guerra C, Mijimolle N, Dhawahir A, Dubus P, Barradas M, Serrano M, et al. Tumor induction by an endogenous K-ras oncogene is highly dependent on cellular context. *Cancer cell*. 2003 Aug;4(2):111-20.
  154. DuPage M, Dooley AL, Jacks T. Conditional mouse lung cancer models using adenoviral or lentiviral delivery of Cre recombinase. *Nature protocols*. 2009;4(7):1064-72.
  155. Siegel RL, Miller KD, Jemal A. Cancer statistics, 2016. *CA Cancer J Clin*. 2016 Jan;66(1):7-30.
  156. Sanchez-Cespedes M. The role of LKB1 in lung cancer. *Familial cancer*. 2011 Sep;10(3):447-53.

157. Singh GK, Miller BA, Hankey BF. Changing area socioeconomic patterns in U.S. cancer mortality, 1950-1998: Part II--Lung and colorectal cancers. *Journal of the National Cancer Institute*. 2002 Jun 19;94(12):916-25.
158. Pisters KM, Le Chevalier T. Adjuvant chemotherapy in completely resected non-small-cell lung cancer. *Journal of clinical oncology : official journal of the American Society of Clinical Oncology*. 2005 May 10;23(14):3270-8.
159. Baylin SB, Esteller M, Rountree MR, Bachman KE, Schuebel K, Herman JG. Aberrant patterns of DNA methylation, chromatin formation and gene expression in cancer. *Human molecular genetics*. 2001 Apr;10(7):687-92.
160. Stoker M, Perryman M. An epithelial scatter factor released by embryo fibroblasts. *Journal of cell science*. 1985 Aug;77:209-23.
161. Soltermann A, Tischler V, Arbogast S, Braun J, Probst-Hensch N, Weder W, et al. Prognostic significance of epithelial-mesenchymal and mesenchymal-epithelial transition protein expression in non-small cell lung cancer. *Clinical cancer research : an official journal of the American Association for Cancer Research*. 2008 Nov 15;14(22):7430-7.
162. Abe K, Rossman KL, Liu B, Ritola KD, Chiang D, Campbell SL, et al. Vav2 is an activator of Cdc42, Rac1, and RhoA. *The Journal of biological chemistry*. 2000 Apr 07;275(14):10141-9.
163. Lai SY, Ziober AF, Lee MN, Cohen NA, Falls EM, Ziober BL. Activated Vav2 modulates cellular invasion through Rac1 and Cdc42 in oral squamous cell carcinoma. *Oral oncology*. 2008 Jul;44(7):683-8.
164. Tamas P, Solti Z, Bauer P, Illes A, Sipeki S, Bauer A, et al. Mechanism of epidermal growth factor regulation of Vav2, a guanine nucleotide exchange factor for Rac. *The Journal of biological chemistry*. 2003 Feb 14;278(7):5163-71.
165. Chan KT, Bennin DA, Huttenlocher A. Regulation of adhesion dynamics by calpain-mediated proteolysis of focal adhesion kinase (FAK). *The Journal of biological chemistry*. 2010 Apr 09;285(15):11418-26.
166. Wittmann T, Bokoch GM, Waterman-Storer CM. Regulation of leading edge microtubule and actin dynamics downstream of Rac1. *The Journal of cell biology*. 2003 Jun 09;161(5):845-51.
167. Nobes CD, Hall A. Rho, rac, and cdc42 GTPases regulate the assembly of multimolecular focal complexes associated with actin stress fibers, lamellipodia, and filopodia. *Cell*. 1995 Apr 07;81(1):53-62.
168. Burgstaller G, Gregor M, Winter L, Wiche G. Keeping the vimentin network under control: cell-matrix adhesion-associated plectin 1f affects cell shape and polarity of fibroblasts. *Molecular biology of the cell*. 2010 Oct 01;21(19):3362-75.
169. Marignani PA, Carpenter CL. Vav2 is required for cell spreading. *The Journal of cell biology*. 2001 Jul 09;154(1):177-86.
170. Citterio C, Menacho-Marquez M, Garcia-Escudero R, Larive RM, Barreiro O, Sanchez-Madrid F, et al. The rho exchange factors vav2 and vav3 control a lung metastasis-specific transcriptional program in breast cancer cells. *Science signaling*. 2012 Oct 02;5(244):ra71.
171. Schuebel KE, Movilla N, Rosa JL, Bustelo XR. Phosphorylation-dependent and constitutive activation of Rho proteins by wild-type and oncogenic Vav-2. *The EMBO journal*. 1998 Nov 16;17(22):6608-21.



172. Chang F, Lemmon CA, Park D, Romer LH. FAK potentiates Rac1 activation and localization to matrix adhesion sites: a role for betaPIX. *Molecular biology of the cell*. 2007 Jan;18(1):253-64.
173. Tse JC, Kalluri R. Mechanisms of metastasis: epithelial-to-mesenchymal transition and contribution of tumor microenvironment. *Journal of cellular biochemistry*. 2007 Jul 1;101(4):816-29.
174. Onder TT, Gupta PB, Mani SA, Yang J, Lander ES, Weinberg RA. Loss of E-cadherin promotes metastasis via multiple downstream transcriptional pathways. *Cancer research*. 2008 May 15;68(10):3645-54.
175. Huber MA, Kraut N, Beug H. Molecular requirements for epithelial-mesenchymal transition during tumor progression. *Current opinion in cell biology*. 2005 Oct;17(5):548-58.
176. Zeisberg M, Neilson EG. Biomarkers for epithelial-mesenchymal transitions. *The Journal of clinical investigation*. 2009 Jun;119(6):1429-37.
177. Fischer KR, Durrans A, Lee S, Sheng J, Li F, Wong ST, et al. Epithelial-to-mesenchymal transition is not required for lung metastasis but contributes to chemoresistance. *Nature*. 2015 Nov 26;527(7579):472-6.
178. Zheng X, Carstens JL, Kim J, Scheible M, Kaye J, Sugimoto H, et al. Epithelial-to-mesenchymal transition is dispensable for metastasis but induces chemoresistance in pancreatic cancer. *Nature*. 2015 Nov 26;527(7579):525-30.
179. Gao Y, Xiao Q, Ma H, Li L, Liu J, Feng Y, et al. LKB1 inhibits lung cancer progression through lysyl oxidase and extracellular matrix remodeling. *Proceedings of the National Academy of Sciences of the United States of America*. 2010 Nov 02;107(44):18892-7.
180. Colucci-Guyon E, Portier MM, Dunia I, Paulin D, Pournin S, Babinet C. Mice lacking vimentin develop and reproduce without an obvious phenotype. *Cell*. 1994 Nov 18;79(4):679-94.
181. Yamashita N, Tokunaga E, Kitao H, Hisamatsu Y, Taketani K, Akiyoshi S, et al. Vimentin as a poor prognostic factor for triple-negative breast cancer. *Journal of cancer research and clinical oncology*. 2013 May;139(5):739-46.
182. Liu S, Liu L, Ye W, Ye D, Wang T, Guo W, et al. High Vimentin Expression Associated with Lymph Node Metastasis and Predicated a Poor Prognosis in Oral Squamous Cell Carcinoma. *Scientific reports*. 2016 Dec 14;6:38834.
183. Javle MM, Gibbs JF, Iwata KK, Pak Y, Rutledge P, Yu J, et al. Epithelial-mesenchymal transition (EMT) and activated extracellular signal-regulated kinase (p-Erk) in surgically resected pancreatic cancer. *Annals of surgical oncology*. 2007 Dec;14(12):3527-33.
184. Burch TC, Watson MT, Nyalwidhe JO. Variable metastatic potentials correlate with differential plectin and vimentin expression in syngeneic androgen independent prostate cancer cells. *PLoS One*. 2013;8(5):e65005.
185. Domagala W, Lasota J, Dukowicz A, Markiewski M, Striker G, Weber K, et al. Vimentin expression appears to be associated with poor prognosis in node-negative ductal NOS breast carcinomas. *The American journal of pathology*. 1990 Dec;137(6):1299-304.
186. Konen J, Wilkinson S, Lee B, Fu H, Zhou W, Jiang Y, et al. LKB1 kinase-dependent and -independent defects disrupt polarity and adhesion signaling to

- drive collagen remodeling during invasion. *Molecular biology of the cell*. 2016 Apr 01;27(7):1069-84.
187. Terzi F, Henrion D, Colucci-Guyon E, Federici P, Babinet C, Levy BI, et al. Reduction of renal mass is lethal in mice lacking vimentin. Role of endothelin-nitric oxide imbalance. *The Journal of clinical investigation*. 1997 Sep 15;100(6):1520-8.
188. Hosseini H, Obradovic MM, Hoffmann M, Harper KL, Sosa MS, Werner-Klein M, et al. Early dissemination seeds metastasis in breast cancer. *Nature*. 2016 Dec 14.
189. Tian W, Wang G, Yang J, Pan Y, Ma Y. Prognostic role of E-cadherin and Vimentin expression in various subtypes of soft tissue leiomyosarcomas. *Medical oncology (Northwood, London, England)*. 2013 Mar;30(1):401.
190. van Zijl F, Krupitza G, Mikulits W. Initial steps of metastasis: cell invasion and endothelial transmigration. *Mutation research*. 2011 Jul-Oct;728(1-2):23-34.
191. Cheung KJ, Gabrielson E, Werb Z, Ewald AJ. Collective invasion in breast cancer requires a conserved basal epithelial program. *Cell*. 2013 Dec 19;155(7):1639-51.
192. Roychowdhury A, Samadder S, Islam MS, Chaudhury K, Roy A, Banerjee D, et al. Identification of Changes in the Human Papilloma Virus 16 (HPV16) Genome During Early Dissemination of Cervical Cancer Cells May Complement Histological Diagnosis of Lymph Node Metastasis. *Pathology oncology research : POR*. 2017 Jan 19.
193. Khalil AA, Ilina O, Gritsenko PG, Bult P, Span PN, Friedl P. Collective invasion in ductal and lobular breast cancer associates with distant metastasis. *Clinical & experimental metastasis*. 2017 Sep 11.
194. Bowden ET, Onikoyi E, Slack R, Myoui A, Yoneda T, Yamada KM, et al. Co-localization of cortactin and phosphotyrosine identifies active invadopodia in human breast cancer cells. *Experimental cell research*. 2006 May 01;312(8):1240-53.
195. Ivaska J, Vuoriluoto K, Huovinen T, Izawa I, Inagaki M, Parker PJ. PKCepsilon-mediated phosphorylation of vimentin controls integrin recycling and motility. *The EMBO journal*. 2005 Nov 16;24(22):3834-45.
196. Dave JM, Kang H, Abbey CA, Maxwell SA, Bayless KJ. Proteomic profiling of endothelial invasion revealed receptor for activated C kinase 1 (RACK1) complexed with vimentin to regulate focal adhesion kinase (FAK). *The Journal of biological chemistry*. 2013 Oct 18;288(42):30720-33.
197. Mouw JK, Yui Y, Damiano L, Bainer RO, Lakins JN, Acerbi I, et al. Tissue mechanics modulate microRNA-dependent PTEN expression to regulate malignant progression. *Nat Med*. 2014 Apr;20(4):360-7.
198. Goldman RD, Khuon S, Chou YH, Opal P, Steinert PM. The function of intermediate filaments in cell shape and cytoskeletal integrity. *The Journal of cell biology*. 1996 Aug;134(4):971-83.
199. Wang N, Stamenovic D. Mechanics of vimentin intermediate filaments. *Journal of muscle research and cell motility*. 2002;23(5-6):535-40.
200. Yang Z, Garcia A, Xu S, Powell DR, Vertino PM, Singh S, et al. *Withania somnifera* root extract inhibits mammary cancer metastasis and epithelial to mesenchymal transition. *PLoS One*. 2013;8(9):e75069.

201. Thaiparambil JT, Bender L, Ganesh T, Kline E, Patel P, Liu Y, et al. Withaferin A inhibits breast cancer invasion and metastasis at sub-cytotoxic doses by inducing vimentin disassembly and serine 56 phosphorylation. *International journal of cancer*. 2011 Dec 01;129(11):2744-55.